



UNIVERSITAT
POLITÈCNICA
DE VALÈNCIA



ESCUELA TÉCNICA
SUPERIOR INGENIERÍA
INDUSTRIAL VALENCIA

INDUSTRIAL ENGINEERING MASTER THESIS

3D PRINTED AUTONOMOUS SOLAR CATAMARAN

AUTHOR: DAAN DE GEYTER

SUPERVISOR: JAVIER OROZCO MESSANA

Academic year: 2020-2021

Acknowledgements

After an exciting half year of studying abroad it is finally time to finish this master's thesis. During this challenging and enlightening period, I was put to the test in many ways. I was given the opportunity to utilize my acquired knowledge from the past years studying, to become a master's in industrial engineering and develop my skill even further.

Many people contributed to the realization of this thesis. I would like to take this opportunity to thank them for their support, help and trust during this project.

First of all, I would like to express my gratitude to my supervisor, Professor Javier Orozco Messana. Javier always steered me in the right direction and would assist me whenever I had questions. I would also like to thank Raimond Calabuig-Moreno for assisting me and checking up on the progress.

Secondly, I would like to thank my parents and family for the support and guidance. They were always there when I needed them.

And lastly, my flatmates and the friends I made during this exchange program. To Daniel Ortega Villalobos for helping me with Spanish, To Moritz Langen for keeping me company in the office and to Sebastian Küpper joining me in exploring places in Spain. With them I made unforgettable memories and stories to tell.

Thank you to all these people for the support, courage and making my work more gratifying.

Keywords: Solar energy, Hydrogen power, Additive manufacturing, 3D printing, Catamaran, Marine energy systems

Summary

Increasing energy shortages, maintainability and technology are key factors in upcoming global energy policies. Solar energy is therefore a great solution for generating clean energy. Also, Hydrogen has the potential to be the sustainable fuel of the future. Combining solar energy capture and hydrogen as storage and fuel source proves to be an interesting method for renewable, transportable, and decarbonized energy.

The aim of this master's thesis is to make an inspiring proposal for sustainable maritime mobility. It will consist of designing and executing a fully autonomous solar catamaran prototype. A photovoltaic system is used to generate electrical energy that can be used directly and/or stored in the form of hydrogen to be able to navigate in conditions of absence of light.

Both solar and hydrogen energies were thoroughly explored. Technologies used for converting and storing energy in hydrogen form are electrolysis and fuel cell technology, in combination with the method of the compressed gas storage.

Inspired by the Alinghi 5, a former race catamaran, a 3D model will be designed. Additive manufacturing was the chosen method to manufacture the model catamaran.

The solar panel, the hydrogen parts and a remote-controlled steering system were fitted into the 3D printed catamaran. An electric system was designed to change power source, followed by an operational performance evaluation of the sailing times in the different modes, resulting in advice for the optimal transition of sailing modes.

The selected materials, devices and technologies chosen for this purpose were tested in order to fully characterise their behaviour, to assess their optimal operating condition and to find their limitations.

The results of this project intend to demonstrate the viability of developing a new proposal for fully sustainable maritime mobility as a first step in eliminating fossil fuels in navigation. It might inspire the future vision on the technologies in the autonomous maritime sector.

Palabras Clave: Energía solar, Hidrógeno, Producción aditiva, Impresión 3D, Catamarán, Sistemas energéticos marinos

Resumen

La creciente escasez energética, la sostenibilidad y la tecnología son factores clave en las políticas energéticas globales del futuro. La energía solar es por ello una gran solución para la generación de energía limpia. A su vez, el Hidrógeno tiene un gran potencial para convertirse en el combustible sostenible del futuro. La combinación de la captura de energía solar y el almacenamiento de hidrógeno como fuente de energía están convirtiéndose en la alternativa más prometedora para una descarbonización energética, renovable y transportable.

El objetivo de esta tesina de máster es ofrecer una propuesta inspiradora para la sostenibilidad en la movilidad marítima. Consistirá principalmente en el diseño y ejecución de un prototipo de catamarán solar completamente autónomo. Utilizando un sistema fotovoltaico para generar electricidad que pueda ser consumida directamente o almacenada en forma de hidrógeno para poder navegar en condiciones de escasez lumínica.

Ambas fuentes energéticas, solar y de hidrógeno han sido exhaustivamente exploradas. Las tecnologías seleccionadas para convertir y almacenar energía en forma de hidrógeno, han sido la electrólisis y la célula de combustible, combinadas con el almacenamiento del hidrógeno generado bajo presión.

Inspirado en el Alinghi 5, un antiguo catamarán de carreras, se diseñará un modelo en 3D. Utilizando como herramienta la fabricación aditiva se procederá a fabricar un modelo de catamarán donde verificar a escala la propuesta integrada.

Partiendo de un panel solar de última generación, unido a una célula de hidrógeno y un sistema de dirección remoto, se ha diseñado una versión a escala del catamarán prototipo, inspirada en el Alinghi. Se diseñó un sistema eléctrico auxiliar para poder cambiar la fuente de alimentación, seguida de una evaluación operacional de desempeño en diferentes modos y tiempos de navegación, a fin de establecer unas recomendaciones para la transición óptima entre los distintos modos de navegación.

Los materiales aparatos y tecnologías seleccionados para este propósito fueron caracterizados para comprobar y dimensionar su comportamiento, con vistas a seleccionar las condiciones óptimas de operación y determinar sus limitaciones.

Los resultados de este proyecto pretenden demostrar la viabilidad del desarrollo de nuevas propuestas para la movilidad marítima sostenible como un primer paso para la eliminación de los combustibles fósiles en la navegación. Podría inspirar una visión futura de las tecnologías en el sector autónomo marítimo.

List of symbols and abbreviations

List of abbreviations

3D	Three-dimensional
AAWA	Advanced Autonomous Waterborne Applications Initiative
ABS	Acrylonitrile butadiene styrene
AC	Alternating current
AFC	Alkaline fuel cell
ASA	Acrylonitrile styrene acrylate
A-Si	Amorphous silicon
AUV	Autonomous underwater vehicles
CAD	Computer aided design
COLREG	Collision Regulations
COP	Coefficient of performance
CSC	Safe containers
DC	Direct current
DMFC	Direct methanol fuel cell
FDM	Fused Deposition Modelling
FF	Fill factor
GDP	Gross Domestic Product
H ₂	Hydrogen
IC	Integrated circuit
IMO	International maritime organisation
IT	Current-Time
IV, IU	Current-Voltage
Lidar	Light detection and ranging
LNG	Liquified natural gas
MASS	Maritime Autonomous Surface Ships
MCFC	Molten carbonate fuel cell

MPP	Maximum peak power point
MSC	Maritime Safety Committee
PAFC	Phosphoric acid fuel cell
PC	Polycarbonate
PEM	Proton exchange membrane
PEMFC	Proton exchange membrane fuel cell
PET	Polyethylene terephthalate
PLA	Polylactic acid
PNG	Pipeline natural gas
PTFE	Polytetrafluorethylene
PV	Power-Voltage
ROI	Return on investment
ROV	Remotely operated vehicles
SAR	Search and rescue
SMR	Steam methane reforming
SOFC	Solid oxide fuel cell
SOLAS	Safety and maritime security
SPACE STP, STP	Special trade passenger ship instruments
STCW, STCW-F	Training of seafarers and fishers
TPU	Thermoplastics polyurethane
UV	Ultraviolet
VT	Volume-Time

List of units

A	Ampere
bar	Barometric pressure
EJ	Exajoule
ft	foot
g	Gram
GW	Gigawatt
GWh	Gigawatt hours
J	Joule
Kg	Kilogram
KW	Kilowatt
KΩ	Kiloohm
l/min	Litre per minute
m ³	Cubic metre
mA	Milliamp
mAh	Milliamp hours
Mhz	Megahertz
ml	Millilitre
mm	Millimetre
Mpa	Megapascal
mV	Millivolt
mW	Milliwatt
PWh	Petawatt hour
Rpm	Revolutions per minute
TW	Terawatt
TWh	Terawatt hours
V	Volt
Vcc	Volt closed circuit
Vmp	Voltage maximum power

Voc	Volt open circuit
W	Watt

List of symbols

F_b	Buoyancy force
°	Degree
°C	Degree Celsius
ρ_{fluid}	Density
V_{displ}	Displaced or submerged volume
η	Efficiency
€	Euro
g	Gravitational force
%	Percent
W	Weight of the object

Figures index

Figure 1: World primary energy supply by source [6].....	15
Figure 2: World electricity generation by power station type [6].....	16
Figure 3: World electricity generation from solar and wind [6].....	18
Figure 4: World final energy demand by carrier [6].....	19
Figure 5: Maritime energy demand and projected fuel mix [6].....	19
Figure 6: Energy storage in relation to time [21]	25
Figure 7: Hydrogen storing methods [21]	26
Figure 8: Electrolysis visualisation [22]	28
Figure 9: PEMFC visualisation [23]	30
Figure 10: SOFC visualisation [23]	31
Figure 11: AFC visualisation [23]	31
Figure 12: DMFC visualisation [23].....	32
Figure 13: PAFC visualisation [23]	32
Figure 14: Polarisation curve [20]	32
Figure 15: Solar panel IV – and PC curve [8]	37
Figure 16: IV – and PC curve stacked solar cells [8]	38
Figure 17: Power curve.....	39
Figure 18: Labview data acquisition program interface.....	42
Figure 19: Labview data acquisition program code blocks	43
Figure 20: Water pressure experiment schematic.....	45
Figure 21: Water pressure experiment setup 1	46
Figure 22: Short term experiment setup.....	47
Figure 23: Volume time characteristics.....	48
Figure 24: Current time characteristics.....	48
Figure 25: Volume time characterisation O ₂	49
Figure 26: Volume time characterisation O ₂	50
Figure 27: Volume time characterisation H ₂	50
Figure 28: Hydrogen to oxygen ratio.....	51
Figure 29: Long term experiment schematic	52
Figure 30: Gaussian distribution and standard deviations [27]	54
Figure 31: 100min experiment IV characteristic 1	55
Figure 32: 100min experiment IT characteristic 1.....	56
Figure 33: 100min experiment significant numbers calculations 1	56
Figure 34: 100min experiment IV characteristic 2	57
Figure 35: 100min experiment IT characteristic 2.....	57
Figure 36: solar exposure level [28]	60
Figure 37: Full day experiment IV characteristic.....	60
Figure 38: Full day experiment PT characteristic	61
Figure 39: Full day experiment IU characteristic.....	62
Figure 40: Full day experiment UT characteristic.....	63
Figure 41: Full day experiment VT characteristic combined H ₂ and O ₂	63

Figure 42: Full day experiment IV characteristic combined H ₂ and O ₂	64
Figure 43: Full day experiment 2 IU characteristic.....	65
Figure 44: Full day experiment 2 IU characteristic capped	66
Figure 45: Full day experiment 2 IU characteristic capped night.....	66
Figure 46: Full day experiment 2 IT characteristic	67
Figure 47: Full day experiment 2 VT characteristic	69
Figure 48: Full day experiment 2 VT characteristic combined H ₂ and O ₂	70
Figure 49: Full day experiment 2 IV characteristic combined H ₂ and O ₂	71
Figure 50: Polarisation curve 2 [29]	73
Figure 51: Fuel cell characterisation schematic	74
Figure 52: Fuel cell IV characterisation	75
Figure 53: Fuel cell PI characterisation.....	76
Figure 54: Fuel cell power curve	77
Figure 55: Fuel cell 2 IV characterisation	77
Figure 56: Fuel cell 2 PI characterisation.....	78
Figure 57: Fuel cell 2 power curve	79
Figure 58: Motor IV characterisation	80
Figure 59: Motor operating point	81
Figure 60: Fuel cell and motor schematic	82
Figure 61: Fuel cell and motor IV characterisation	83
Figure 62: Fuel cell and motor PI characterisation.....	84
Figure 63: Fuel cell and motor power curve	84
Figure 64: Fuel cell and motor operating point.....	85
Figure 65: Fuel cell 2 and motor operating point.....	87
Figure 66: Fuel cell 2 and motor significant numbers for calculating the operating point.....	87
Figure 67: Additional fuel cell schematic	88
Figure 68: Additional fuel cell IV – and power curve	89
Figure 69: Additional fuel cell IV – and power curve motor 1	89
Figure 70: Additional fuel cell IV – and power curve motor 2	90
Figure 71: Series experiment schematic	93
Figure 72: Series control experiment PT curve	94
Figure 73: Series experiment 1 PT curve	95
Figure 74: Series experiment 1 IV- and PV curve	95
Figure 75: Series experiment 2 motors in series schematic.....	97
Figure 76: Series experiment 2 motors in series PT curve	97
Figure 77: Series experiment 2 motors in series IV- and PV curve	98
Figure 78: Series experiment 2 motors in parallel schematic.....	99
Figure 79: Series experiment 2 motors in parallel PT curve	99
Figure 80: Series experiment 2 motors in parallel IV- and PV curve.....	100
Figure 81: Parallel experiment schematic	101
Figure 82: Parallel experiment PT curve	101
Figure 83: Parallel experiment IV- and PV curve.....	102
Figure 84: Dual extruder print head.....	106

Figure 85: Xyz cube before-after tuning: ringing	107
Figure 86: Xyz cube before-after tuning: outer wall error	107
Figure 87: Benchy sideview	108
Figure 88: Benchy bottom view	108
Figure 89: Second picture: complete dual colour cone.....	109
Figure 90: First picture: alignment of the two nozzles.....	109
Figure 91: Prime tower.....	109
Figure 92: Ooze shield	109
Figure 93: Complex dual colour frog 2	110
Figure 94: Complex dual colour frog 1	110
Figure 95: Alinghi 5 drawing [35]	111
Figure 96: Completed catamaran in CAD	112
Figure 97: Hull	113
Figure 98: Top hull cover.....	114
Figure 99: Servomotor mount.....	115
Figure 100: Rudder assembly side view	116
Figure 101: Rudder assembly bottom view.....	116
Figure 102: Propellor assembly top view	117
Figure 103: Propellor assembly side view	117
Figure 104: Power unit mount	119
Figure 105: Deck.....	119
Figure 106: Model ship internals.....	125
Figure 107: Hydrogen station.....	126
Figure 108: Fuel cell connections	126
Figure 109: Hydrogen power unit	127
Figure 110: Servo control components	128
Figure 111: Power system integration electrical circuit.....	129
Figure 112: Mode pilot switches	130
Figure 113: Advised sailing mode.....	132
Figure 114: OceanVolt electric motor system [37]	136
Figure 115: Luxyacht cost calculator [42].....	138
Figure 116: Luxyacht cost calculator 3 [42].....	139
Figure 117: Luxyacht cost calculator 2 [42].....	139

Table index

Table 1: Energy efficiency improvements by sector [6]	17
Table 2: Short term experiment results	49
Table 3: Statistical formulas	54
Table 4: 100min experiment statistics	55
Table 5: 100min experiment statistics	55
Table 6: 100min experiment significant numbers calculations 2.....	58
Table 7: 100min experiment statistics	58
Table 8: Full day experiment statistics	60
Table 9: Full day experiment significant data	61
Table 10: Full day experiment 2 statistics table 1	67
Table 11: Full day experiment 2 significant data table 1	68
Table 12: Full day experiment 2 significant data table 2	69
Table 13: Full day experiment 2 statistics table 2	69
Table 14: Fuel cell and motor significant numbers for calculating the operating point.....	86
Table 15: Fuel cell and motor efficiency calculations 1.....	92
Table 16: Fuel cell and motor efficiency calculations 2.....	92
Table 17: Series control experiment significant data.....	94
Table 18: Series experiment 1 significant data	96
Table 19: Series experiment 2 motors in series significant data.....	98
Table 20: Series experiment 2 motors in parallel significant data	100
Table 21: Parallel experiment significant data	102
Table 22: Print time and mass calculations.....	124
Table 23: Solar vs internal combustion engine	141
Table 24: Retrofit of the boat.....	141
Table 25: ROI	142

Index

Acknowledgements	III
Summary	V
List of symbols and abbreviations	IX
Figures index	XIII
Table index	XVI
1 Introduction	3
1.1 <i>Contextualization</i>	3
1.2 <i>Main goals</i>	4
1.2.1 Research objectives:	4
1.2.2 Development plan.....	5
1.3 <i>Required functionality of the model</i>	6
1.4 <i>Methodology</i>	7
1.5 <i>Framework</i>	8
2 Theoretical contextualisation	11
2.1 <i>Autonomous vehicles</i>	11
2.1.1 Regulation of autonomous ships	11
2.1.2 Autonomous ships in operation.....	11
2.1.3 Autonomous ships: The next step	12
2.1.4 Technology.....	12
2.1.5 Safety	13
2.1.6 Legal aspect.....	13
2.1.7 Economical.....	14
2.1.8 Benefits of Autonomous shipping	14
2.2 <i>Future predictions</i>	15
2.2.1 Highlights	15
2.2.2 Electricity	15
2.2.3 Energy efficiency.....	16
2.2.4 Renewables on the rise.....	17
2.2.5 Technology.....	18
2.2.6 Transport.....	18
2.2.7 Maritime	19

2.2.8	Hydrogen.....	20
2.3	<i>Solar energy</i>	21
2.3.1	Introduction	21
2.3.2	Characteristics.....	21
2.3.3	Materials	21
2.3.4	Impact of radiation and temperature	22
2.3.5	Implementation and upcoming tests.....	23
2.4	<i>Hydrogen energy</i>	24
2.4.1	Introduction	24
2.4.2	Characteristics.....	24
2.4.3	Storage	25
2.4.4	Electrolysers.....	27
2.4.5	Fuel cells.....	29
2.4.6	Implementation	33
3	Developments and results	36
3.1	<i>Solar energy capture</i>	36
3.1.1	Solar cell characterization.....	36
3.1.2	IV measurements	39
3.2	<i>Data acquisition program</i>	42
3.3	<i>PEM reversible fuel cell</i>	44
3.4	<i>Electrolyser practical experiments</i>	45
3.4.1	Water pressure experiment.....	45
3.4.2	Short term experiment	47
3.4.3	Long term experiment	52
3.4.4	Setup	52
3.4.5	Statistics	54
3.4.6	100 min experiment.....	55
3.4.7	Full day experiments.....	59
3.4.8	Conclusions electrolyser	71
3.5	<i>Fuel cell practical experiments</i>	72
3.5.1	Graph comparison	73
3.5.2	Fuel cell characterisation with potentiometer	74
3.5.3	Second fuel cell characterisation with potentiometer	77

3.5.4	Fuel cell characterisation using the motor	80
3.5.5	Fuel cell and motor testing	81
3.5.6	Second fuel cell characterisation using the motor	86
3.5.7	Additional fuel cell characterisation	88
3.5.8	Fuel cell conclusion	91
3.6	<i>Series and parallel tests combining solar panel, electrolyser, and motor</i>	<i>93</i>
3.6.1	Setup series circuit.....	93
3.6.2	Series experiment	95
3.6.3	Series experiment 2 motors in series	97
3.6.4	Series experiment 2 motors in parallel.....	99
3.6.5	Parallel experiment.....	101
3.6.6	Circuit conclusions	103
3.7	<i>Additive manufacturing</i>	<i>104</i>
3.7.1	Material choice	104
3.7.2	3D printer and setup.....	105
3.8	<i>Design of the catamaran</i>	<i>111</i>
3.8.1	Tolerance	112
3.8.2	Complete model	112
3.8.3	Print settings	120
3.8.4	Total print time and mass	123
3.9	<i>Power system integration</i>	<i>125</i>
3.9.1	Functional explanation of the model ship	125
3.9.2	Assembly	125
3.9.3	Printed parts	125
3.9.4	Hydrogen related components.....	126
3.9.5	Solar panel	127
3.9.6	Servo and radio control	127
3.9.7	Circuit.....	128
3.9.8	Modes	129
3.10	<i>Operational performance evaluation of the design.....</i>	<i>131</i>
3.10.1	Specifications	131
3.10.2	Hydrogen runtime.....	131
3.10.3	Electrical runtime.....	131

3.10.4	Open water evaluation	131
3.10.5	Advised sailing mode	132
4	Budget.....	135
4.1	<i>Energy observer</i>	135
4.2	<i>Solar panels and battery</i>	135
4.3	<i>Wind turbines</i>	136
4.4	<i>Electric motors</i>	136
4.5	<i>Fuel cell</i>	136
4.6	<i>Electrolyser</i>	137
4.7	<i>Hydrogen compressor and storage</i>	137
4.8	<i>Retrofit</i>	137
4.9	<i>Annual expenses</i>	138
4.10	<i>Income</i>	140
4.10.1	Charter as research vessel	140
4.10.2	Charter for pleasure.....	140
4.10.3	Charter for daytrips and island transport	140
5	Evaluation.....	141
6	Conclusions.....	145
7	References and other sources of information.....	149
8	Annexes.....	155
8.1	<i>Additional pictures</i>	155
8.2	<i>Datasheets</i>	157

1 INTRODUCTION

1.1 Contextualization

1.2 Main goals

1.3 Required functionality of the model

1.4 Methodology

1.5 Framework



1 Introduction

1.1 Contextualization

The vision behind the making of this master's thesis finds its origin on the development of UN sustainability goal 7 (affordable and clean energy) and its application to sustainable sea mobility. In order to focus this research, the idea to breathe new life into the Alinghi 5 catamaran was selected as the factual environment for concentrating work on an engineering environment. Since the full development of the idea would be far beyond the scope of a Master thesis the project concentrated on a scaled down objective by making an autonomous model ship.

The catamaran was a gift to the city of Valencia by the Alinghi Team but has been left unused for 11 years. The Alinghi 5 was built to compete as the defender in the 33rd America's cup in 2009. Two years after the victory in the 32nd cup. It was the American BMW Oracle Racing team who were challenging the Swiss by a rare Deed of Gift match. The Challenger versus the Defender, the time chosen by the American team and a place chosen by the Swiss. A Deed of Gift match meant that the winner made the rulebook for the design of the catamaran and the guidelines for the upcoming America's cup.

As opposed to the more common mutual consent. This induced a lengthy court battle. The duel for the trophy was decided to be a "best of three" race. The most significant design parameter for the Deed of Gift match was the load water line. This parameter must be 90ft or 27.5m. Because Alinghi was very limited in time they chose their Alinghi 5 model. To their saying, one of the most revolutionary catamarans of all time. The Alinghi 5 was built out of a carbon fibre composite construction. Built in Switzerland by Alinghi Villeneuve and Décision Corsier. Its beam has a length of 27m. The mast length is equivalent to a 17-story high building. The sail has a span of 1100m² and a total of 100.000 hours were needed to build the catamaran.

Eventually Alinghi's team was beaten 2-0 by the American 110ft trimaran with its radical wing. Because of their defeat and Alinghi leaving his base at the Valencian port facilities, the famous catamaran was gifted to the city. It was stored at the Valencian port and has been left there ever since without use.

[1] [2]

1.2 Main goals

The aim of this master's thesis is to make an interesting proposal for sustainable maritime mobility and consists of designing and executing a fully autonomous solar catamaran prototype. A photovoltaic system will be used to generate electrical energy that can be used directly and stored in the form of hydrogen to be able to navigate in conditions of absence of light.

Given that the prototype is going to be functional and in order to link it to Valencia, it will be based on an advanced design catamaran, the Alinghi 5 catamaran. Doing so by making a small-scale model equipped with state-of-the-art-technology respect for the environment.

Increasing energy shortages, maintainability and technology are key factors in upcoming global energy policies. Solar energy is therefore a great solution for generating clean energy. In recent years solar became more and more popular all around the world for various applications. Therefore, implementing a solar cell will make the model ship self-sufficient.

Considering the long-term view, autonomous or even unmanned (and remotely controlled ships) will become significant marine applications. For this reason, this thesis sets up a research scenario through a model. Allowing a first approach to the problem where different measuring devices will evaluate alternative possibilities for maritime applications.

With the results of this project, it is intended to demonstrate the viability of developing a new proposal for fully sustainable maritime mobility as the first step in eliminating fossil fuels in navigation.

1.2.1 Research objectives:

Building on the thesis proposal, the following objectives are presented as research topics:

- Energy technology and - storage selection: researching which methods of hydrogen production and storage are available. Determining which method is most viable for the purpose. Characterising the chosen devices and implementation in combination with the solar panel. Incorporation in the model ship.
- Solar panel capture characterization: the optimal solar technology which is industrially available for the application is amorphous silicon. A commercial sized panel will be fitted into the proposed model. The setup will be characterized and analysed for evaluating the power generation and its possibilities. The analysis will be done to determine the significant parameters and make adjustments for optimization.
- Model catamaran: using the available catamaran design, a model will be engineered to fit on the power system. This will be done by using 3D additive manufacturing.
- Power system integration: finally, a test rig will be assembled with the required electric motor, propeller, and power unit. From there on, the design can be further improved, and the assembly can be characterized and evaluated.

1.2.2 Development plan

The following tasks are deduced from the previous objectives.

- Solar energy capture:
 - Solar panel characterization:
 - IV curve evaluation.
 - Daily power generation under different sun exposure conditions.
- Energy storage:
 - Bibliography search on hydrogen technologies and hydrogen storage.
 - Test rig for evaluating performance.
 - Energy production and storage selection.
- Model catamaran:
 - Selection of catamaran structural design.
 - Computer model design.
 - 3D model printing
 - Assembly of the solar catamaran.
 - Operational performance evaluation of the design.
- Power system integration:
 - Design of the power system assembly for a catamaran.
 - Incorporation of selected components.
 - Evaluation.

1.3 Required functionality of the model

The model will need 4 key components: solar panel for electricity generation, an electromotor for propulsion, an electrolyser for hydrogen production, and a fuel cell to convert hydrogen back into electricity. The goal is to monogamously combine these components in order to achieve propulsion in sunny conditions as well as in dark conditions.

The initiative is, during sunny conditions, solar energy will be directly used to power the motor. In addition, hydrogen is produced if there is excess energy. This will be performed with the use of an electrolyser and then stored. Secondly, when there is not enough solar irradiation, the stored hydrogen can be used by the fuel cell to produce electricity and power the motor.

If the ship is docked and there is enough sunlight it should be possible to power the electrolyser in order to produce and store hydrogen.

1.4 Methodology

- 1 Comprehending the assignment.
- 2 Assessing the scope of the project in consultation with the mentor, dividing the project in four major parts which are: solar energy capture, hydrogen generation and storage, modelling of the catamaran and power system integration.
- 3 Theoretical study on solar energy to get a greater understanding of its limitations.
- 4 Understanding the current state of the solar energy capture project, evaluating work done by previous students and catching up. Gathering specific information about the tools and programs used.
- 5 Set up of the solar data acquisition software and performing tests.
- 6 Solar cell characterisation and performance analysis.
- 7 Theoretical study on hydrogen technologies including – generation, storage, and consumption.
- 8 Setup of testing facilities for hydrogen generation via electrolysis with controlled current source as well as using the solar panel.
- 9 Electrolyser characterisation.
- 10 Fuel cell characterisation.
- 11 Electrical motor characterisation.
- 12 Combining previous test results and comparing and evaluating power curves and calculating efficiencies.
- 13 Deciding on the configuration that will be used in the actual model.
- 14 Theoretical study on additive manufacturing, suitable materials, and methods of 3D printing.
- 15 Setup and preparation of the 3D printer available.
- 16 Study on the Alinghi 5 reference catamaran, design in CAD software, buoyancy calculations.
- 17 Printing and assembly of the catamaran.
- 18 Installation of the power unit, electronics, and radio control. Outdoor testing and evaluating.
- 19 Operational performance evaluation of the build.
- 20 General conclusions.

1.5 Framework

The structure of this final work consists out of five parts:

1 Introduction

The reader will learn about the theme and the general direction of the thesis. The goals and objectives that are described and the methodology which is used to conquer difficulties.

2 Theoretical approach and literature review

The literature review will give a wider view on the subjects used and needed for the practical part of the thesis. This will ensure a better understanding of the topics and theme related to this thesis. It also includes reviewing the predictions, technical developments and scientific publications and journals related to the topics.

3 Developments and results regarding the practical work

A thorough representation of the work carried out is illustrated in this part. The hands-on developments and a judgemental assessment of the results are described. It will explain the approach taken on how to practically solve the research objectives. As well as the results those methods yield. Divided in 10 topics researching solar – and hydrogen solutions, design and manufacturing of the catamaran, power system integration, and to end with operational performance evaluation.

4 Budget

An economical study will be made to find a logical purpose for the Alinghi 5. Several scenarios will be looked into such as retrofitting the vessel to a research vessel for coastal missions. Calculations will be made to determine a rough estimate for the cost of the construction and the new equipment. A supplementing return on investment will be made as well to verify the feasibility of the retrofit.

5 Conclusions

The summarisation and breakdown about the work, here it will be discussed whether or not the research objectives are met. The conclusions are drawn. The positives and negatives are weighted and reviewed to form a final standpoint on the work done.

2 THEORETICAL CONTEXTUALISATION

2.1 Autonomous vehicles

2.2 Future predictions

2.3 Solar energy

2.4 Hydrogen energy

2.5 Implementation



2 Theoretical contextualisation

2.1 Autonomous vehicles

Autonomous vehicles are progressively becoming a more viable option among many fields of industry. For example, self-driving cars are on the rise and being developed, having eyes on the near future. Nowadays a lot of vehicles are equipped with driver assistant technology and partial automation with the user monitoring the tasks and controls. Although the future goal is a full automation where the user does not have to do anything anymore. In the maritime industry this is also becoming a trend. Remotely operated vehicles (ROV) are advancing to autonomous underwater vehicles (AUV) for progressively more tasks such as underwater mapping or survey missions. The difference between the two is that the working of the AUV is completely intervened by an operator. The AUV is pre programmed and will adapt itself regarding its sensor inputs. Where the AUV is autonomous, the ROV is not. The ROV is connected to the main ship by cables and operated from a different location. It allows remote navigation and operation.

2.1.1 Regulation of autonomous ships

Based on the significant impact of autonomous ships and the role they play to a more competitive and sustainable shipping future, the International Maritime Organisation (IMO) has decided to look at the regulation for autonomous ships. This is of great importance because it means that the IMO is striving forward by giving autonomous ships a chance to be implemented in large overseas cargo transport in the long run. The IMO has made a strategic plan to integrate new and advancing technologies in the regulatory framework. It involves balancing the benefits from the advancing technologies against safety and security concerns, as well as the impact on the environment and international trade facilitations. They also focus on the personnel on board and ashore. [3]

Primarily they agreed to include the issue of marine autonomous surface ships. This is done by a scoping exercise with the goal to determine the safety, security, and the environmental impact. To continue introducing the Maritime Autonomous Surface Ships (MASS) to the IMO instruments, they want to take a proactive and leading role, considering the commercially operated ship regarding the rapid technological advancements. The experiment is expected to put certain points in perspective including the human factor, safety, security, liability and compensation for damage, interactions with ports facilities, pilotage, responses to incidents and protection of the marine environment. [3]

2.1.2 Autonomous ships in operation

In some sea areas there are running trials using autonomous and remote-controlled ships. The use of autonomous ships in the near future is focussed on short voyages, for instance the port-to-port transport. This is rather recent, in June 2019 the Interim guidelines for Maritime Autonomous Surface Ships (MASS) trials were approved. The main points of these guidelines are the safekeeping of safety, security, and protection of the environment with at least the same degree provided by relevant instruments. Also measures to reduce risks to as low as reasonably practical and acceptable are put in place. [3]

Special methodology and framework are put in place to assure these concerns. Regarding the degrees of autonomy identified for the purpose of the scoping, a ranking from one to four is put in place. From ships with crew supported by automated processes, which is supervised by the crew. To degree four, where the operating systems make decisions completely autonomous and carry out actions by itself. Specific instances of the Maritime Safety Committee (MSC) focus on safety and maritime security (SOLAS), collision regulations (COLREG), loading and stability (Load Lines), training of seafarers and fishers (STCW, STCW-F), search and rescue (SAR), tonnage measurement (Tonnage Convention), Safe Containers (CSC) and special trade passenger ship instruments (SPACE STP, STP). [3]

2.1.3 Autonomous ships: The next step

“Autonomous shipping is the future of the maritime industry. As disruptive as the smartphone, the smart ship will revolutionise the landscape of ship design and operations”. A study conducted by Rolls-Royce is working on a project called the Advanced Autonomous Waterborne Applications Initiative (AAWA). It started in 2017 to set sail in 2020. It concerns an autonomous cargo vessel which is driven from the shore. The AAWA project joins all sides of the maritime industry to address all factors needed to make autonomous ships a reality. Parties resembling universities, ship designers, classification bureaus, economical researchers, social, legal, and technological, remote, and autonomous operation. Their research conducts how to keep ships as safe as existing ships, what risk they face and how they can be mitigated. Incentive for owners and investors in autonomous vessels are looked for. Legal and liabilities in case of an accident are examined. They examine what technology is needed and how it can be linked with autonomous operation. This research will result in the form of a proof of concept. It will inform the specification and preliminary designs. Their aim by 2020 is to achieve their first step, which is reducing crew by remote support and operation of functions integration. The second step is to have a remote-controlled unmanned vessel by 2025. The third step is to have a remote-controlled unmanned ocean-going ship by 2030. Finally, the fourth step is to have a fully autonomous unmanned ocean-going ship by 2035. [4]

2.1.4 Technology

2.1.4.1 Sensor combining

The technology they are developing to make autonomous shipping work is mostly concerned with sensing the world around the ship. It also includes monitoring its own health and communications with nearby objects or vessels to make decisions based on the acquired information. Sensing technology is already well developed and can be found in many autonomous vehicles. The AAWA project explored this field by implementing different sensor technologies to get an accurate picture on the vessel's surroundings in any situation, at all times. This allows safe navigation and avoids collisions. They deep dived into different radar types, high-definition camera equipment, thermal imaging, and LIDAR technology. Finding the best way to combine multiple sensor inputs regarding quality and cost efficiency considering the difficult marine environment. This sensor fusing resulted in a series of sea trials. [5]

2.1.4.2 Algorithms

The method used for collision avoidance is based on control algorithms. This is particularly important for autonomous ships because the aim is not needing a shipper on board and being fully autonomous. The algorithm receives sensor data, and the decision on the next action is handled by the algorithm. Algorithms like these will need adaptations regarding evolving maritime rules and regulations. This leads to challenges for the programmers on the subject of interpretation. The key to develop successful algorithms is to iterate and perform extensive testing to optimise the code. [5]

2.1.4.3 Communications

To communicate between the shore and the crew on board, human communication will still be needed. Therefore accurate, bidirectional, scalable, and multiple system supported connectivity is crucial. As in existing ships, redundancy is put in place to reduce risk. Sufficient capacity has to be ensured at all times. The project will combine existing communication technologies such as satellite connection and land-based systems, allowing complete monitoring of the behaviour of the ship at a chosen location. [5]

2.1.5 Safety

As mentioned before safety and security regarding working with autonomous ships are a top priority. In perspective of the crew, nearby persons, the environment and structures, the ship has to be at least as safe as existing vessels. Autonomous ships have the ability to reduce risk regarding human made mistakes. There is also the possibility to reduce the total amount of people working on board. At the same time autonomous ships induce new risks. They will have to be uncovered looking at the circumstances of the involved risks. The marine industry has comprehensive risk assessments but are not yet up to speed with the newly evolving technologies and its hazards. Comprehending these new factors and calculating them into renewed risk assessments are required to build a safe environment for autonomous ships. Cybersecurity will be critical to have safe remote operations, without risk of hacking and losing ships to cyber pirates. The project is adapting best practices already used by various marine environments. This will result in making recommendations to the regulators and classification bureaus for a first set of standards for autonomous vessel management. [5]

2.1.6 Legal aspect

Current ships are bound by a great range of legalities. This will be no different for autonomous vessels. For the moment, the maritime law does not cover any legal development regarding autonomous and remote-controlled ships. When autonomous ships become a reality, the legal aspects will have to be in order at regulatory levels. This concerns the operating and constructing of such vessels. Appropriate rule changes by the IMO are already in the making as described in the previous part but these will have to be made concrete. Liability for autonomous vessels is subjected to national differences, what is to be explored is how product liability would affect current maritime rules. In regard to the insurance of the goods and vessels. Researching this extent of the law and supplementing the law is to be addressed. The AAWA team is proposing solutions to its end but in the end, national and international decisions will have to be made by the governments. [5]

2.1.7 Economical

Autonomous vessels have the capability to reinvent the shipping industry and the role of the companies operating in it. They have an effect on ship builders, cargo transport companies, technology companies and so on. The benefits in this sector are the cost reduction regarding more efficient ship design, less crew and thus accommodation space needed, more efficient use of the crew and their skills and better use of fuel. The shipping will also benefit indirectly of the optimised processes and operations as a result of real time data analysis. The factor of human mistakes will be reduced and support safety and service quality. The AAWA team sees that these benefits are giving a long-term advantage in the shipping sector. Research will be conducted to find assignments where an autonomous ship will pay off exceptionally. By implementing autonomous ships, the resources and management will be impacted, also the way businesses operate. Also, global logistics will see benefits by integrating an adaptable fleet in the best possible way. [5]

2.1.8 Benefits of Autonomous shipping

Complementing the previous paragraph, there are many advantages and benefits in relation to the use of autonomous and remote-controlled vessels. Reducing the necessary crew or completely eliminating them during voyage would greatly reduce the salary cost. Also provisions and accommodation that have to be in place to accommodate these people will decrease significantly. This is more important for smaller vessels where usable space is scarce and costs of the crew make up a bigger share of the total cost.

The automation of ships will increase safety by elimination of human error. Better space management and ship layout. Fuel efficiency will increase. By redesigning the ship layout, certain components can be placed in a manner that they are more efficient or cost effective. For example, shorter cables or pipe systems reducing drag or other new ways of improvement. Risk of traditional piracy will decrease when using an autonomous ship. They are the next generation of ships with no staff members on board, being controlled from ashore and monitored by engineers. Using innovative technology for navigation such as high-definition cameras, radar, and LIDAR, as well as improved satellite communication.

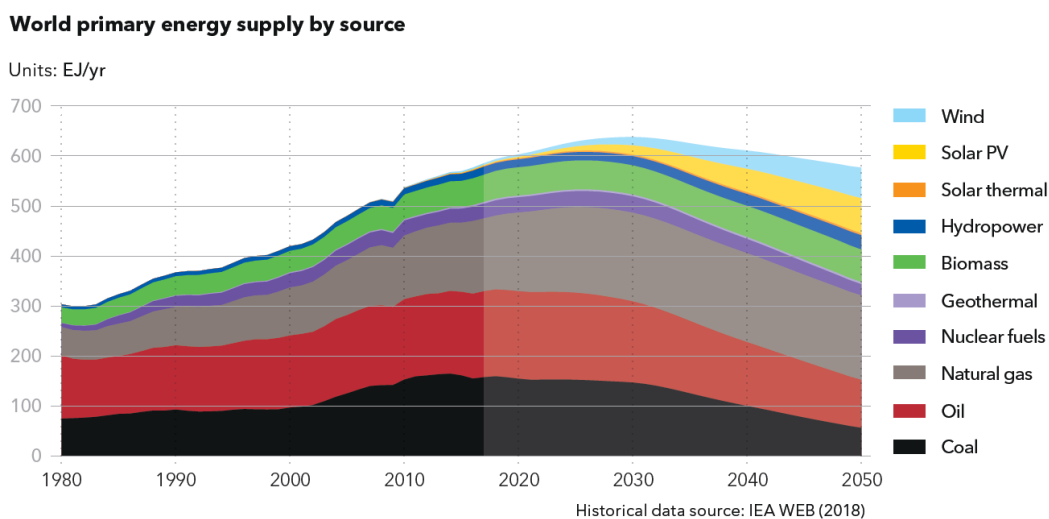
Autonomous ships will revolutionise the shipping industry focussing on vessel and supply chain efficiency. Changing the way businesses operate.

2.2 Future predictions

Since the world is in a fast-moving pace considering energy usage, some comments will be made about the future of energy production and usage. This covers a time period to 2050 and is a forecast of the global transition including 10 world regions. In the next three decades the world will go through tremendous shifts in the energy system. The focus will be held on the relevant matter to this project namely renewable energy and the maritime industry. This will summarise certain parts of the energy transition outlook 2019 executive summary by DNV GL.

2.2.1 Highlights

Highlights of this report are the feasibility of the 1.5°C COP target agreed upon under the Paris Agreement, which technology can deliver but only with strong enforced policies. A rapid energy transition is forecasted within a timespan of a generation. The share of the demand in electricity will double from today's level. 50% Of passenger vehicles will be electrically driven by 2032. Oil will gradually decrease after 2030 but gas will continue to grow and eventually level out. Renewables will take a more prominent share in the energy distribution. The forecasted transition will not be fast enough, emissions will only peak by 2025 and will not fall enough therefore it will be difficult to keep global warming below 2°C. Energy usage peaks in 2030, this will be a turning point as energy efficiency will outperform the economic expansion. The biggest contributor will be the electrification power by renewables. [6]



We are approaching a future where the world will need less energy, even as the global population increases and the economy continues to grow. Large energy efficiency improvements in all sectors and accelerated electrification see primary energy supply peaking at 638 EJ in 2030. The fossil fuel share of the energy mix will decline from 81% today to 56% by 2050.

Figure 1: World primary energy supply by source [6]

2.2.2 Electricity

Current energy demand consists of only 19% electricity, by 2050 this will more than double to 40% and 49PWh. A two times multiplication looks remarkable, there is also a notable shift in the generation of this power. Forecasted by the mid century, 63% of the electric energy will be wind or solar powered.

Coupled to significant energy efficiency gains. As a point of view, over the last 30 years there has already been a doubling in the energy share. However, in that time mostly fossil fuelled power plants were used where an efficiency increase is seen from 28% to 34%. The energy loss in power plants by wasting heat, as well as in the distribution lines, increased considerably. By using renewable energy, a significant drop in heat loss can be expected.

A large share in renewable energy will require a more flexible system, current 650 GWh storage will expand to 31TWh with the focus on batteries. Power grid expansion and power to gas will create extra flexibility as well as the conventional generation technology will remain to be important. Another factor is the reduced prices for wind and solar energy when these sources contend among themselves. This can be observed by modelling of the market at hourly intervals. The main sources for demand will rise from 0,3 PWh in 2017 to 9,1 PWh in 2050. Investments in the power grid will be made to connect the renewable power sources. [6]

World electricity generation by power station type

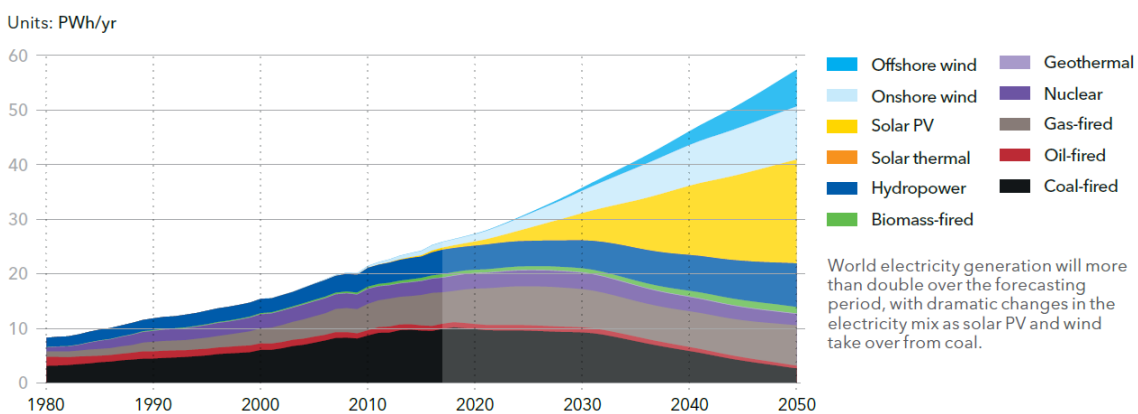


Figure 2: World electricity generation by power station type [6]

2.2.3 Energy efficiency

For the forecasted time, energy efficiency is a crucial part. For the last 20 years energy intensity, as units of energy per unit of gross domestic product (GDP), has decreased by 1.6% per year. In the next three decades energy intensity will improve to 2.5% annually worldwide, with the strongest improvement in the year 2030. At that point, the global energy use will peak. The main driver intensity improvement is the rising renewable stake in electric energy reducing immense heat losses.

Efficiency derives from how energy is supplied but also from how it is used. On the consumer side, the greatest improvement is related to road transport, with the side effect of introducing electric vehicles. As indicated in Table 1: Energy efficiency improvements by sector [6], there are sectors with many other efficiencies such as the replacement with electricity of biomass and oil for heat and cooking as examples. The analysis shows that solid progress will be made to emphasise the need to enhance the rate of improvement in energy efficiency. Without efficiency improvements, the final energy demand by 2050 would be 70% higher than forecasted. [6]

Energy efficiency improvements by sector

Sector	Sub-sector	Sectoral output		Energy used		Improvement per year
		2017	2050	2017	2050	(2017-2050) CAGR
Transport 	Road	28T km	60T km	90 EJ	84 EJ	2.5%
	Aviation	4G pass-trips	11G pass-trips	13 EJ	18 EJ	2.0%
	Maritime	57T tonne-miles	81T tonne-miles	11 EJ	9 EJ	1.7%
Buildings	Average all sectors	6.2 EJ	12.2 EJ	121 EJ	144 EJ	1.5%
Manufacturing 	Base materials	32G tonnes	46G tonnes	74 EJ	62 EJ	1.7%
	Manufactured goods	14G tonnes	27G tonnes	52 EJ	74 EJ	0.9%

Sectoral energy efficiency improvements will be significant in all sectors, but highest in road transport with the dual effect of the steadily improving efficiency of combustion vehicles and the introduction of highly efficient EVs.

Table 1: Energy efficiency improvements by sector [6]

2.2.4 Renewables on the rise

The main incentive for the fast-rising solar power usage is the decreasing cost, determined to drop more than 60% of the current amount by 2050. In comparison with nuclear power, hydropower and wind energy, solar installations induce less disapproval from preservationists. The installed capacity is presumed to be 12 TW by 2050, producing 33% of the world's electricity demand. Due to its variability, solar combined with battery storage will become notably cheap and efficient with increased connectivity and demand side response. On the other hand, solar will obtain the lowest market price of technologies as result of its variability. Combined with storage cost explains why gas will hold a sizable share of power generation until 2040. China will hold 40% of the global solar installations by 2050. [6]

Forecasting wind electricity generation to increase from 1.1 PWh per year in 2017 to 17 PWh in 2050. Therefore producing 29% of the world electricity. The largest part is produced by China, North America, and Europe. Onshore wind will see a more prudent support in developed regions while offshore will receive a more strengthened backing from countries with less available land. Therefore, the offshore share in the global electricity generation will gradually rise from 4.5% to 40% by the end of 2050, having 1.5TW installed power. Capacities will continue to rise with 21% as well as base and tower size with 34% by 2050, totalling a combined power of 3.4 TW. Offshore capacity is already 29% because of the more favourable wind conditions and is also presumed to rise to 51% by mid century. [6]

World electricity generation from solar and wind

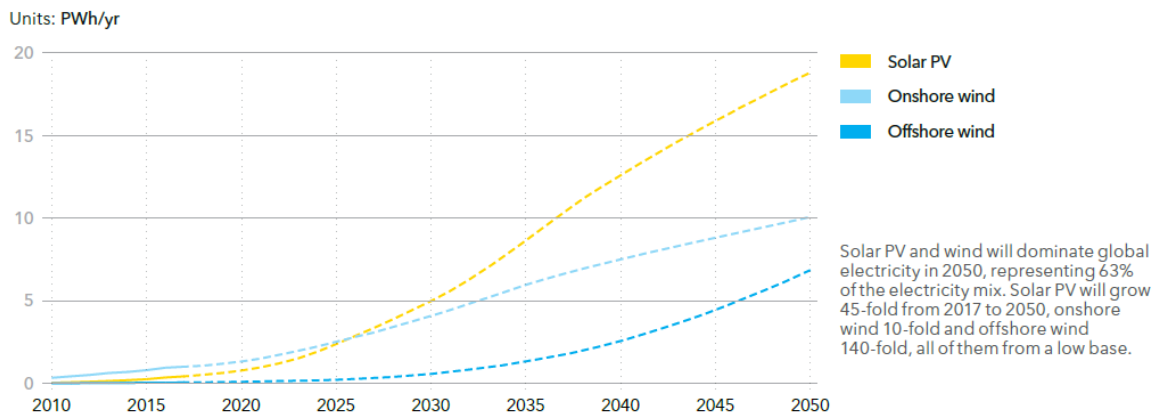


Figure 3: World electricity generation from solar and wind [6]

2.2.5 Technology

As a result of years of academic and applied studies, powered by developing energy markets, solar technology still manages to surprise many. Materials, supply chains and technology constantly innovate all to the benefit of the evolution of solar energy possibilities. Breakthroughs have resulted in 18% core technology cost learning rate. Continuing this rate would result in a global capacity 30 times as big as present by 2050, reaching close to 12000 GW. By 2050 cost will drop nearly 60% of recent levels. Large scale installations will become ruling with high efficiency technologies grow into a widespread knowledge therefore continuing cost reduction. Additional advancements and incorporation of digital technologies will globally boost capacity factors by almost 50% by 2050. [6]

The energy transition is becoming more and more urgent, previously being an important step to now being a source of great and pressing risk but also an opportunity. Current technology can deliver the 1.5°C global warming ambition set in the Paris agreement for the future we desire. The critical question is how and when this technology will be applied, as well as the strengths of the decarbonization policies. [6]

2.2.6 Transport

28% Of the global energy demand is due to transport, road transport taking account for an 80% share of this number. A rising energy demand can be seen until 2030 because of the improvements in energy efficiency. In 2017 116EJ was demanded by the transport sector, by 2050 this will reduce slightly to 112EJ. Regardless of this minor decrease, transport is one of the big contributors of the energy transition as fossil fuel makes its way for electrification. [6]

World final energy demand by carrier

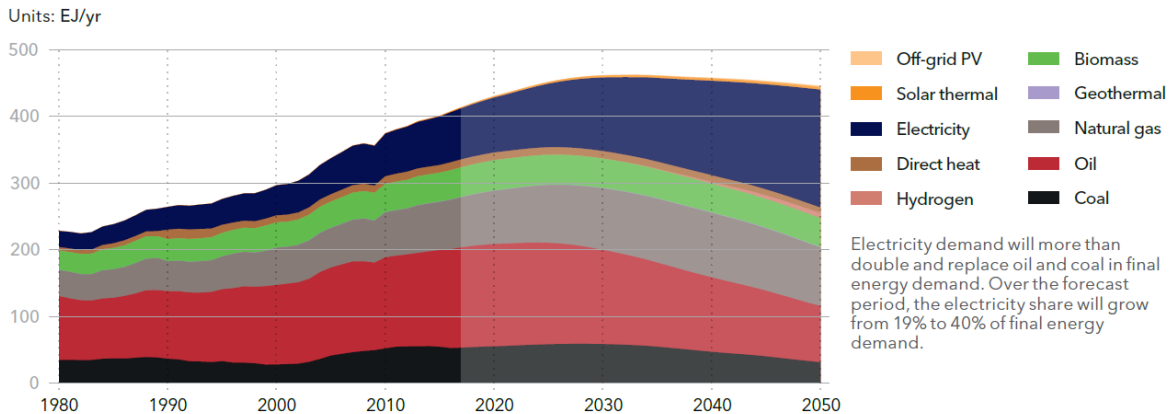


Figure 4: World final energy demand by carrier [6]

2.2.7 Maritime

Consuming nearly 2% of the world’s energy, it can be said that the shipping industry is a big player. In addition, the shipping industry is the most energy efficient method of transport by energy/tonne-kilometre. By rising demand in overseas shipping, an increase in global fleet size is expected towards 2030 to then back down, as oil and coal demands will start to decline. Gas, container, and bulk trades will continue to grow. Stricter limits on sulphur emissions are already ongoing by demand of the international maritime organisation (IMO). This change is supported by the shipowners and governments, and they have a target of 50% CO₂ emission from 2008 to 2050 as well. This will be crucial for shipping policies for the coming decades. The forecast is that there will be a shift in asset use and an energy efficiency increase. A substantial shift from conventional fuel to low and zero carbon fuels (such as LNG, PNG, electricity, ammonia, and biofuel use) allows for this goal to be reached. At last, a vital challenge for the maritime sector is that they cannot easily electrify. [6]

Maritime energy demand and projected fuel mix

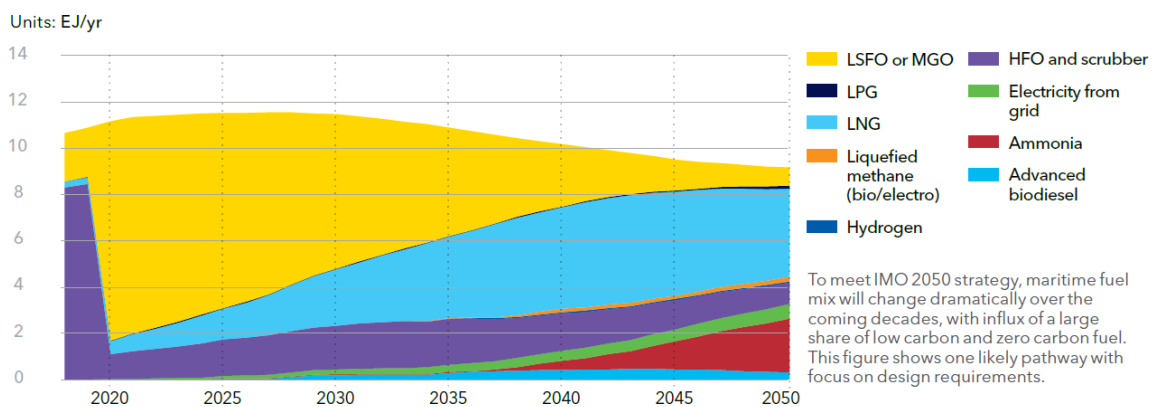


Figure 5: Maritime energy demand and projected fuel mix [6]

2.2.8 Hydrogen

By focusing on hydrogen as a zero-emission energy source, there are two major routes forecasted. One is steam methane reforming (SMR), the other is electrolysis. By the mid 2030 a global growth in hydrogen use will be provided by SMR. Thereafter, high shares of variable renewables will introduce periods of cheap electricity thereby allowing affordable hydrogen generation by electrolysis. Decarbonation through hydrogen will be expensive, also caused by conversion losses. Therefore, no hydrogen uptake in the passenger segment is forecasted. Although a limited uptake in a heavy transport sector in countries such as China, where decarbonization policies will be strong. Likewise, the reuse of refurbished gas pipelines will reduce cost and will make hydrogen for heating use competitive. [6]

For transportation, the overarching technical challenge for hydrogen storage is how to store the amount of hydrogen required for a conventional driving range (>300 miles) within the vehicular constraints of weight, volume, efficiency, safety, and cost. Durability over the performance lifetime of these systems must also be verified and validated. Acceptable refuelling times must be achieved. Requirements for off-board bulk storage are generally less restrictive than on-board requirements; for example, there may be no or less-restrictive weight requirements, but there may be volume or "footprint" requirements. The key challenges include:

- **Weight and Volume.** The weight and volume of hydrogen storage systems are presently too high, resulting in inadequate vehicle range compared to conventional petroleum fuelled vehicles. Materials and components are needed that allow compact, lightweight, hydrogen storage systems while enabling a mile range greater than 300 miles in all light-duty vehicle platforms.
- **Efficiency.** Energy efficiency is a challenge for all hydrogen storage approaches. The energy required to get hydrogen in and out is an issue for reversible solid-state materials. Life-cycle energy efficiency is a challenge for chemical hydride storage in which the by-product is regenerated off-board. In addition, the energy associated with compression and liquefaction must be considered for compressed and liquid hydrogen technologies.
- **Durability.** Durability of hydrogen storage systems is inadequate. Materials and components are needed that allow hydrogen storage systems with a lifetime of 1500 cycles.
- **Refuelling Time.** Refuelling times are too long. There is a need to develop hydrogen storage systems with refuelling times of less than three minutes over the lifetime of the system.
- **Cost.** The cost of on-board hydrogen storage systems is too high, particularly in comparison with conventional storage systems for petroleum fuels. Low-cost materials and components for hydrogen storage systems are needed, as well as low-cost, high-volume manufacturing methods.
- **Codes and Standards.** Applicable codes and standards for hydrogen storage systems and interface technologies, which will facilitate implementation/commercialization and ensure safety and public acceptance, have not been established. Standardized hardware and operating procedures, and applicable codes and standards, are required.
- **Life-Cycle and Efficiency Analyses.** There is a lack of analyses of the full life-cycle cost and efficiency for hydrogen storage systems.

A detailed list of the barriers to hydrogen storage as well as the technical targets to meet these challenges and guide the development of hydrogen storage technologies are presented in the Hydrogen Storage section of the Fuel Cell Technologies Office Multi-Year Research, Development, and Demonstration Plan. [7]

2.3 Solar energy

2.3.1 Introduction

Solar power is already a very well known and popular technology used in many applications to power them. Solar cells can be found in power banks, in street signs, on roofs of a building to supply power for the needs of the residents. As long as there is enough light these devices are a great source for electricity. Solar panels are made from individual cells stacked together. These cells are made from semiconductors. The semiconductors are silicon which has been produced from pure crystalline form. The film of silicon absorbs photons from the sun's radiation and releases them as electrons. This triggers a current to flow when a load is added to the solar cell. [8] Solar cells were discovered by a French physicist named Edmund Becquerel. He observed the photovoltaic effect by the use of an electrode in a conductive solution subjected to light [9]

Solar panels do not have moving parts and the biggest cost of keeping them operational comes from cleaning the panels to allow them to receive light. Therefore, solar panels are very useful to be used over extended time periods in an outdoor environment to harvest energy. In Addition, solar panels have been made lighter and more efficient over time.

Using solar panels in combination with fuel cells as a way to power an autonomous ship is an excellent choice because the power and charging system has to be independent. Using a wired system would prove inconvenient as the ship has to be anchored and connected to a dock as well as the high cost of installation required. The efficiency of energy conversion has to be as high as possible since deck space on a ship is limited. By using solar energy, the powering of the ship can only happen during the day, an electric motor can be directly powered from the solar panel. Meanwhile hydrogen can be created and stored for when there is insufficient solar radiation to power the solar panel. Hydrogen can then be supplied to the fuel cell to generate electricity and power the electric motor once again. Therefore, being completely self sufficient, off grid and autonomous.

2.3.2 Characteristics

Photovoltaic cells are one of the most important modern energy producers because of the current improvements in conversion efficiencies and lowering of the cost of solar panel production. A single solar cell produces around 0.5V [10] this means it is not able to power most devices independently. Therefore, these cells are connected in series to produce a workable voltage. For example, the solar panel which will be used has a voltage of 12V and as an array of individual cells connected in series. If a higher current is required, the cells can be connected in series. To protect the cell from the environment a glass layer is added on top of the semiconductor wafers, this allows light to pass through and adds durability. The power of a solar panel is measured in watts, for bigger arrays kilowatts is used.

2.3.3 Materials

The most developed commercial materials will be shortly discussed as well as their differences and efficiencies.

2.3.3.1 Amorphous silicon

In the solar power industry, a widely used type of solar panel is the amorphous silicon (A-Si) type. This is the non crystalline form of silicon. It is used as the semiconductor material for the solar cells. The silicon is deposited in thin layers on a surface which is most of the time glass, metal, or plastic. Amorphous solar cells commonly have a lower efficiency of around 6-7% [11] compared to the mono- and polycrystalline configurations. Apart from this, amorphous are more environmentally friendly because they do not use materials like cadmium or lead. A-Si panels are also cheaper, they save on material cost because amorphous silicon can be laid down thinner than crystalline silicon [12].

2.3.3.2 Crystalline silicon

The more popular than the amorphous silicon type solar panels are the crystalline silicon type panels. There are two different variations namely mono- and poly crystalline. [13] The difference is in the way the structural orientation. Monocrystalline has an homogenous structure and is constant throughout the material. While polycrystalline consists of silicon grains with varying crystallographic orientation. As far as efficiency is concerned, commercial crystalline silicon modules have an efficiency up to 16 percent. Lab cell record efficiency is 25.6% for mono silicon cells and 20.4% for poly silicon cells. [14] Monocrystalline and polycrystalline silicon type solar cells are the most used due to their high efficiency with a current market share of 90% [15]

2.3.4 Impact of radiation and temperature

The energy output of a solar panel is affected by several parameters such as tilt angle, panel contamination, shade, temperature, and radiation. However, temperature and radiation are the most prominent. Radiation is the emission and transmission of energy which lays closely to the parameter irradiance. Irradiance is the power received by a surface per unit area and is expressed in W/m^2 this reflects the process by which an object is exposed to radiation [16]. This parameter has a lot in common with the UV index, which is used to describe the strength of the sun's UV radiation. The scaling system ranges from 0-11 corresponding to a level ranging from low to extreme. It is also colour coded from green to purple. But both parameters, irradiance and UV index can not be compared directly because UV radiation is linked to the wavelength being more- or not damaging to human skin. A weighted curve is used for conversions. [17]

The sun's radiation level and UV index progress in a similar way which is relevant for this topic and are highly affected by the location on the earth, time of day and the month of the year. Looking at the more accessible UV index curves the radiation level can be estimated and, in a glance, it can be forecasted whether the irradiance will be high or not. If the solar radiation level is high, the solar cells will have a higher output power. Oppositely, if the ambient temperature rises a negative effect on the output power of the solar cells can be observed. [18]

Therefore, in the practical part the irradiation will have to be determined to dimension the solar system and calculate the efficiency because it is related to the input power of the solar panel.

2.3.5 Implementation and upcoming tests

The solar panel will be placed flat on the deck of the ship, where solar radiation can be collected most efficiently disregarding the heading of the ship. The cells will be connected to the motor and electrolysers, the practical tests will prove the most optimum configuration of the circuit. For dimensioning the system, it is required to construct the power- and iv-curve. The fill factor and efficiency of the solar panel will be calculated. This information can then be used to dimension the system to get the optimal performance working together with the fuel cell. These experiments will be discussed in the practical part.

2.4 Hydrogen energy

2.4.1 Introduction

Hydrogen is a great step in the direction of a less polluted world. Designing an autonomous catamaran with the use of hydrogen will allow for a carbon free propulsion. The storage of energy is a vital part of the design of the autonomous solar catamaran but proves to be difficult and is dependent on scale.

In this part the use of hydrogen will be discussed with the challenges including storage, hydrogen generation and hydrogen powered technologies. Advantages and disadvantages will be addressed, and a thought-out choice will be made to fit the needs of the boat with respect to the scale of the project. Doing so will ensure a solution that's energy efficient and practically executable.

2.4.2 Characteristics

Hydrogen (H_2) can be found everywhere on earth but is rarely found alone, therefore it is made by breaking it down from a compound. The most common compound where it can be found is water or H_2O where it is combined with an oxygen atom. Hydrogen can be produced by different processes, some produce CO_2 and others have no carbon emission. Using electrolysis, there is a zero-carbon footprint. If the electricity used to produce hydrogen is renewable, then this hydrogen is also renewable. The low polluting fuel has many uses such as transport, heating, and power generation in situations where electricity is no option. Hydrogen has a high energy density making it suitable for long-term storage. It can be transported over long distances allowing distribution of energy between countries. [19]

Hydrogen has the greatest energy content of any conventional fuel by mass but has the lowest energy content by volume. When hydrogen is produced in its molecular form, the energy which is available in the molecule can be released by reacting with oxygen to produce water. This can be done with an internal combustion engine or with fuel cells. [19]

The most common way of producing hydrogen is to create it from natural gas, with a share of 70%, followed by oil and electricity. This is done by a process called steam reforming. Smaller amounts of hydrogen have been made using renewable energy, though this is determined to increase in the future. Electrolysis only accounts for 5% of the world's production. Electrolysis uses an electric current and splits the water into oxygen and hydrogen allowing the gasses to be individually extracted. If the electricity used is carbon free or renewable than the gasses produced have a zero-carbon footprint, this is called green hydrogen. Because hydrogen is created by extracting it from a compound of other primary sources, it is an energy carrier which is used to store, transport, and deliver energy produced from these sources. [19]

In addition, hydrogen is a small molecule which can escape through pores and small openings more easily than other gasses and liquids such as fuels. Natural gas has an energy density which is three times the energy density of hydrogen, this means in case of a leak the natural gas releases three times more energy than a hydrogen leak. If a hydrogen leak takes place, hydrogen disseminates much quicker than other fuels. It is more light and more diffusive than gasoline, propane, and natural gas. If hydrogen is ignited, the explosive energy released per unit of stored fuel is the lowest. [20]

2.4.3 Storage

Batteries do not hold large amounts of electricity over time very well. Hydrogen, unlike electricity, can be stored in large quantities for extended periods of time. Therefore, producing hydrogen on an industrial scale is an important step in the energy transition phase. Nevertheless, hydrogen can be a great addition to batteries in the transport sector. With hydrogen providing the largest part of the energy and batteries being used for regenerative braking and cover peak power or act as a buffer to extend its lifetime expectancy. This arrangement is now at work in Honda's hydrogen car. [21]

Energy storage can play an important role in improving system integration. Short term storage is great for batteries and small energy demands for plants. However, for larger amounts of hydrogen and long-term storage, a new type of storage is needed. More particularly chemical storage in the form of hydrogen. [21]

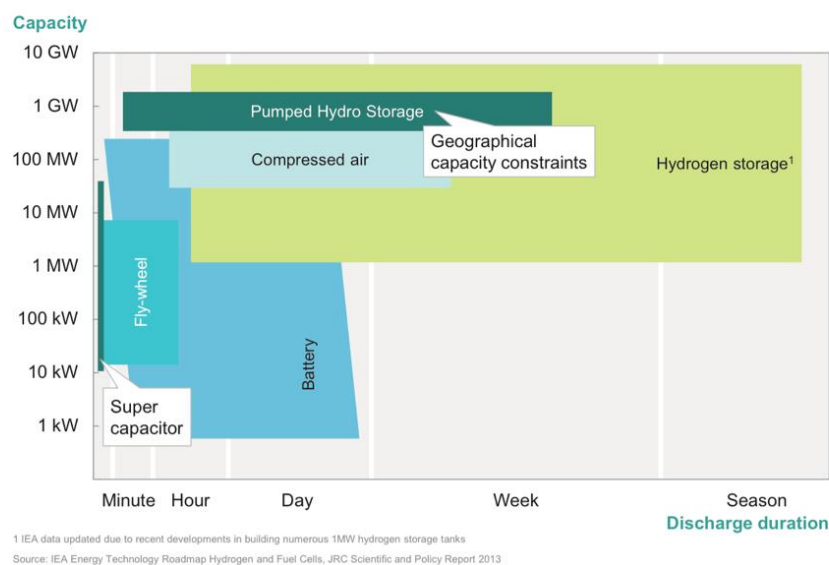


Figure 6: Energy storage in relation to time [21]

The substitution of marine fuels with renewable energy (sailing apart), mainly wind turbines and photovoltaic modules, leads to significant reduction of polluting emissions. In this framework, the coupling between hydrogen storage systems and electrical batteries is the most suitable solution in stand-alone power generation plants, which may lead to autonomous systems following load demand and ensuring both long (batteries) and short-term (hydrogen) energy storage.

Hydrogen can be produced from electricity with incorporation of renewables. When there is a subsequent energy demand, hydrogen can deliver directly. On the other hand, it can also be stored in large tanks as pressurised gas and reclaimed when there is a shortage. Hydrogen has the highest energy density as an energy carrier based on mass. The density is almost three times higher than liquid hydrocarbons, although the volumetric energy density is comparably rather low. Hence, for handling the material it is needed to substantially increase the density of hydrogen. [21]

Most essential approaches of storing hydrogen involve physical storage based on compressing hydrogen, or cooling, or a combination of both, which is called hybrid storage. In addition, many more methods are being developed to find new suitable ways of storing hydrogen. These methods can be categorised as material-based storage and contain solid, liquid and even surface bonding. [21]

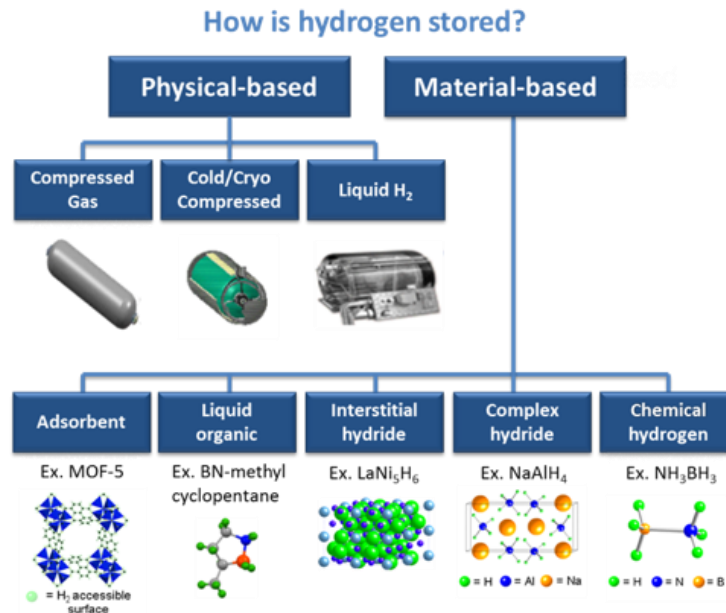


Figure 7: Hydrogen storing methods [21]

2.4.3.1 Liquid hydrogen

The first method is liquefying the hydrogen, the gas is cooled to -253°C where it condenses and turns into a fluid. This method is in demand because it ensures high levels of purity in the liquified hydrogen. In addition, in liquid form hydrogen has a higher energy density than its gaseous form. On the other hand, liquefying brings extra complexity and economical costs along. In order to contain the cold, the storage tanks need to be very well insulated to keep the evaporation under control. Evaporation can occur when exposed to heat due to conduction, radiation, or convection. Liquid hydrogen is mainly used in space exploration technology. [21]

2.4.3.2 Cold- and cryo compressed hydrogen

Combining the two compression methods, cooling, and compressing results in a further development of hydrogen storage for mobility objectives. The hydrogen is cooled first and then compressed. Working with cryogenic compressed hydrogen has the advantage of being higher in energy density in comparison with compressed hydrogen. Field stations using this technology went recently in production. The downside on the other hand is that cooling requires extra energy. [21]

It requires from 9 to 12% of the total energy available to compress hydrogen from 1 to 350 bar. On the contrary, liquefying hydrogen, which implies cooling, requires 30% energy. However, the energy input depends on the method used and quantity. Researchers are looking for more economical methods with a considerably lower energy input. [21]

2.4.3.3 Material based hydrogen storage

The other method opposed to physical storage of hydrogen is to suspend it in solids and liquids or on top of surfaces. The majority of these storage methods are still under development. Although the storage densities are not adequate yet, the time and expense of charging and discharging the hydrogen are too high. The media used for material-based storage can be divided into three groups, hydride storage systems, liquid hydrogen carriers and surface systems. [21]

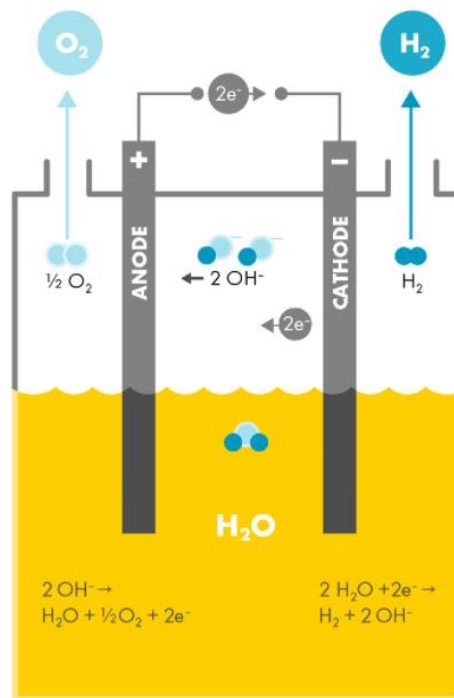
2.4.3.4 Conclusions

The many unique properties of hydrogen make it suitable for applications both stationary, portable and for transportation. Hydrogen can be stored in various ways. They can be categorised in physicals and material based. The latter one being still in development. Material based storage suspends hydrogen in solid, liquid or on surfaces. Physical storage can be categorised in compressed gas, liquid hydrogen or cold/cryo compressed gas. Each has its advantages and disadvantages. With the Liquid hydrogen method, it is necessary to cool the hydrogen -253°C . This requires adequate insulation when transported. The cryo compressed hydrogen method first cools the gas and then compresses it. This is a mixture of two methods and takes a fair percentage of the energy capacity. The ultimate goal with this technology is to power fuel cells with hydrogen which is produced from renewable energy sources and therefore having a zero-carbon pollution.

2.4.4 Electrolysers

Hydrogen can be produced using multiple different processes and from a large number of primary energy sources. Electrolysis is one of these methods and this option can produce hydrogen from renewable energy. In the process of electrolysis, electricity is used to split water into hydrogen and oxygen. The reaction takes place in a device, called an electrolyser. These units vary in sizes from small to as large as a shipping container. Electrolysers can be used for small-scale hydrogen production as well as for large-scale and central production facilities that can be directly coupled to renewable or non-greenhouse-gas emitting electricity production. [22]

Hydrogen production by use of electrolysis offers opportunities for renewable energies with variable power generation. For instance, a wind farm, the intrinsic variability of wind is a drawback to the effective use of wind power. Hydrogen fuel and power generation can be integrated in the wind farm. This creates flexibility to shift production depending on the availability of the resource. In times of excess electricity production hydrogen can be made through electrolysis instead of curtailing the electricity as is mainly done. [22]



Shell Hydrogen Study © Shell

Figure 8: Electrolysis visualisation [22]

2.4.4.1 Process

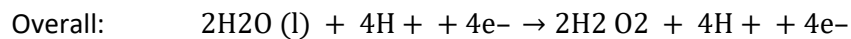
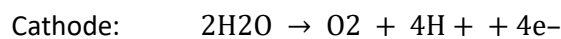
Electrolyzing water breaks it down into oxygen and hydrogen by the use of electricity. The electrolyser consists of a DC source and two noble metal plated electrodes which are separated by an electrolyte. When a high enough voltage is supplied, a current will be drawn and the process will start. Electrolysers consist of cells and can be combined to form a stack, which can be dimensioned and adapted for individual needs. Electrolysis can be differentiated by the materials they are made of as well as temperature they operate at. [22]

Low temperature electrolysis includes alkaline-, proton exchange membrane- (PEM) and anion exchange membrane or alkaline PEM electrolysis. Next there is the high temperature electrolysis, this group is most known for solid oxide electrolysis. However, this method is still being researched and has not reached a commercial level yet. The advantages are increased conversion efficiency and the possibility to produce synthesis gas from steam and CO_2 which is used for synthetic liquid fuels. The efficiency of electrolysers is dependent on the method used. The efficiency of water electrolysis is around 60-80% based on the calorific value. [22]

Electrolysers are already integrated in many operations, however research continues to be done. In order to improve operating life, power density and stack size, we need to reduce material cost and introduce fully pressurised systems. The latter eliminates the need to compress the hydrogen after it has been produced. [22]

2.4.4.2 PEM electrolyser

The polymer electrolyte membrane (PEM) based electrolyser is a commonly used electrolyser type. It uses the same type of electrolyte which is being used in the PEM based fuel cell. The electrolyte is a slim solid ion conduction membrane. The electrolysers are bipolar by design and can handle high differential pressure across the membrane. The reactions that occur are as following:



The membrane in the PEM electrolyser allows H^+ ions to transfer from the anode to the cathode side of the membrane. This separates the hydrogen from the oxygen gas. The hydrogen is produced at the anode side and oxygen is produced at the cathode. The membrane that is used in most cases, consists of a platinum catalyst which is applied to each side to efficiently split the water molecules in hydrogen and oxygen. [20]

The catalyst converts the electrical energy into chemical energy and is needed to split the water into hydrogen and oxygen. Whereas platinum is the most used for the reaction it is rather expensive. Catalysts which are cheaper and work as efficient as platinum have not been found yet. Less effective catalyst causes a greater voltage drop, which reduces the efficiency. [20]

2.4.4.3 Conclusions

Electrolysis is a popular way of producing hydrogen, this process breaks down water into hydrogen and oxygen. The hydrogen produced is of ultra pure quality and is non-polluting when produced from renewable energy. An electrolyser can be activated at any time and at any place if hydrogen is needed. Therefore, hydrogen does not necessarily have to be stored. This is a great method for hydrogen production that will be used by fuel cells. Dimensioning such a system can be cheaper than supplying pressurised gas containers. Electrolyser systems can also be made portable, allowing integration in vehicles or boats.

Electrolysis and hydrogen storage can also be a great way to add flexibility for an energy grid, by shifting energy production to best match intermittent resource availability regarding wind and solar power.

2.4.5 Fuel cells

A fuel cell is a device that generates electricity from an electrochemical reaction. An external supply of chemical energy is used and as long as the fuel cell is supplied with hydrogen and oxygen it can run indefinitely with water as a side product. Feeding the fuel cell oxygen from the air instead of pure oxygen is commonly done too. The "fuel" mentioned in the name of the fuel cell refers to the source of hydrogen even though there is no combustion taking place. Instead, electromechanical oxidation of the hydrogen takes place in a very efficient process. Hydrogen and oxygen atoms react with each other to form water. Electrons are released and if a peripheral circuit is connected, the electrons will flow through as an electrical current. [23]

Energy production values of fuel cells vary from producing only several watts to producing a number of megawatts, the size of these devices varies accordingly. The central design of a fuel cell is based on two electrodes separated by a solid or liquid electrolyte. The electrolyte carries the electrically charged particles. To speed up the reaction at the electrodes a catalyst is often used. Fuel cells are divided in several classes according to the nature of the electrolyte they are using. Each type uses different materials and fuels and is suitable for different applications. [23]

Industrially, in the field of energy, hydrogen is mostly used to power fuel cells. A fuel cell is an electrochemical device which uses hydrogen and oxygen to produce electric energy. Water and heat are the by-products. The basic form of a fuel cell consists of two electrodes with an electrolyte separating them. The hydrogen reacts with the catalyst which creates a positively charged ion and a negatively charged electron. This happens at the anode side. The proton travels through the electrolyte while the electron flows through an electric circuit in the form of a current. At the cathode side, the oxygen is reacting with the ion and the electron, to form water and heat. [23]

2.4.5.1 Proton exchange membrane fuel cell

The type of fuel cell used in this thesis is the proton exchange membrane fuel cell (PEMFC). Thereby the focus will be held on this particular one. Apart from these PEMFCs there are several other types of fuel cells which will be described briefly by the use of summarising pictures and schematics.

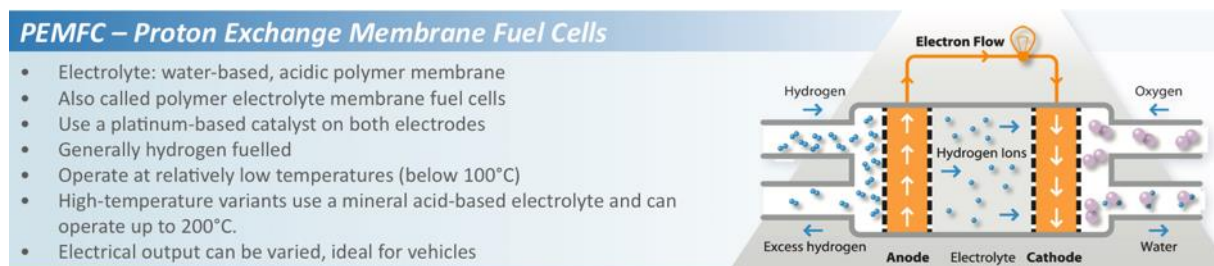


Figure 9: PEMFC visualisation [23]

The proton exchange membrane fuel cell provides high power density and has some advantages related to its low weight and volume compared to other types of fuel cells. The proton exchange membrane is a polymeric membrane which is used as the electrolyte in the fuel cell. The membrane contains a platinum catalyst. This type of fuel cell only needs hydrogen and oxygen from the air to operate. The operation does not involve corrosive fluids like some other fuel cells do. Typically, the hydrogen is supplied from storage tanks containing the pure gas. The operation temperature is usually between 20 and 80°C. Because of its density, they are a suitable choice for mobility applications and purposes that demand an initial high power. [23]

Current PEM fuel cells do not operate at high temperatures because the membrane will otherwise deteriorate too quickly. This is one of the limitations of current fuel cells. The advantage of the low operation temperature is that they reach their operating temperature quickly and are therefore rapidly operational. The inconvenience is that they need a platinum catalyst in order to operate and these are comparably expensive. The platinum catalyst is also prone to CO poisoning, therefore it is necessary to use an additional reactor in the fuel gas, resulting in reduced CO. This only needs to be done if the gas is coming from alcohol or hydrocarbon fuel. Including this step makes this type of fuel

cell more expensive. Ongoing research is trying to reduce or eliminate the use of platinum with some form of success, already the quality of the platinum used in PEM fuel cells has decreased substantially. Additionally, the platinum catalyst can be recycled. These days PEM fuel cells are a consensus choice for transport applications however they are also used in some stationary applications. [23]

Fuel cells are able to achieve power densities of over 1kW/litre, this makes them competitive with internal combustion engines. Other advantages include:

- Potential for high operating efficiency.
- Multiple fuel source possibilities and supply methods for the gas.
- The design is scalable.
- Fuel cells produce no pollutants.
- Low maintenance due to no moving parts.
- Fuel cells do not need to be recharged and provide power instantly when fuel is supplied.

Following limitations regarding fuel cells:

- Manufacturing fuel cells is costly because of the specific materials for the electrolyte and there are issues finding low-cost replacements.
- Fuel reformation technology is expensive, heavy equipment is needed as well as power in order to operate. [24]
- Performance decreases if other fuel besides hydrogen is fed into the fuel cell because of catalyst degradation and electrolyte CO poisoning.

2.4.5.2 Other common types of fuel cells

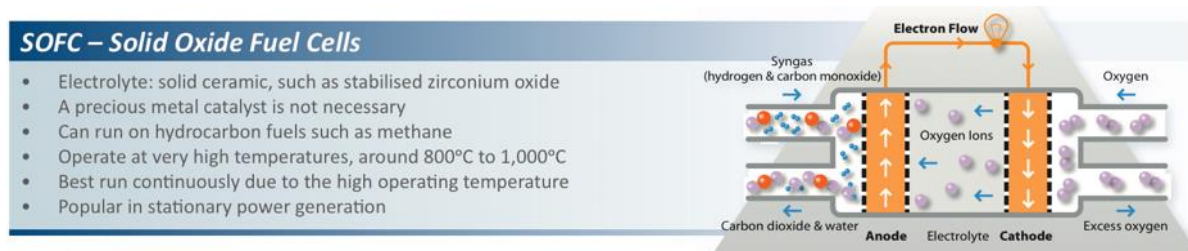


Figure 10: SOFC visualisation [23]

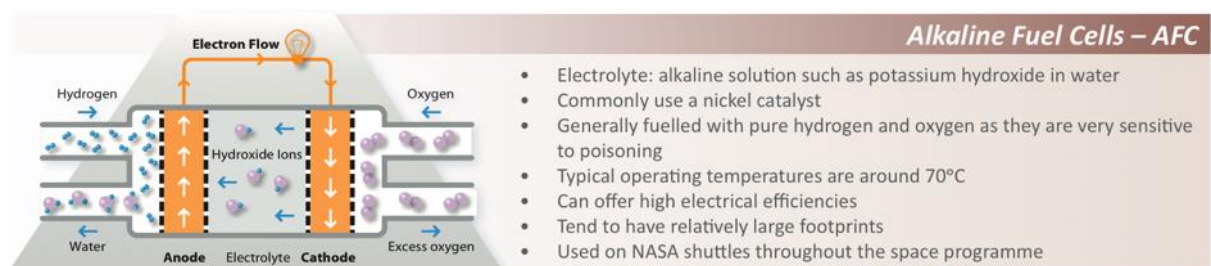


Figure 11: AFC visualisation [23]

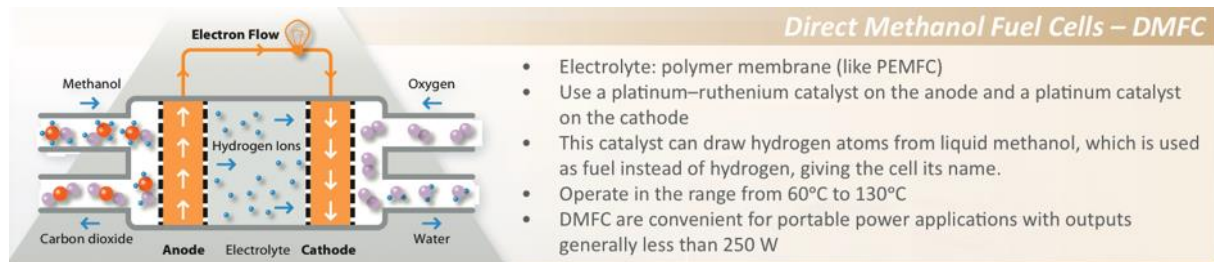


Figure 12: DMFC visualisation [23]

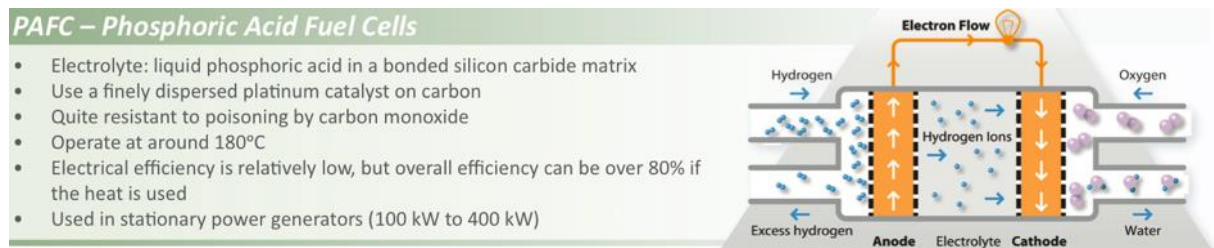


Figure 13: PAFC visualisation [23]

2.4.5.3 Polarization curves

The method of characterising fuel cells is through polarisation curves. This is a plot of the cell's voltage potential and the current density. The IV curve is the most common method for characterizing and comparing fuel cell performance. The polarisation curve displays the voltage-current relation based on operating conditions such as temperature, load, fuel rates and humidity. Below an example of a typical polarisation curve can be found and its regions of importance. [20]

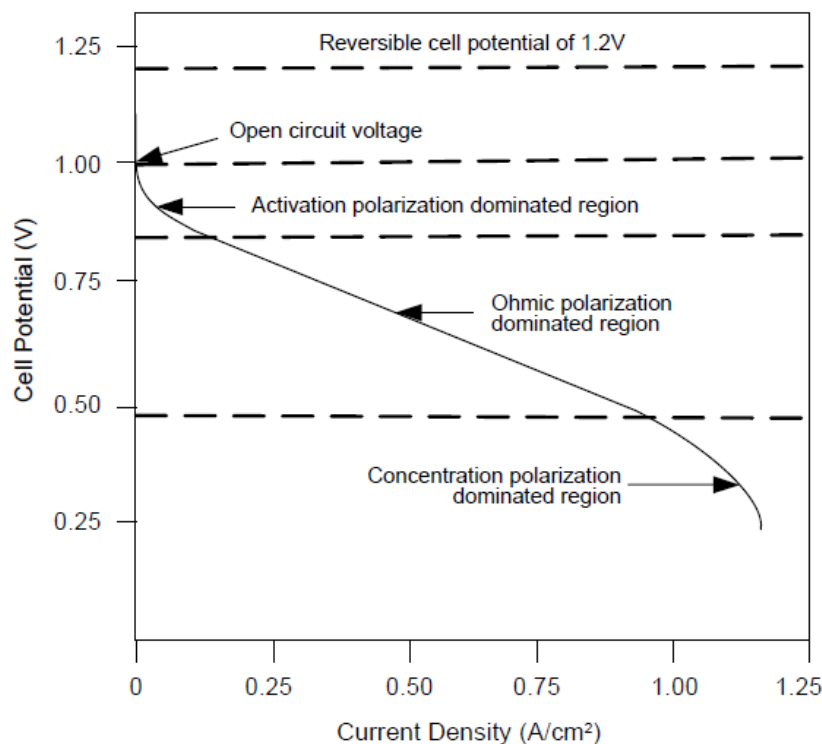


Figure 14: Polarisation curve [20]

The curve can be partitioned into three parts: the activation overpotential region, the ohmic overpotential region, and the concentration overpotential region. During the initial activation stage, a voltage drop occurs. This happens because the electrochemical reactions are slow to produce current. It is the oxygen's electrochemical reaction on the cathode which is responsible for most of the activation overpotential. When the fuel cell produces more current, the activation losses increase at a slower rate than the ohmic losses. Then, the ohmic overpotential is subjected to the resistance of the transfer of charged species in the polymer electrolyte membrane and catalyst. [20]

The concentration overpotential region is because of mass transport limitations which means that the rates of electrochemical reactions in the catalyst are impeded by the lack of reactants. The mass transport limitations are due to both diffusional limitations in the electrode backing layer and water flooding in the cathode catalyst layer. This implies that at high currents the produced water in the cathode catalyst exceeds the amount of water that can be displaced. [20]

2.4.5.4 Conclusions

This section explained how fuel cells work and how they are an indispensable part of the renewable energy market. Fuel cells are able to produce power in stationary, transportation and portable applications. The most common type of fuel cell used for transportation solutions is the polymer electrolyte membrane (PEM) fuel cell. They mostly use pure hydrogen as fuel source, but they are also capable of using other types of fuels, involving gasses derived from ethanol and biomass. Apart from the PEM fuel cells, the most important other fuel cells are: SOFCs, AFCs, DMFCs, PAFCs, MCFCs and DMFCs. Fuel cells require low maintenance, and their power density makes them competitive with internal combustion engines. On the other hand, the manufacturing process for fuel cells is expensive because of the material used for the catalyst.

2.4.6 Implementation

The implementation of a hydrogen driven system in the thesis is done in following ways: The process for producing hydrogen is electrolysis with the use of a proton exchange membrane electrolyser. This method is chosen because electrolysers are available in small form factors and can be electrically powered in a completely renewable way, in the project's case, with the use of a solar panel.

For storing the hydrogen, the compressed gas method is the most suitable, mainly because only a small volume of 10ml has to be stored. The other methods are not economical at this limited scale. The hydrogen will be stored using a latex balloon connected to the electrolyser and a series of valves which can be opened and closed if needed. The pressure using this method is low, but as seen in the results, this will be sufficient.

When it comes to using the stored hydrogen, it will be converted back into electricity by the use of a proton exchange membrane fuel cell. The PEM type fuel cell operates at a low temperature and is ideal for transportation applications because of its high energy/volume density. Therefore, the device can be small in size and still produce sufficient power.

More about the configuration and component description will be explained in the part: "Power systems integration."

3 DEVELOPMENTS AND RESULTS

- 3.1 Solar energy capture
- 3.2 Data acquisition program
- 3.3 PEM reversible fuel cell
- 3.4 Electrolyser practical experiments
- 3.5 Fuel cell practical experiments
- 3.6 Series and parallel tests combining solar panel, electrolyser, and motor
- 3.7 Additive manufacturing
- 3.8 Design of the catamaran
- 3.9 Power system integration
- 3.10 Operational performance evaluation of the design



3 Developments and results

3.1 Solar energy capture

The first part of this project is to figure out how to collect solar energy and how to analyse and study the energy collection. The energy collection will be done by a solar cell made by Xunzel. The goal is to determine current and voltage characteristics under different lighting conditions and loads. The goal is to use this solar cell as a power supply for the hydrogen generator. For analysing and acquisition of the data the software Labview and Excel are used. The code for logging the current and voltage data in Labview is written by two students who contributed to this project before me. This code will be reused resulting in a faster process of acquiring and analysing data. Nevertheless, a good understanding of the software is needed to comprehend the program and make adjustments to it.

The precise measuring device which is used for measuring the current is the Keithley 2601 source meter. A source meter is a tool to analyse source code. It can perform deep static program analysis of complex programs. The Keithley 2601 Source Meter can make precision DC, pulse, and low frequency AC source-measure tests. The precision of this device at the range used for the measurements which 100mA is 0.02% + 20 μ A. The main interest in this device is the ability to do I-V functional testing. The Keithley is connected to the computer and thus Labview via a usb-cable. Another precise measuring device used for measuring current, is the Agilent 34401A multimeter. This multimeter is also used for measuring current. Its accuracy is 0.0035%. The latter is used when the Keithley is occupied for doing simultaneous tests. [25]

In combination with the previous measuring devices there is the National Instruments DAQ 9174 Ni 9129 Card Equipment used for measuring the voltage. In the experiments the voltage meter is used in various ways to either measure over the hydrogen fuel cell, or the voltage produced by the solar panel. This device is chosen because of the compatibility with the LabView software.

3.1.1 Solar cell characterization

One of the first requirements is the characterisation of the IV curve of the solar panel. The panel is an Amorphous Silicon (a-Si) type panel. The IV curve shows the current in relation to the voltage. This graph can be made for arrays of solar panels in series or parallel or in this case the single cell characteristic. The graph gives a detailed description of the solar energy conversion capability and efficiency. It is also important for determining the output performance of this particular solar cell.

The aim of the IV curve is to summarise the key electrical characteristics of the photovoltaic cell. It projects the current and voltage. The intensity of the solar radiation or isolation which hits the solar cell, dictates the current. The negative effect is the heating up of the solar cell therefore reducing the voltage produced by the cell. The solar cell provides direct current, as known power equals voltage times current. The rated power of the Xunzel solar cell is 7W and it measures 32,5 cm long by 34 cm wide.

The IV curves of the solar cell graphically represent its operation. Summarising the affiliation between voltage and current at the circumstances which are present, related to temperature and irradiation. [8]

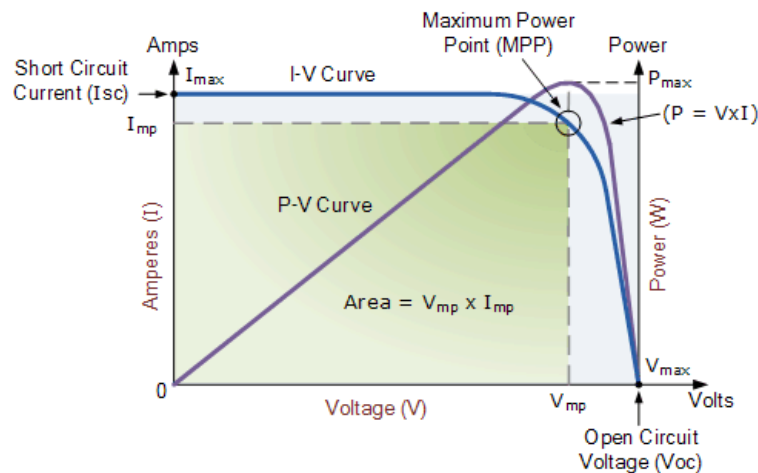


Figure 15: Solar panel IV – and PC curve [8]

The curve offers information needed to construct the system to operate as close to the maximum peak power point (MPP).

The above graph consists of the current-voltage (IV) curve and the power-voltage (PV) curve. Shown here is the typical amorphous silicon type solar panel graph, behaving in normal conditions. The first thing to notice in this graph is the IV curve. The starting point on the Y-axis is I_{max} or I_{sc} ; this is the short circuit current. This value can be measured by simply shorting the positive and negative terminals from the solar panel, without any load. The voltage is then at its minimum and the current at its maximum. By implementing an ampere meter, this can be read. The voltage can be read on the x-axis. The maximum point V_{max} here is the open circuit voltage. The value of the open circuit voltage can be measured by adding a voltage meter in parallel to the positive and negative terminals, also without any load in between. The voltage is now at its maximum and the current at its minimum point. If a variable resistor is added to the circuit, the progression of the graph can be constructed between the points I_{sc} and V_{oc} . This is how this graph is constructed.

The second curve to notice is the power-voltage graph. This curve is constructed by multiplying the current and voltage value at each point. For all values from short circuit to open circuit conditions. The power curve is given for a certain radiation level. Neither of the conditions, open circuit or short circuit gives a power output. A point on this power curve, in between the extremes, gives the maximal power produced.

There is one point where the multiplication of the current and voltage is at its maximum, this is when the maximum electrical power is produced. This point is called the “maximum power point” (MPP). Given the ideal operation point for the solar cell. The value of this point is shown in the datasheet of the solar panel, in this case it is 7W. The maximum power point is located at the bend in the IV curve. This point has its coordinates corresponding in the IV graph which are V_{mp} for Voltage maximum power and I_{mp} for current maximum power. Generally speaking, V_{mp} is roughly 0.8-0.9 times V_{oc} and I_{mp} is roughly 0.85-0.95 times I_{sc} . Depending on the temperature the solar panel operates, this point will change regarding the current and voltage, thus the actual max power output.

Having looked at the single cell characteristics of a solar panel, this can also be done for arrays of solar panels. The biggest difference is in the connection of multiple panels. The next graph shows the influence of connecting the panels in series and parallel. Depending on the desired effect, the connection method can be chosen accordingly. [8]

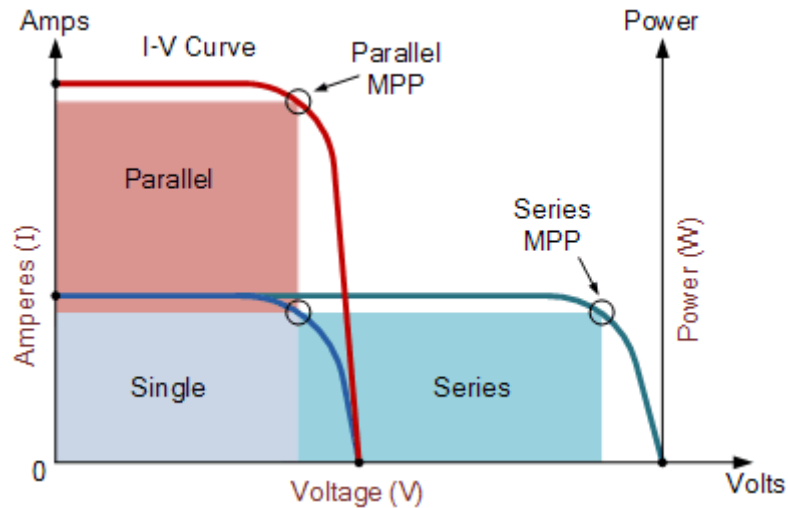


Figure 16: IV – and PC curve stacked solar cells [8]

Connecting the cells in parallel will result in a higher current output. On the other hand, if a higher voltage is required the connection would be made by putting the cells in series. The produced electrical power in watts will be the same either way because power is equal to the voltage times current.

Another important parameter concerning these solar panels is the fill factor (FF). This is the relation between the maximal deliverable power in normal operating conditions, and the open circuit voltage multiplied by the closed-circuit current. The result of this calculation gives an initiative of the quality of the solar cell. The optimal value is 1, the closer the result of the fill factor is to 1, the more power will be produced. Standard, these values lay between 0.7 and 0.8. Again. The formula which will be used to calculate the fill factor is:

$$FF = \frac{I_{max} * V_{max}}{I_{sc} * V_{oc}}$$

The efficiency of the solar cell is the ratio between the maximal deliverable electrical power and the amount of solar irradiance exerting the solar panel. This is usually rather low, between 6-7% is a normal value. This is depending on the type of cell which is being used. In this case amorphous, which is the least efficient of the series monocrystalline, polycrystalline, amorphous, and thin film amorphous. The formula which is going to be used to calculate the efficiency:

$$\eta = \frac{P_{max}}{P_{input}}$$

In conclusion these IV curves are a good way to understand the capabilities of the solar panel and its maximum available output power. Considering a given temperature and irradiation level. It represents the panel's ability to convert sunlight into electrical power. The most important numbers for the calculation are the current, voltage and maximal power. [8]

3.1.2 IV measurements

As written above, the first thing to do is to make the concrete IV curve for this particular solar cell. This is done under the conditions that all coming experiments will experience. The solar panel is placed in the laboratory in direct sunlight. One disadvantage is the presence of sun blinds which can be opened but there is a remaining shade overcasting some portions of the solar panel. This is a given that must be taken into account later.

The open circuit voltage (V_{oc}) is measured between the positive and negative terminals of the solar panel. The value equals 22.967V. Now the short circuit current is measured (I_{sc}). The value equals to 71.87mA. Furthermore, by connecting a variable resistance of 4.7K Ω it is possible to range through the IV curve and map it accordingly. The mapping is done by varying the resistance, then writing down the current and voltage numbers accordingly. The current is measured by the Keithley 2601 source meter and the voltage is measured by the Agilent 34401A multimeter. Combining these two datasets into an Excel sheet results in the following IV and PV-curve of the system.

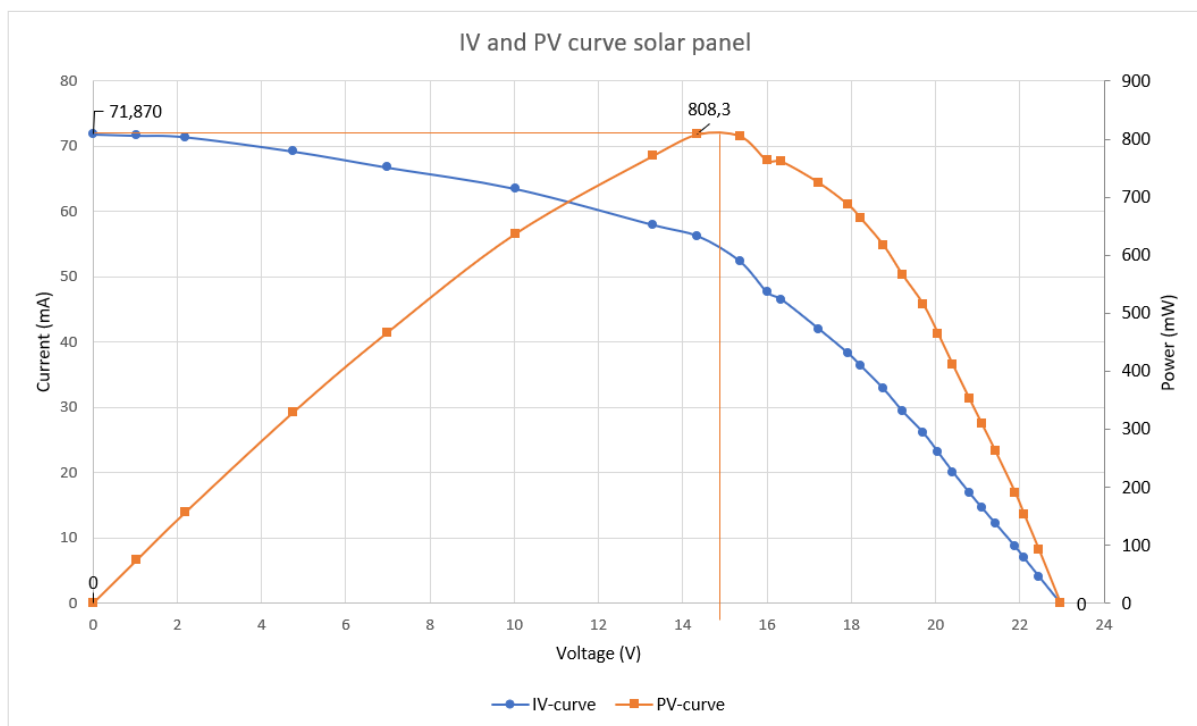


Figure 17: Power curve

Unfortunately, the weather was not ideal, and it was rather cloudy. Therefore, it was not possible to reach the maximum current stated in the datasheet or as seen in other experiments. Nevertheless, it is still possible to construct an IV-curve and a PV-curve. It can be expected to see less than optimal results because of these conditions. The blue curve in the graph represents the IV-curve. The shape of this curve is similar to the theoretical curve seen in the illustration above. As well as the PV-curve the maximum power point is positioned in the bend of the PV curve. In this case the maximum power in these cloudy conditions is 808,3mW. The max peak point is located at 15V exactly what the datasheet describes.

For calculating the efficiency of the solar panel, it is needed to know the input power. There is no available way of measuring, so an approximation is going to be made. On average the irradiation by the sun during a sunny day is 1000 W/m^2 . Because of the sun blinds not being able to pass through 100% of the sunlight there is a need for a correction factor. About 20% of the panel is covered by shade so the correction factor is 0,8. The area of the surface of the solar panel is known, namely 32,5 cm long by 34 cm wide. As result we get:

$$P_{input} = 0.8 * 1000 \frac{W}{m^2} * 0.325m * 0.34m = 88.4W$$

To give an example what the efficiency would be in optimal condition, regarding the datasheet of the solar panel. In this case we cannot use the correction for the sun blinds, and we know that the output power is equal to 7W. Assumed the manufacturer calculated his values with a sunny day in mind and thus using the 1000W/m^2 :

$$P_{input} = 1000 \frac{W}{m^2} * 0.325m * 0.34m = 110.5W$$

$$\eta = \frac{P_{max}}{P_{input}} * 100\% = \frac{7W}{110.5W} = 6.335\%$$

This is in the range of the theoretical performance of an amorphous solar cell, which ensures for the practical test. A similar calculation for the fill factor (FF) cannot be made because the datasheet only provides the open circuit voltage (Voc). The values for I_{max} and V_{max} are given, these can be compared to the ones in this particular test. The values are $I_{max}=467\text{mA}$ and $V_{max}=15\text{V}$ also the open circuit voltage is given this is $V_{oc}=21.5\text{V}$.

Now comparing this to the experiment, a recalculation of the irradiation has to be done because of the cloudy conditions. In a previous experiment on a sunny day, it was measured that the short circuit current equals to 225.013mA. Assuming the 1000W/m^2 [26] irradiance at that point in the day. Recalculating to 71.87mA on a cloudy day gives a new irradiance of 319.4W/m^2 , roughly a third of the value of the sunny day. This is plausible if compared to other research papers, also ranging around 300W/m^2 .

Out of the practical test and the IV curve we can make the calculations for the fill factor (FF) and the efficiency of the solar cell. The values of the short circuit voltage are needed as well as the open circuit voltage. $I_{sc}=71.87\text{mA}$, $V_{oc}=22.967\text{V}$. read from the graph, the values for the current and voltage at the maximum power point are $I_{max}= 71.8\text{mA}$, $V_{max}= 14.9\text{V}$.

$$FF = \frac{I_{max} * V_{max}}{I_{sc} * V_{oc}} = \frac{0.0718A * 14.9V}{0.07187A * 22.967V} = 0.6481$$

As explained above, the closer this value lays to 1 the better. This gives an idea about the quality of the solar panel. The number 0.6481 compared to the normal values which range between 0.7 and 0.8 is okay, considering the suboptimal conditions. Calculating the efficiency of the solar panel in these conditions with the new value for the irradiation:

$$P_{input} = 0.8 * 319.4 \frac{W}{m^2} * 0.325m * 0.34m = 28.24W$$

$$P_{max} = I_{max} * V_{max} = 0.0718A * 14.9V = 1.077W$$

$$\eta = \frac{P_{max}}{P_{input}} * 100\% = \frac{1.077W}{28.24W} = 3.814\%$$

The efficiency is not in the theoretical 6-7% range, this is also to be expected because the solar panel is not made to be operating in these low light conditions. Nonetheless it is half as efficient as theoretically possible. Comparing the manufacturers presumed optimal efficiency and the practical sub optimal conditions there is a difference of 6.335%-3.814% = 2.521%. These results are not that far apart.

3.2 Data acquisition program

The program in Labview version 18.0.1f4 consists of a human interface, the front panel as it is called and the code, the block diagram. In the front panel there are a few parameters to adjust. First a data file path must be chosen. This can be a file in .txt format. The program will write the raw data to this file which can be plotted in excel later. This must be done for the voltage data and the current data as well. Next to the data path items there are toggle switches. These switches make it possible to write or not write the data to the file. This can be useful if only one of the datasets is desired.

The set time function makes it possible for the user to fill in the time in seconds the program will run. Below a progress bar can be found, this gives a visual representation of how far the experiment has gone in perspective to the set time. This happens in real time. In contribution to this feature an elapsed time function has been added which shows the exact elapsed data in hours minutes and seconds. This ensures an extra convenience.

A designated button to stop the measurement can be found below the elapsed time, this feature can be used in case of an emergency or to end the process prematurely. Below are three error fields that are used to show any occurring error. For example, if the measuring device is not well connected or there are driver issues, this will show up according to its nature in one of the boxes. As can be seen there is a box error in and error out.

During an experiment, the voltage data and current data can be viewed in real time. Alongside with the starting time point and dt value, the dt value is the update interval of shown measurement values.

In this picture the code block is shown. There are three processes going on at the same time. Looking at the upper row of the box, the code for the voltage data collection can be seen.

The voltage is measured through the NI-DAQmx equipment. A DAQ system is a data acquisition platform in this case built by National Instruments. It includes a set of compatible hardware and software to enable the collection, processing and analysing the sensor data.

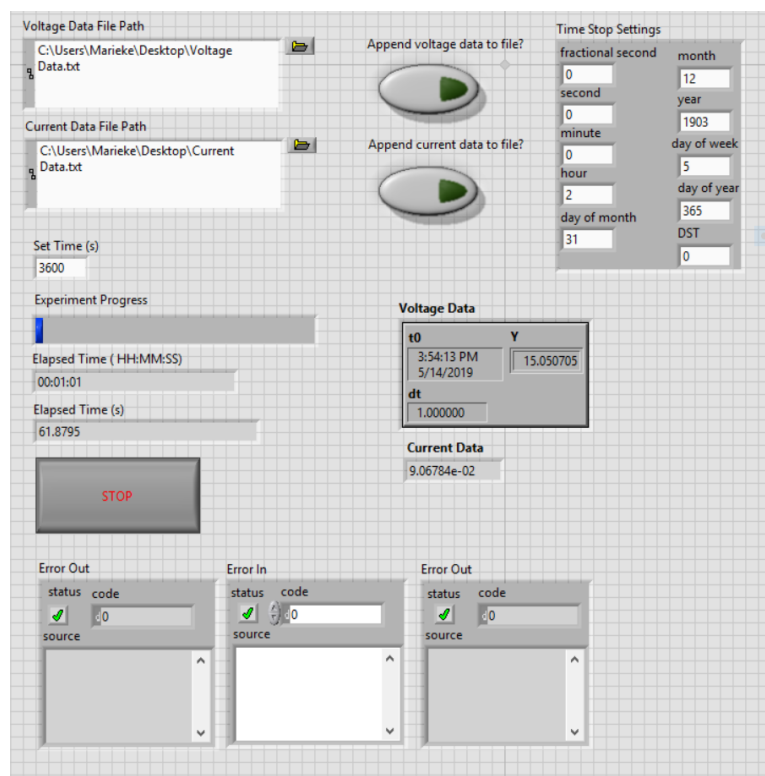


Figure 18: Labview data acquisition program interface

The second row of the program is the code for measuring the current that flows through the circuit. The current is measured by the Keithley 2601. These blocks also drive the sensing unit by measuring and saving the circuit current data.

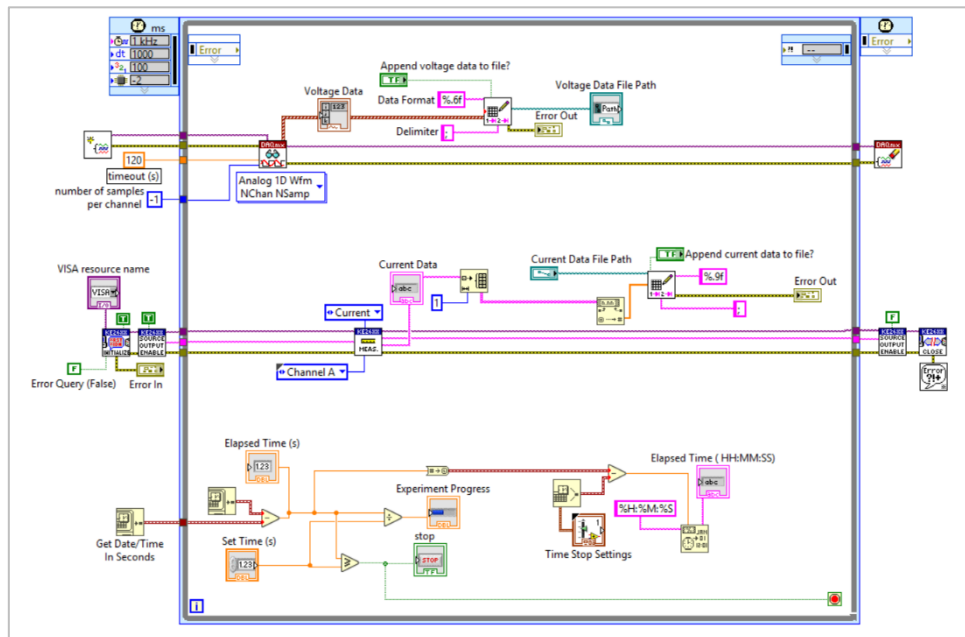


Figure 19: Labview data acquisition program code blocks

Finally, the third line of the program code has the function to stop the experiment when it reaches a certain time. This code compares the computer's time to the current time elapsed during the experiment. Thus, to see how long it has been since the beginning of the experiment.

When the duration of the experiment reaches the time restraint chosen by the user, the experiment will stop. This safety is implemented for the one-day experiments to ensure that the testing procedure would stop and does not continue to produce hydrogen gas.

3.3 PEM reversible fuel cell

This fuel cell is used to produce hydrogen and oxygen gas. As this is a reversible fuel cell it is also used for the opposite, the production of electricity. Then it is called an electrolyser. The PEM (Polymer Electrolyte Membrane) fuel cell is supplied by Cebekit. The size of the fuel cell is 54 x 54 x 17mm and the weight is only 14 grams this makes it an ideal component for portable applications. In the following experiments two of these PEM reversible cells will be used, one for generating the hydrogen and oxygen gas and the other for the electricity production. The PEM reversible cell consists of a membrane connected to two output terminals and two connection ports at each side of the membrane. Distilled water must be used to prevent corrosion of the membrane.

The PEM reversible cell is in electrolysis mode when a charge is supplied to the terminals. Then water will start to ionize, and hydrogen and oxygen will form. It is important that the water is only supplied at the oxygen side, at the lower connection port. The lower port of the hydrogen side must be blocked off. The two remaining ports must be connected to the gas containers. The negative side will produce hydrogen gas and the positive side will produce oxygen gas. As the electrolyser is possibly sensitive to pressure at either of its inputs, the impact of the water pressure, thus height of the supplied water column will be investigated. A study to characterize all scenarios for the gas production has been carried out. This is to fully understand the behaviour of the PEM reversible cell in electrolysis mode. More details about that in the experiments part of the thesis.

In fuel cell mode power is generated by doing the reverse process. Hydrogen and oxygen gas must be supplied under pressure. A charge will form at the output terminals. Negative at the hydrogen side and positive at the oxygen side. It is then possible to connect a load to the fuel cell and calculate the efficiency of the system. A study to characterize all scenarios for the power production has been carried out. This is to fully understand the behaviour of the PEM reversible cell in fuel cell mode. More details about that in the experiments part of the thesis. Based on these results it is possible to design a good working circuit for the model boat.

3.4 Electrolyser practical experiments

Before the first experiment could be done, a connection had to be made with the Keithley 2601 and the DAQ 9174 Ni 9129 Card in the Labview program. Then a sample rate of one measurement per minute was chosen because the experiments take up a lot of time, some in the range of several hours up to a day. This sample rate of one measurement per minute is more than enough for a good overall scope and not having too many samples to work with.

First the program and measuring equipment were tested in small experiments to confirm proper working of the setup. This was done by connecting the volt and ampere meter to the solar panel. When the sampling rate was confirmed and the values of the measuring devices were compared, a test setup with the PEM reversible cell could be made.

The main goal of this part of the research is to characterise the Horizon's C7121 PEM reversible cell in electrolysis mode, understand the working properties and its limitations. This way implementation and future calculations can be made. The solar panel is first used as a power supply to determine the current draw of the system. Then a lab bench power supply is used for the short-term experiments where constant current is required. Later, the solar panel is used again for the long-term experiments and the final setup.

3.4.1 Water pressure experiment

Experiment schematic:

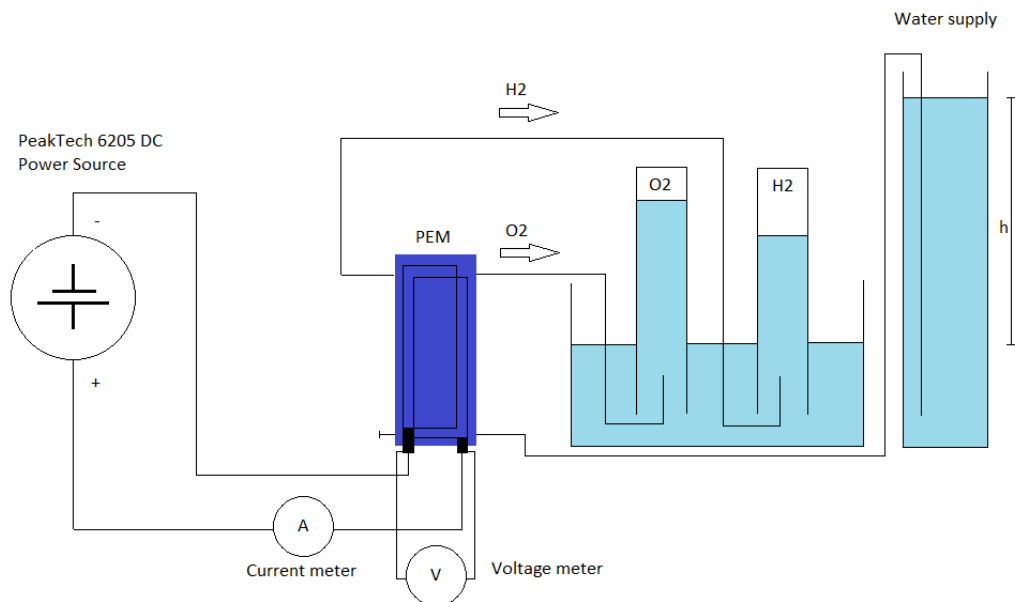


Figure 20: Water pressure experiment schematic

After learning how the PEM reversible cell worked and had to be configured in the setup the first test was concluded. As pressure on the membrane is an important factor, the supply water pressure was tested by altering the height of the water column. Since the formula of pressure is:

$$p = \rho * g * h$$

With p: pressure in pa, density of the fluid $\rho = 1000$ (kg/m³) gravitational force $g = 9.81$ and h represents the height of the water column.

Height of the water column is measured between the highest level of the water in the supply flask and the highest level of water in the receiving flask where the flasks of the H₂ and O₂ are put in. The measurement took place at the beginning of the experiment. Four tests with different heights were performed: one with a water level equal to the height of the electrolyser membrane. The other ones with a height difference of 3cm, 11cm and 35cm above the height of the electrolyser membrane.

To conclude these height tests, the height of the water level does not affect the volume of the hydrogen production. It just ensures that the electrolyser has a sufficient water level, which was completely filled. If the height of the water column is too low, the oxygen gas is able to flow back through the water supply line and stops the water from reaching the membrane. The production process stops at that point. It is important to have a high enough water column thus pressure, or to elevate the supply water beaker to a sufficient height. What could be seen at the 35cm test is that a lot of extra water is siphoned through the electrolyser thus excessively filling the lower beaker. A height difference of 3 cm above the top of the electrolyser is sufficient to keep the process going. The membrane must be completely hydrated for maximal gas production. Otherwise, the rate of gas production will be inconsistent. The rate of the volume production of the hydrogen and oxygen gas is dependent on the current flowing through the electrolyser if the membrane is completely hydrated.

Practical setup:

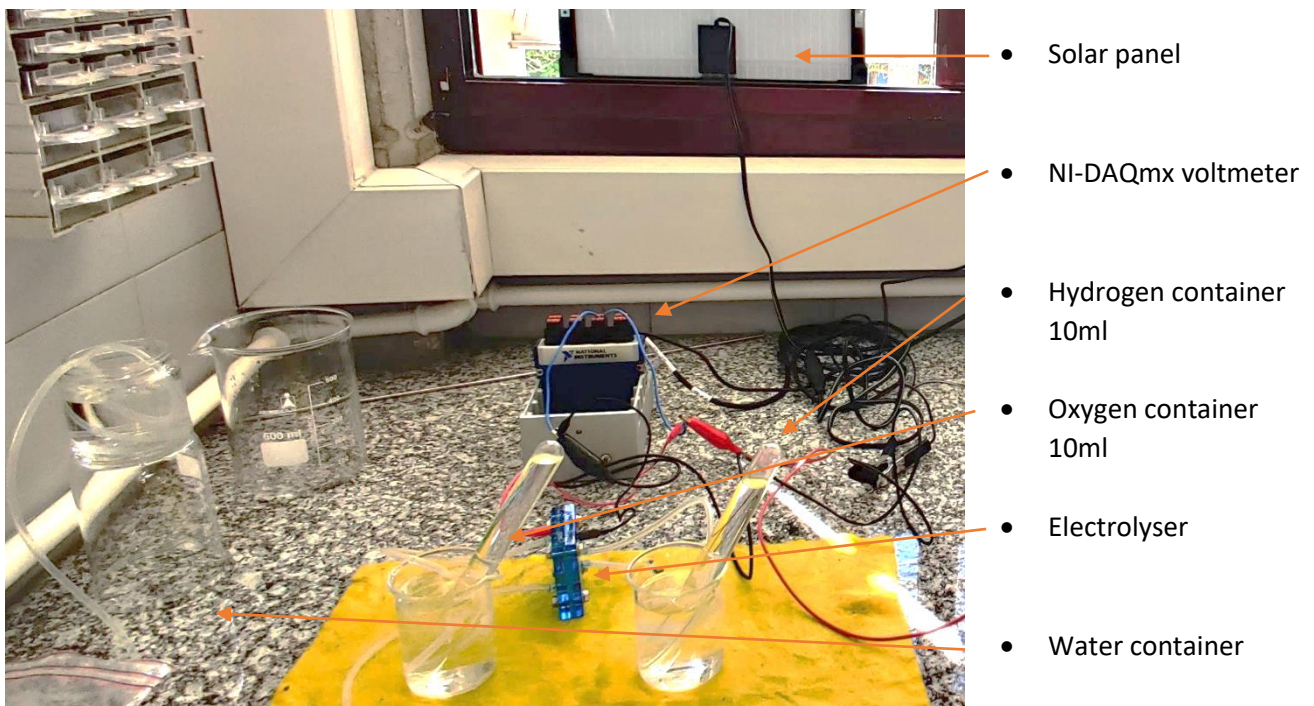


Figure 21: Water pressure experiment setup 1

3.4.2 Short term experiment

The volume production or flow rate is an important factor of the performance of the electrolyser. It represents the volume in millilitres (ml) of gas produced in a certain time. This figure is going to be needed later in the reverse process and for the consumption of a motor. This value is dependent on the supplied current and the relation of the two will be investigated. By performing small scale tests, it is tried to determine these flow rate values at certain current values.

The current that the electrolyser draws from the solar panel is limited between 0.1A and 0.3A. The tests are conducted in that range for that exact reason. Also, the current must be higher than 0.1A otherwise the production of the gasses is too few. This is done with a variable lab bench power supply, PeakTech 6205 DC Power Source. This way the current can be kept consistent and changed in small increments of approximately 0.2A. To get an accurate current reading the Agilent 34401A multimeter was connected in series with the electrolyser.

Practical setup:

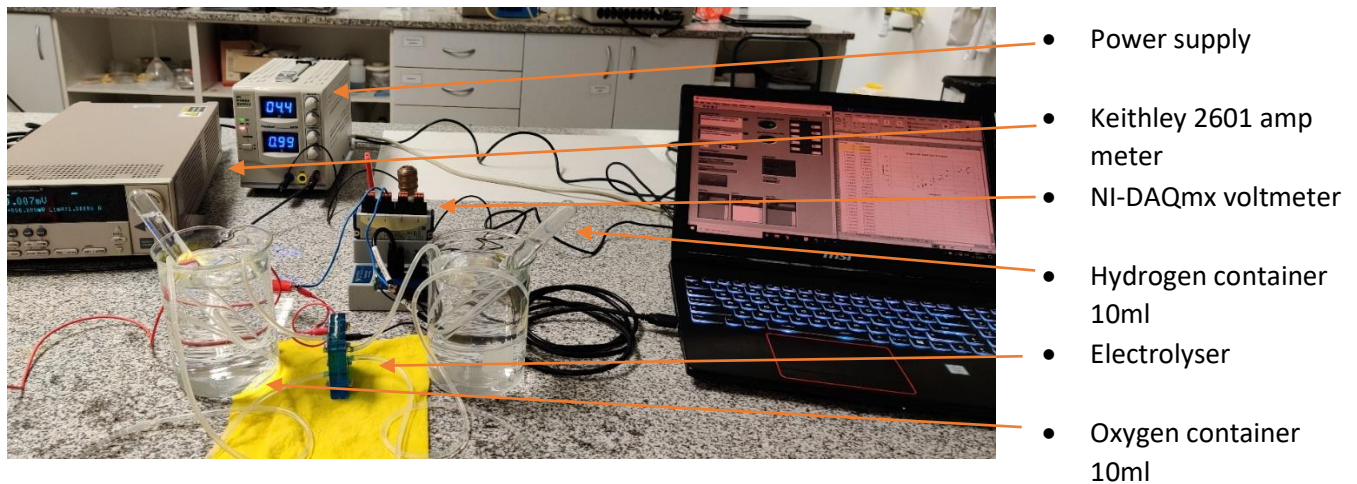


Figure 22: Short term experiment setup

Each test was performed at a fixed current value, then every second the volume of the produced hydrogen and oxygen levels were read of the flasks. The time measured during the full experiment is to reach approximately 10ml of Hydrogen. Then the ratio between the volume of Hydrogen and Oxygen calculated, as to see if there were anomalies from the two to one ratio. The slope of the curve of the volume-time graph will be investigated. The average of the supplied current is taken because the supposed to be steady current values dropped slightly over the period of the time. Because the time of the experiment is known, it is possible to calculate the volume production per minute. The volume production per minute per ampere is also calculated to compare the test results with each other and with the specification of the electrolyser.

The theoretical production of the fuel cell is 5ml/min of hydrogen gas and 2.5ml/min of oxygen gas. This happens at a current of 0.7A and 2V DC. Recalculated this becomes 7.14ml/A*min of Hydrogen and 3.571ml/A*min of oxygen. With this data it is also possible to approximate missing data points in later experiments conducted with a longer time span. The first graph is shown below. This represents the volume-time graph. The left graph is the volume of oxygen generated in ml on the y-axis and time on the x-axis in minutes. The right one is for hydrogen.

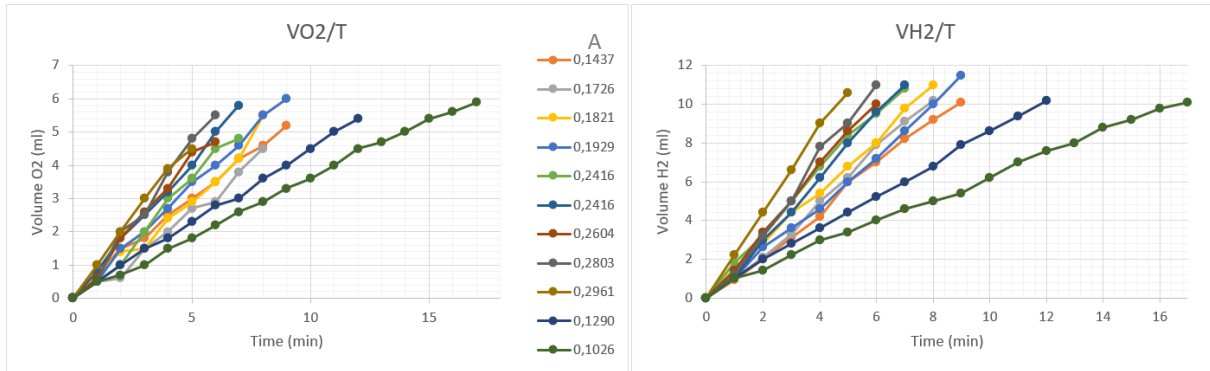


Figure 23: Volume time characteristics

In these graphs the curve of each test can be seen. They are represented in the legend by its average current. What can be concluded is that the slope of the curve gets steeper the more the current rises. This means the higher the current the faster the gas production of the electrolyser. The curve is linear, the gas is produced at a consistent linear rate.

This graph shows the steady current during the experiments as well as a better view on the duration of each experiment. It is clear to see that a lower current equals a longer duration. Also, under 0.1A the gas production would be unrealistically low to keep track of.

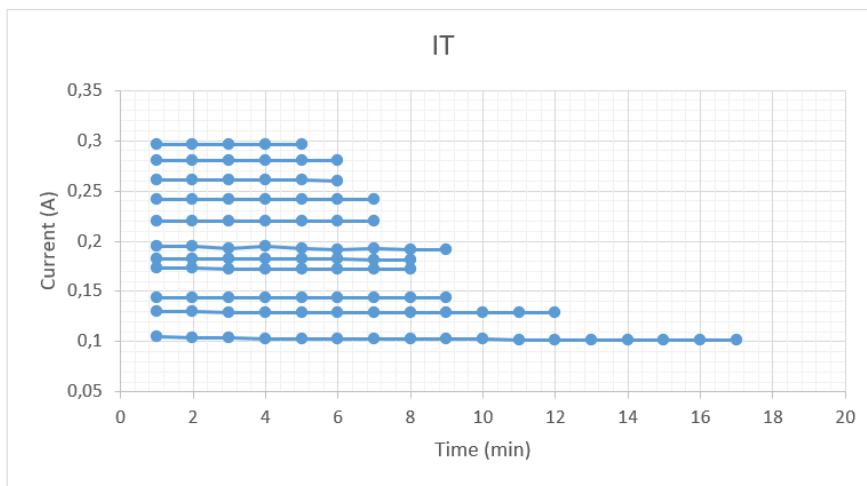


Figure 24: Current time characteristics

Test	I av (A)	O2 (ml/min)	H2 (ml/min)	O2 (ml/A*min)	H2 (ml/A*min)	volume O2 (V)	volume H2 (V)	Ratio H2/O2	Time (min)
1	0,1026	0,347	0,594	3,383	5,791	5,9	10,1	1,71	17
2	0,1290	0,450	0,850	3,489	6,590	5,4	10,2	1,89	12
3	0,1437	0,578	1,122	4,021	7,810	5,2	10,1	1,94	9
4	0,1726	0,563	1,275	3,259	7,387	4,5	10,2	2,27	8
5	0,1821	0,688	1,375	3,775	7,551	5,5	11	2,00	8
6	0,1929	0,667	1,278	3,457	6,626	6	11,5	1,92	9
7	0,2198	0,686	1,543	3,119	7,018	4,8	10,8	2,25	7
8	0,2416	0,829	1,571	3,430	6,505	5,8	11	1,90	7
9	0,2604	0,783	1,667	3,008	6,400	4,7	10	2,13	6
10	0,2803	0,917	1,833	3,270	6,541	5,5	11	2,00	6
11	0,2961	0,900	2,120	3,040	7,160	4,5	10,6	2,36	5

Table 2: Short term experiment results

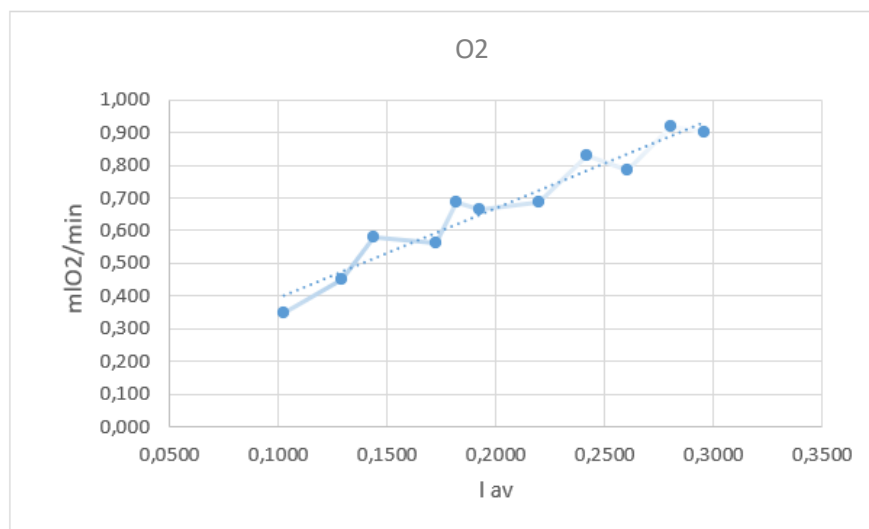


Figure 25: Volume time characterisation O₂

This table combines the significant values from the previous experiment data with the calculations made regarding the volume production. Following graphs and conclusions can be conducted out of this table.

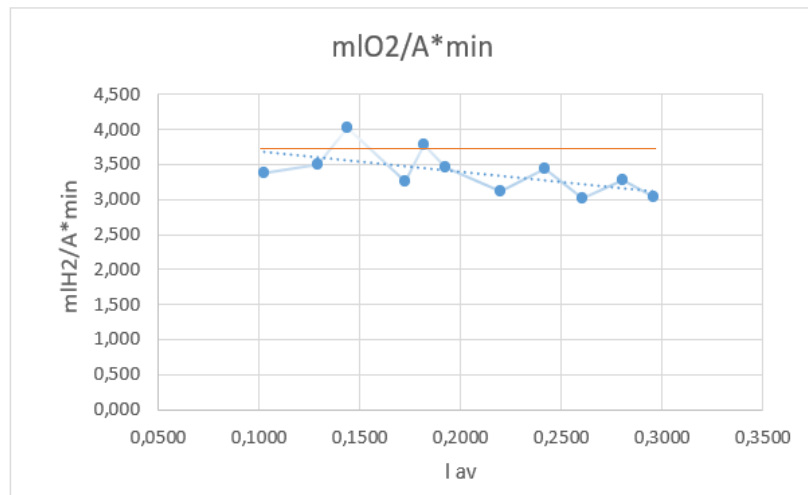


Figure 26: Volume time characterisation O₂

In the graphs above it shows that there is a positive correlation between volume production and current over the eleven tests. From 0.1A to 0.3A this is still the beginning of the workable range of the electrolyser but as the statistics show, it behaves in a linear manner. Each individual test value does not deviate much from the trendline. There is a consistent rise in volume production when a higher current is applied. Because the specification of the electrolyser is relatively far beyond this range, it is not shown on the graph. For completeness and to be compared to the specifications, the theoretical gas production values are 2.5ml/min for oxygen and 5ml/min for hydrogen at a current of 0.7A.

Because the curve has a linear characterisation it is possible to use simple calculations. This becomes more important in further and more complex experiments when the current during the experiment is not consistent. This way it is not needed to calculate volumes with integral functions, but the average can be used.

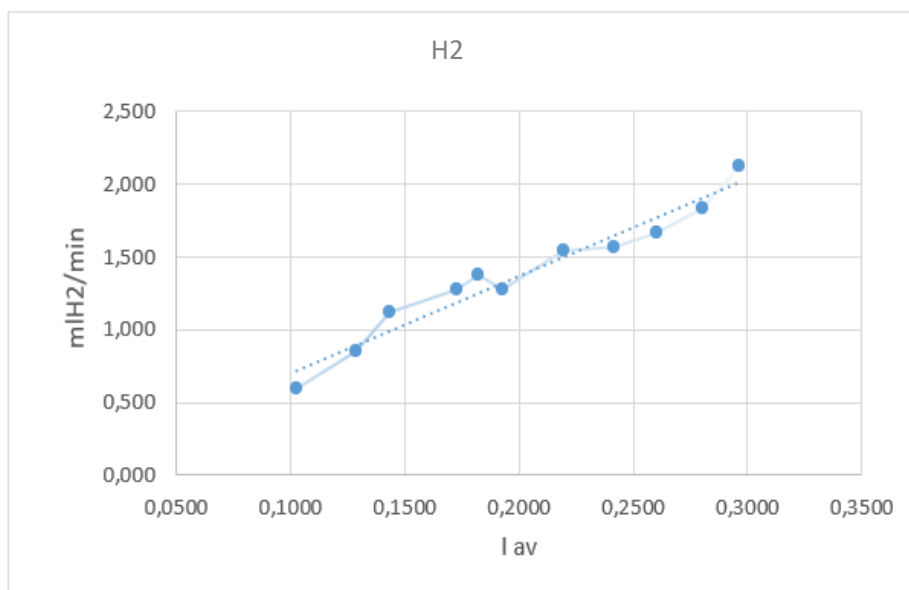


Figure 27: Volume time characterisation H₂

In this chart, the values of the volume production are recalculated to the volume production per minute per ampere. This way it can be easily compared to the specification of the electrolyser, which is 3.571ml/A*min of oxygen and 7.14ml/A*min for hydrogen. They are represented on the graph by the orange line. The trend for the hydrogen is constant and lays close to the desired theoretical value, even at this low current. The oxygen curve starts off close to the base value but drops off slightly, it has a negative linear dependency.

It must be noted that the first two tests took a significantly longer time to complete and it observed that there is a lower production hydrogen production compared to the oxygen and the base value. This is because the limitation of the electrolyser is reached and below that point almost no hydrogen is formed. For the oxygen gas, this point is lower. Theoretically every water molecule is split in one oxygen molecule and two hydrogen molecules. It could be that there is not enough pressure to push the hydrogen gas out. The oxygen gas is transported up through the waterline and gets siphoned through to the gas container, so it has less problems with creating enough pressure.

This last graph of the short-term experiments shows the relation between the volume of hydrogen and oxygen gas regarding a change in current. In the diagram it seems that there is a positive correlation, a lower ratio at lower current and higher ratio at a higher current. Theoretically this should be constant at 2. But because the test is executed rather at the limits of the electrolyser and there might be some slight reading errors, there is a deviation from the constant ratio of two.

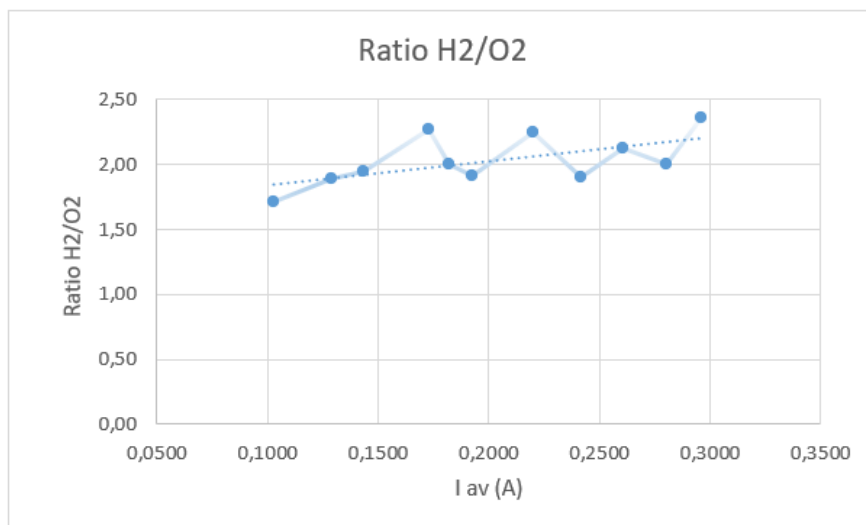


Figure 28: Hydrogen to oxygen ratio

3.4.3 Long term experiment

The next step is to eliminate the lab bench power supply and use the solar panel again as a power source. This brings a new set of variables. The current and volume progression during the day is researched. This means from dark to light times and reverse. The influence of clouds and temperature of the panel may affect the measurements. To understand the working and get enough data, the runtime of the experiment will be gradually increased from a few hours to a full day. After that, conclusions are drawn. The goal of these experiments is to determine the IU (current – voltage) graph and the total volume production to interpret this data in the catamarans design for the propulsion system.

3.4.4 Setup

The setup for the following experiments is not much different than the setup for the short-term experiments except for the implementation of the solar panel and the use of bigger gas containers. The Keithley 2601 and the DAQ 9174 Ni 9129 Card are still used for the current and voltage measurements, the one-minute interval sampling is done in the Labview program. The duration of the experiment is put into the program, so it safely stops the gas production at the given time. The solar panel is placed in direct sunlight in the laboratory. The lab is equipped with shades, these are tilted for maximum solar exposure.

Experiment schematic:

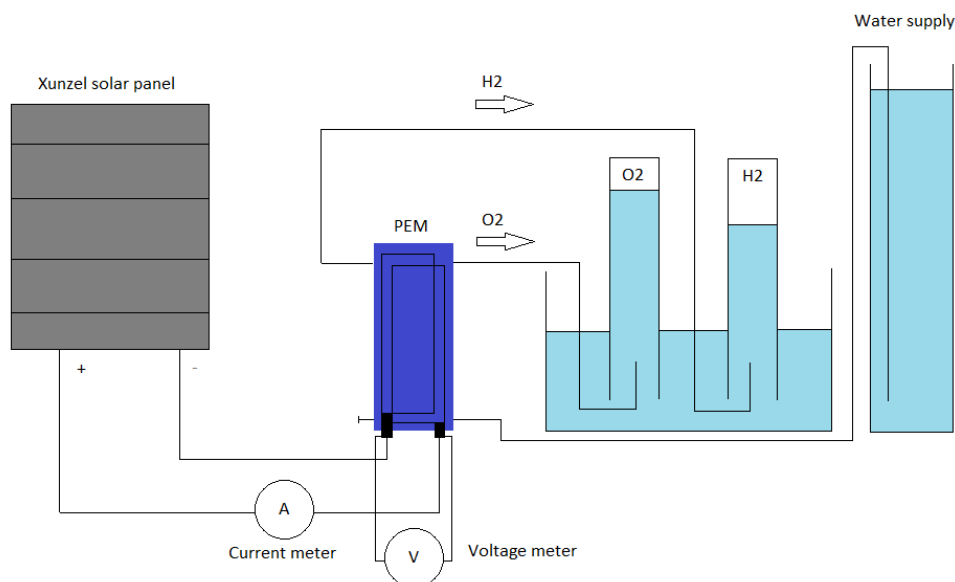
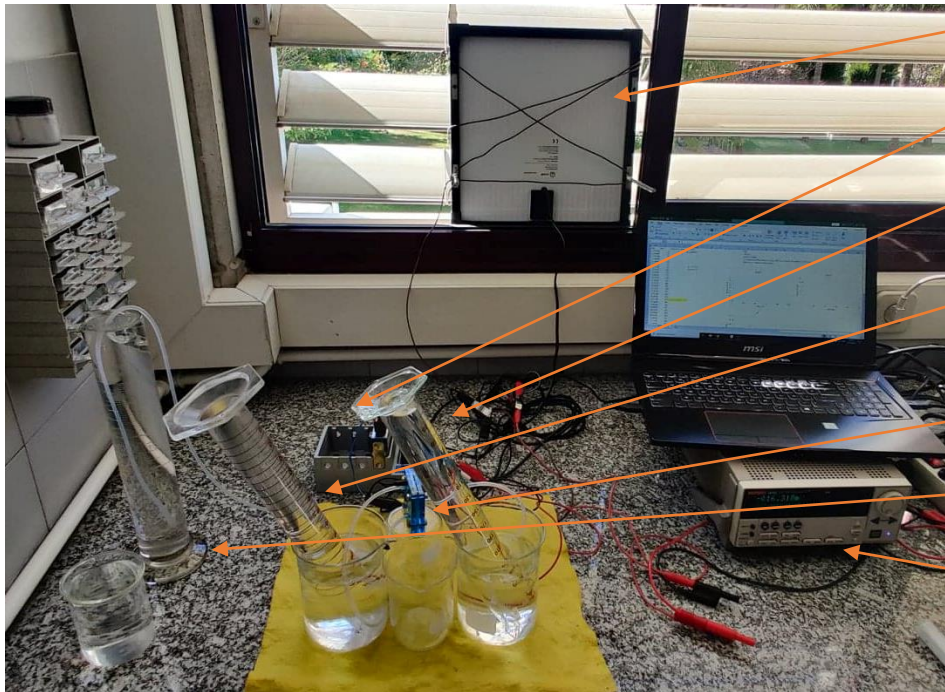


Figure 29: Long term experiment schematic

Practical setup:



- Solar panel
- NI-DAQmx voltmeter
- Hydrogen container 250ml
- Oxygen container 250ml
- Electrolyser
- Water container
- Keithley 2601 amp meter

3.4.5 Statistics

In some rare occasions the Keighley 2601 current meter gives a false value. For that reason, it was decided that some statistics were needed to find all the significant values and to reject peculiar data. The use of a 95% Bell-curve is decided to be sufficient. This means that the 5% of data finds itself outside of this curve is rejected. The remaining 95% is accepted. This is done by performing an analysis on the whole dataset received from the measuring devices. The analysis consists out of the use of following calculations:

Statistics

```

min =MIN(B2:B100)
max =MAX(B2:B100)
average  $\mu$  =GEMIDDELDE(B2:B100)
sigma =STDEV.P(B2:B100)
 $\mu - 2 * \text{sigma}$  =J38-(2*J39)
 $\mu + 2 * \text{sigma}$  =J38+(2*J39)
values below  $\mu - 2 * \text{sigma}$  =+AANTAL.ALS(B2:B100;"<0,070131924")
values above  $\mu + 2 * \text{sigma}$  =+AANTAL.ALS(B2:B100;">0,325124948")

```

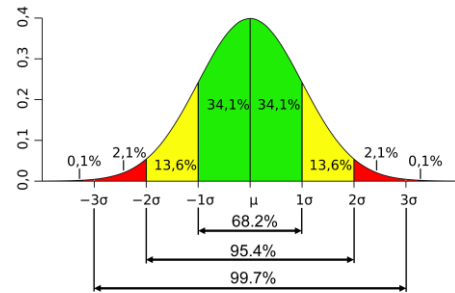


Table 3: Statistical formulas

Figure 30: Gaussian distribution and standard deviations [27]

The first line calculates the minimum value of the dataset. The second line calculates the maximum value. The third line calculates the average value. The fourth line calculates the standard deviation. The fifth line calculates the left limit of the curve, which is the average value minus two times the standard deviation. The sixth line calculates the right limit of the curve. The seventh line calculates the amount of data points below the left limit. Coloured in orange. The eighth line calculates the amount of data points above the right limit. Coloured in red.

By colouring the whole dataset, it is easy to find and exclude peculiar data points out of the graphs and calculations. This will be done on all further datasets of the experiments.

3.4.6 100 min experiment

Two experiments were conducted in a 100-minute time frame. The first one is performed under stable lighting. The second one studies the shut-off behaviour of the system.

3.4.6.1 Experiment 1

The first experiment took place at 15:00h and took 98 minutes to complete. At that time, the weather was very sunny for the most part and very few clouds. When the experiment was complete 132ml of hydrogen and 75 ml of oxygen was collected in the gas containers. Current voltage and time were measured as well, and the current-voltage (IV) and current-time (IT) graphs could be made. Some values were very peculiar and could not be explained by the passing of a cloud. In some rare occasions the Keighley 2601 current meter gives a false value. For that reason, the statistics mentioned above were used to solve this problem. At first there were 14 peculiar values. After taking a deeper look there were two errors in the measurement with values of 9.91E37, these were discarded. The other 11 values cannot be discarded. Although they seem extremely low, it is possible that at that point in time a cloud is moving over, blocking sunlight, and temporarily stopping the process. Thus, explaining the 11 sub-0.07013A values

Statistics				
min	0,0241243	1,541383	0,0318	38
max	0,244106	1,539838	0,2433	39
average μ	0,197628436	1,657004	0,1773	40
sigma	0,063748256	1,622794	0,0274	41
$\mu - 2 * \text{sigma}$	0,070131924	1,535010	0,0264	42
$\mu + 2 * \text{sigma}$	0,325124948	1,533744	0,2342	43
values below $\mu - 2 * \text{sigma}$	11	1,654000	0,1931	44
values above $\mu + 2 * \text{sigma}$	0	1,638422	0,2363	45
		1,657984		46
		1,536477	0,2344	47
		1,655023	0,0264	48
		1,533952		49
				9,91E+37
				9,91E+37

Table 5: 100min experiment statistics

Table 4: 100min experiment statistics

To proceed the analysis of the first experiment, the graphs are made and shown in Figure 31: 100min experiment IV characteristic 1. The first graph is the IV graph providing the current and voltage at the electrolysers operating point. There is a small spread in voltage of around 0.13V in a range of 1.53V to 1.67V. However, the low points in the diagram are notable too. These points can be explained by

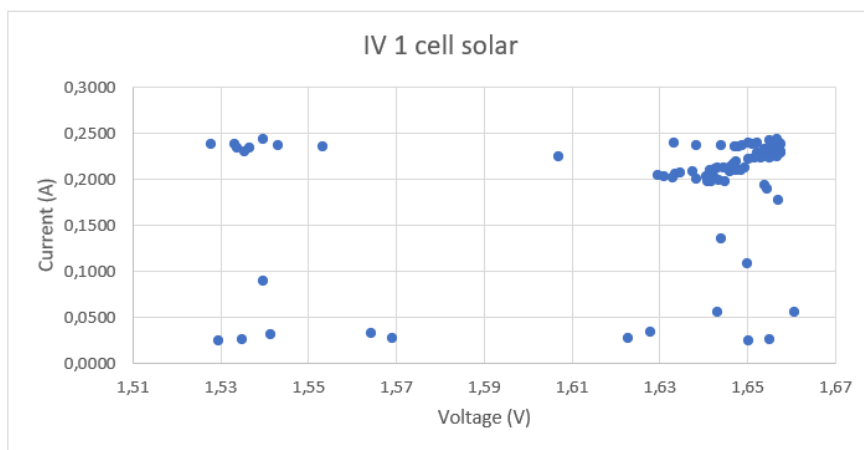


Figure 31: 100min experiment IV characteristic 1

passing clouds. The voltage over the electrolyser holds its value but the current drops to almost none. Thereby not generating any gas.

The second graph shows the current in function of the passed time. Again, the low spots are from the passing clouds but in this graph, it can be seen at what point in time they passed over the solar panel. Furthermore, a gradual decline of the curve can be seen due to the position of the sun.

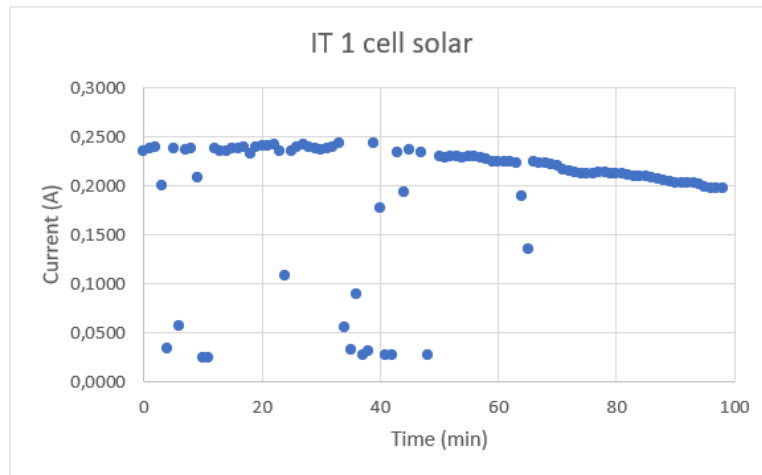


Figure 32: 100min experiment IT characteristic 1

The volume production calculations could then be made. The captured gasses were filled in alongside the measured time. The average current was calculated from the dataset. Then the rates were computed. As seen in the table, the values come close to the specification of the electrolyser, which is 3.571ml/A*min of oxygen and 7.14ml/A*min for hydrogen. The values are on par with the short-term experiments. This is because the current did not change very much.

Average	test 1		V	t_full
0,1976 A				
0,684 ml/min	O2		67 ml	98 min
1,347 ml/min	H2		132 ml	
3,459 ml/A*min	O2	1,96153846 ratio		
6,816 ml/A*min	H2			

Figure 33: 100min experiment significant numbers calculations 1

3.4.6.2 Experiment 2

The second experiment took place at 16:45h and took 138 minutes to complete. The sun was shining all the time, no clouds during the experiment. When the experiment was complete 95ml of hydrogen and 42ml of oxygen was collected in the gas containers. This is less than in the previous experiment because the overall current was lower. This is the result of the time of day. Current voltage and time were measured as well, and the current-voltage (IV) and current-time (IT) graphs could be made. Statistics were used once again but there were no exceptional values.

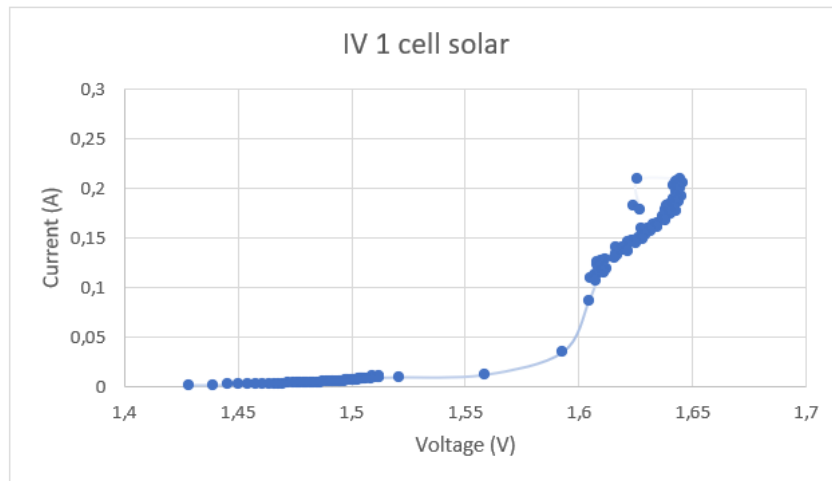


Figure 34: 100min experiment IV characteristic 2

This first graph shows the IV characteristic. The stable operation of the cell with solar plate feed can be seen. The left data points in the lower spectrum refer to the measurements taken when the solar panel did not get sufficient light. Therefore, a low current passed through the system and the voltage is low as well. Considering looking at the right data points in the higher spectrum, a positive linear relationship between voltage and current can be seen. When the voltage goes up, the current also rises.

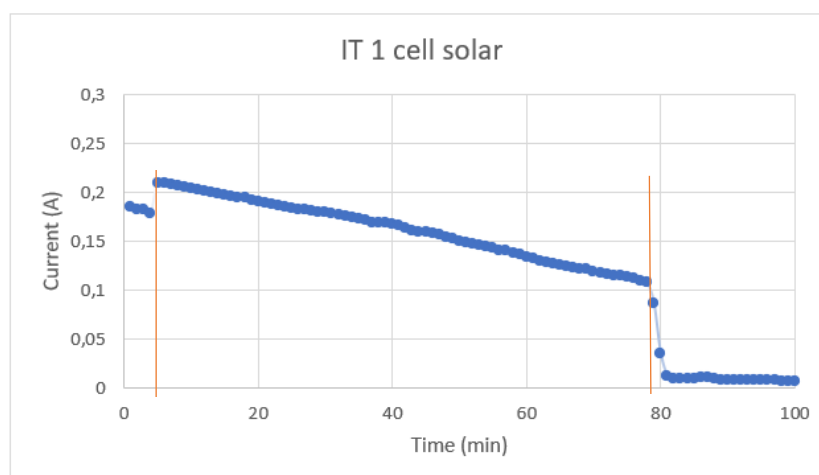


Figure 35: 100min experiment IT characteristic 2

The second graph displays the IT characteristic. The first jump can be explained by a change in the sun blinds, they were adjusted to a better angle to provide more light exposure. Then the intensity gradually decreases according to the position of the sun. Until the light is too few, the current drops and the electrolyser shuts off. This happens at around 0.1A.

To calculate the volume production and the average current an appropriate range must be chosen first, otherwise the value of the average current and rate will be incorrect due to the incorporation of the low values. Thus, the range]5;78[is chosen this includes the linear interval of the curve. This equals a time of 77 analysed minutes.

Performing the statistical analysis on this range gives us no peculiar data points. Calculations give results shown in Table 7: 100min experiment statistics. The ratio hydrogen to oxygen is close to two, which is normal. As well as the ml/A*min. It surpasses the specification on the datasheet for the value of Hydrogen but not for oxygen gas. This explains why the ratio is higher than two.

Statistics

min	0,107618
max	0,210184
average μ	0,16256165
sigma	0,0299418
$\mu - 2 * \text{sigma}$	0,10267805
$\mu + 2 * \text{sigma}$	0,22244526
values below $\mu - 2 * \text{sigma}$	0
values above $\mu + 2 * \text{sigma}$	0

Average	test 2	V	t_full
0,1626 A			77 min
0,545	O2	42 ml	
1,182 ml/min	H2	91 ml	
3,355 ml/A*min	O2	2,167 ratio	
7,270 ml/A*min	H2		

Table 6: 100min experiment significant numbers calculations 2

Table 7: 100min experiment statistics

3.4.6.3 Conclusion of the 100-minute experiments

These experiments were a great first long-term test to see the influence of the moving sun passing over the solar panel during daytime, the program worked like it should without flaws. It appeared that some statistics are needed for the filtering of peculiar values. This will be implemented to the following tests as well. A more detailed and full day experiment can now take place. This will give more insight in the volume production which is a key feature for determining the range of the catamaran.

3.4.7 Full day experiments

Two more experiments will be conducted to the electrolyser. The first one performed over 8 hours during the daytime with a clear sky all day long, no clouds. The other one is a 24h experiment to get the full cycle. During this experiment there were a lot of clouds, this way the impact of clouds can be seen. Also, the night and morning can be compared to daytime and evening behaviour of the electrolyser. In other words, the start-up and shutdown of the system. The current-time (IT) and current-voltage (IV) characteristics will be made and analysed to then make conclusions about them. The rate of volume production will be calculated as well as the rate of volume production per ampere. So, comparisons can be made.

A second dataset for each experiment is made where the progression of the volume is noted every 15 minutes. That way it is possible to make a detailed volume-time (VT) and current-volume (IV) characteristics and interpret them.

3.4.7.1 Day 1 experiment

The first day experiment started at 10:00h. The solar panel was placed in direct sunlight in the laboratory but at this time the shade of the building was still overcasting the solar panel. So, there was no gas production yet. This was the perfect moment to start because this way the start-up of the system could be witnessed and studied. The test took 8 hours to complete. The weather was very sunny for the most part with almost no clouds. This is good because this way the data is consequent and stable, providing a nice graph. The setup is the same as the long-term experiments. The solar panel is connected to the electrolyser, this is the power supply. A voltage meter is put in parallel over the electrolyser and the ampere meter is put in series with the electrolyser. The Keithley 2601 and the DAQ 9174 Ni 9129 Card are again used for the current and voltage measurements. The duration of the experiment is put into the program, so it safely stops the gas production when the given interval expires. The windows in the lab are equipped with shades, these are tilted for maximum solar exposure.

Two datasets were acquired. The first one is automatically made by the Labview program with one-minute interval sampling and saved onto the computer. This dataset will be used for a very accurate current-voltage (IV) graph of the day experiment as well as the current-time (IT) and voltage-time (VT) diagrams.

In the second dataset the volume is measured every 15 minutes. As well as the current, which is retrieved from the file made by the Keithley current meter. This dataset is more general and not as precise concerning the reading method. Nevertheless, this was the only way to measure the progression of the volume production. The volume was manually read from the test tubes. This makes it possible to create the volume-time (VT) and current-volume graphs which will be discussed later.

Starting off with the current-time (IT) graph. The first thing to notice is the gradual start-up of the electrolyser. The current slowly rises to 0.05A, then rises with a steep slope to 0.15A, to then gradually increase according to the position of the sun. At around two in the afternoon the current reaches its peak. This is when the sun’s exposure level is at its maximum. This can also be seen on the exposure graph of that day. The slight difference in timing can be caused by the orientation of the window blinds. Coupled with the further progression of the sun, the measured current declines. Until the point of 0.08A is reached where the power is insufficient, and the electrolyser shuts down. This results in a steep decline at the end. Lastly the current stagnates just below zero.

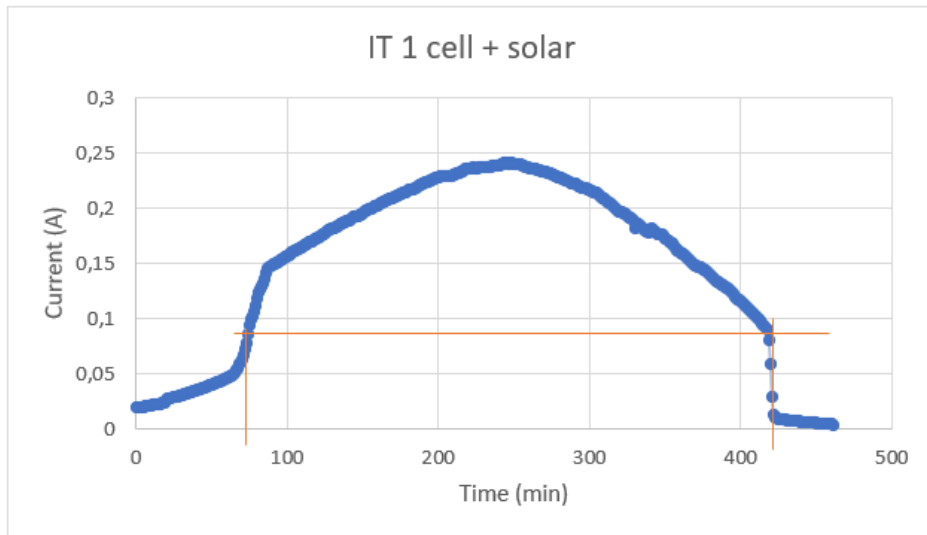


Figure 37: Full day experiment IV characteristic

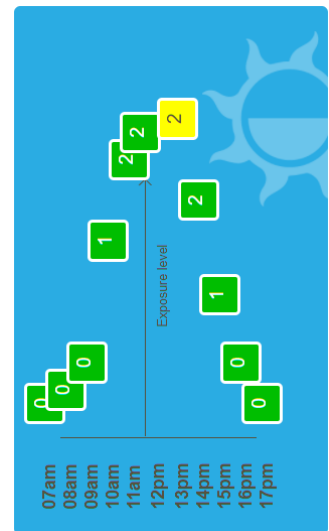


Figure 36: solar exposure level [28]

Statistics were once again used to calculate the general average of the current and whether or not presence of peculiar values. An appropriate range had to be chosen, the cut-off value of 0.08A was a logical choice because then the gas production stopped. The chosen range is [80;420]. This resulted in 13 peculiar values, these were the last values in the range. These values were excluded in the further calculations.

Statistics	
min	0,0578398
max	0,240867
gemiddelde μ	0,18897726
sigma	0,04105353
$\mu - 2 * \text{sigma}$	0,10687019
$\mu + 2 * \text{sigma}$	0,27108433
aantal waarden onder $\mu - 2 * \text{sigma}$	13
aantal waarden bover $\mu + 2 * \text{sigma}$	0

Table 8: Full day experiment statistics

Average	considering max prod only = graph $I > 0,08A$		
0,1890 A	V		t_full
0,759 ml/min	O ₂	258 ml O ₂	340 min
1,153 ml/min	H ₂	392 ml H ₂	
4,015 ml/A*min	O ₂	1,519 ratio	
6,101 ml/A*min	H ₂		

Table 9: Full day experiment significant data

To explain these values, we look back and compare with the previous test results. The time in the interval is 340 minutes. The average current is 0.189A. A total of 258 ml of oxygen gas and 392ml hydrogen gas is produced. This means that the ratio of hydrogen to oxygen equals to 1.519. this is rather low and deviates quite a lot from the theoretical 2. This is because although the calculation takes the values above 0.08A into account, the electrolyser still operates at a rather low current. As seen in the short-term experiments this causes more oxygen gas generation than hydrogen. Thus, lowering the hydrogen to oxygen ratio. The values for the rate of the volume production are not too far of the specifications, 3.571ml/A*min of oxygen and 7.14ml/A*min for hydrogen. This can be explained by the inefficiencies of the system.

Also, interesting, and closely related, is the power curve of the system. The curve has the same shape as the IT curve. It can be seen that in order to power the electrolyser it can take up to 400mW. This translates to roughly 250mA and a production of around 1.6mlH₂/min and 0.8mlO₂/min at the peak of the curve. The average power generated in the capped time period is 314mW, the time passed is 5.7h. Therefore, the solar panel produced a total of 1780mWh.

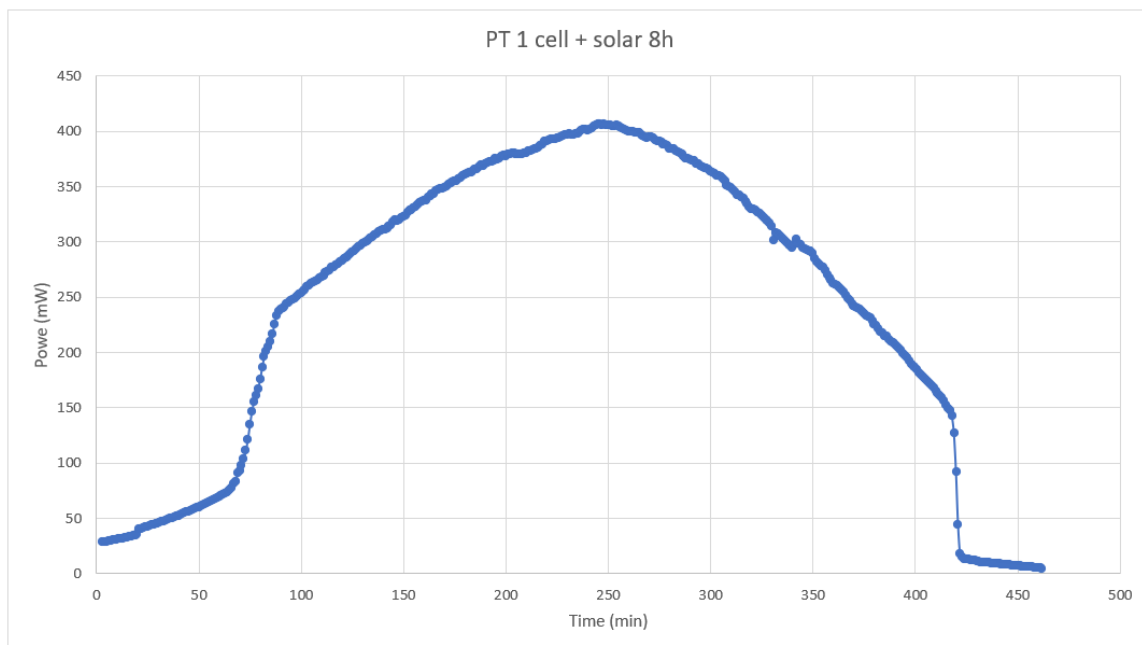


Figure 38: Full day experiment PT characteristic

The more intricate current-voltage (IV) graph will now be investigated. The experiment started with a voltage over the electrolyser at 1.5V. The curve then progresses up linearly and makes a counter clockwise loop. It then proceeds to go down again in a rather swirly matter to finalize at the bottom of the chart after a rapid drop-off. This is the first time perceiving the start-up and shutdown of the electrolyser in one experiment using the solar panel. The linear progression is to be expected as seen in the second long-term experiment. Then there is the loop and returning of the graph, this can be explained by the solar panel operating, and thus, behaving in different circumstances. The temperature of the panel will have risen in the second part of the day. As well as the solar panel receiving different wavelengths of light due to filtering.

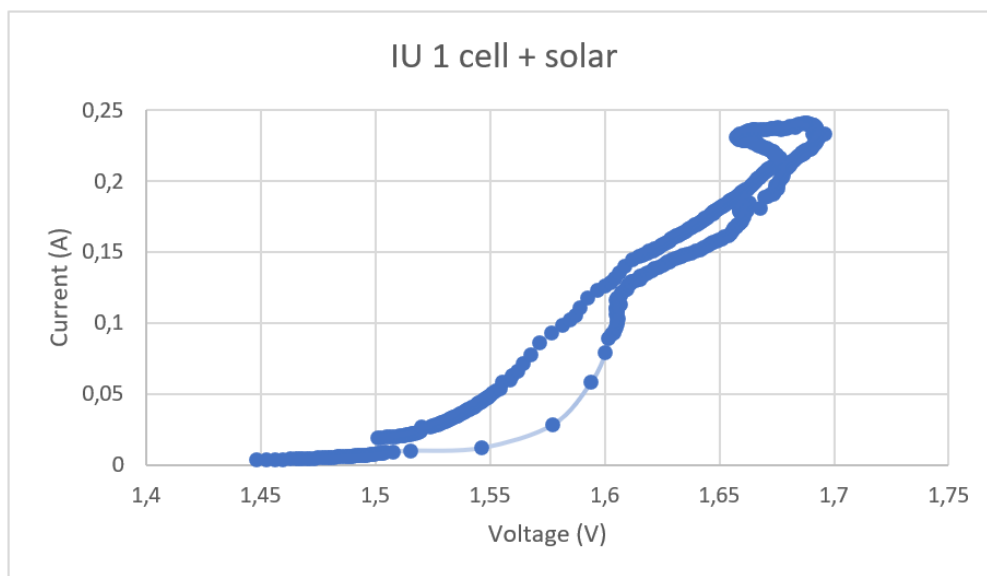


Figure 39: Full day experiment IU characteristic

Still regarding the first dataset, the voltage time curve has a rather stable curve. Immediately the voltage over the electrolyser is 1.5V. Although there is still no gas production or significant current at this point, the voltage is already at an operating value. The first decent rise and kink in the curve is at minute 80. On the current-time (IT) graph this is the point where the current increases rapidly to 0.08A and the gas production starts. Equal to the drop in the end, this is the point on the IT graph where the current drops from 0.08A to almost zero, stopping the gas production. It is interesting to see the voltage over the electrolysis and current do not rise and drop simultaneously. In the second day test the dilation of the UT curve will be more visible due to the longer timespan, capturing the rise and fall of the voltage.

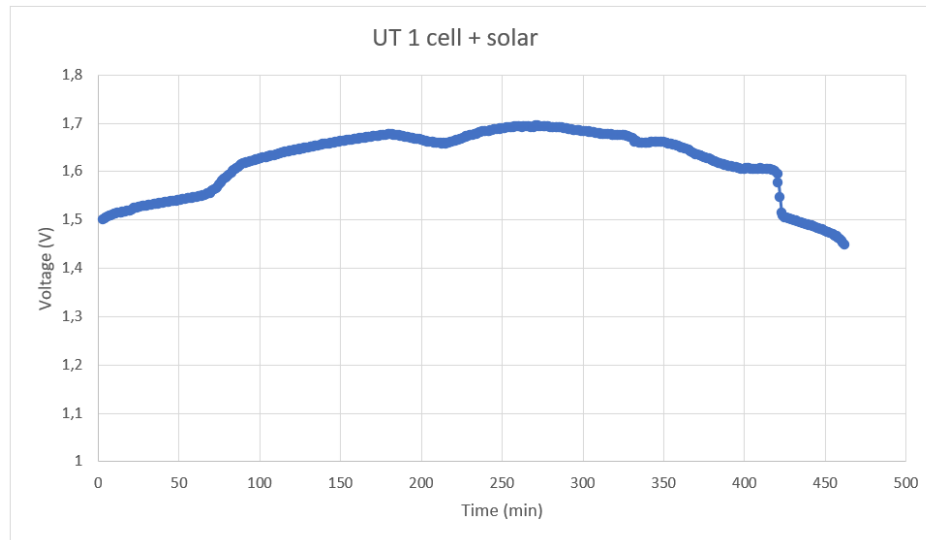


Figure 40: Full day experiment UT characteristic

Now the second data set is used where the volume production will be studied furthermore in detail. To retake, every 15 minutes the volume was manually read together with the current at that time point to be able to make graphs considering the volume progression.

In the volume-time graph the general “S” form of both curves can be seen. Implicating a slower volume production at the beginning and end of the experiment. Above all it seems that the first 100 minutes the volume of hydrogen and oxygen were near identical. This fact gives more insight why the ratio of hydrogen to oxygen was rather low. It must be noted that the five red coloured data points were calculated using the formulas and figures from the short-term experiments, due to the absence of the observer. Nevertheless, these calculations fit rather well in the model. To conclude, the curve has a gradual and predictable development with a slower progression at the start and end.

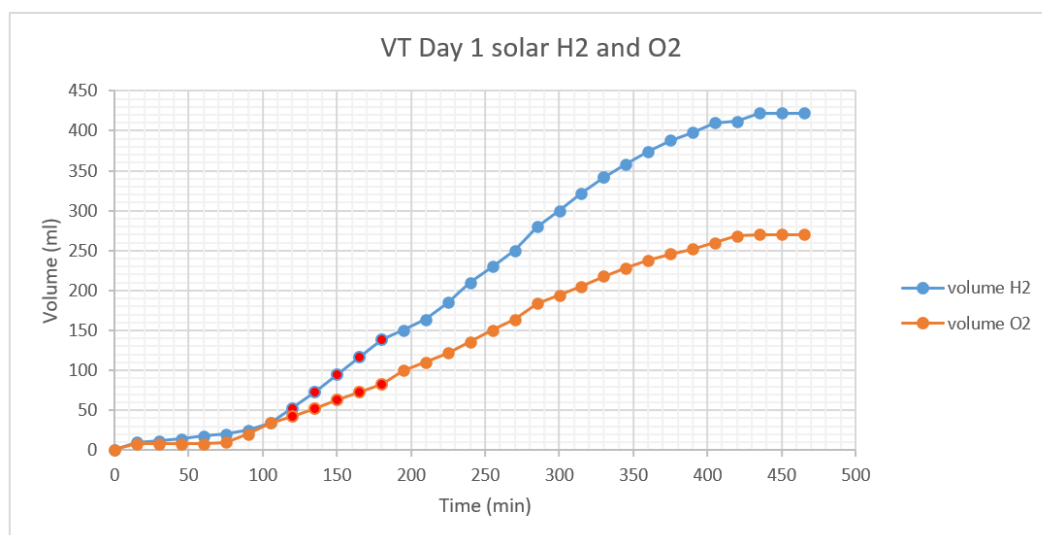


Figure 41: Full day experiment VT characteristic combined H_2 and O_2

The next graph which can be made is the current-volume (IV) characteristic. Here it can be seen that the slope of both curves is steep in the beginning and end. It means that there is very little gas production in that period. This can also be seen by the aggregation of data points. The dilation of

datapoints starts to occur when the current reaches a value of 0.1A, as found in previous tests. Furthermore, it seems that the hydrogen graph is more spread out but not twice as long as the graph of oxygen, because the ratio is not 2. Once again, the progression of the sun moving can be seen by the gradual rise and decline of the current until it drops when the intensity does not suffice anymore.

3.4.7.2 Day 2 experiment

The second full day experiment took place at 10:45h the next day, the position of the solar panel and the setup was exactly the same. The weather was very different, this day it was sunny, but many clouds passed over. Interfering with the continuity of the test but providing a more realistic dataset to study. The model catamaran must be able to operate in less-than-optimal conditions once it is fully assembled and installed. Consequently, this is an interesting day to perform the experiment. The experiment will run for 24h this way the start-up and shutdown of the system can be reviewed. Yet again the Solar panel is used as power supply. The DAQ 9174 Ni 9129 Card is used for capturing the voltage data and the Keithley 2601 measures the current flowing through the circuit. The solar blinds were not adjusted since the previous experiment, so their position is completely open.

Two datasets were acquired. The first one is automatically made by the Labview program with one-minute interval sampling and saved onto the computer. This dataset will be used for a very accurate current-voltage (IV) graph of the day experiment as well as the current-time (IT) and voltage-time (VT) diagrams. This time it is hoped to see more irregularities due to the clouds. It will be interesting to see how these events reflect on the data and therefore the graphs. Because there is data sampling every minute, these changes should be very noticeable.

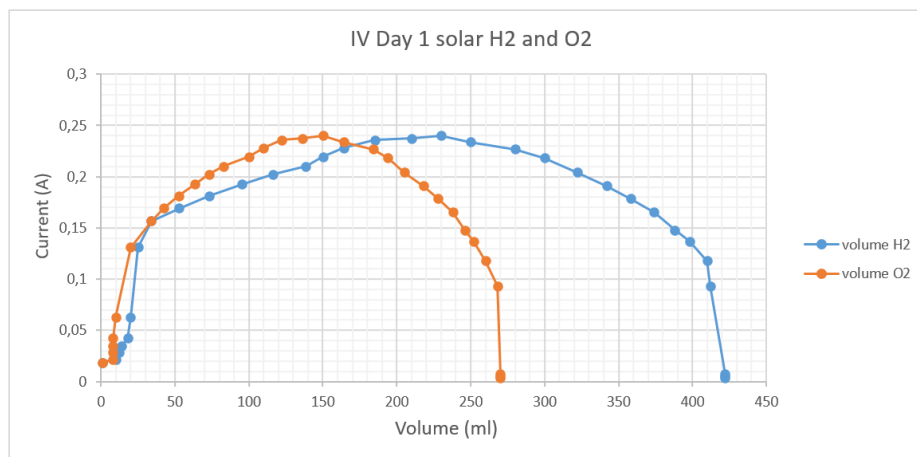


Figure 42: Full day experiment IV characteristic combined H_2 and O_2

In the second dataset the volume is measured every 15 minutes. As well as the current, which is retrieved from the file made by the Keighley current meter. The volume was manually read from the test tubes. This makes it possible to create the volume-time (VT) and current-volume graphs which will be discussed later. Because of the long-time interval, it is tricky to get the right current date. It is not viable to simply take the current at the time of the measurement because it is not accurate if at that exact moment a cloud passes by and causes a low value. The solution to this is to take the average current of the past 15 minutes. The graphs of the second dataset will be made using this method.

The first graph to talk about is the current-voltage (IU) graph. To make examining this graph easier, it will be divided into three parts. The first part from 0V to 1.4V can be discarded because these numbers are not so relevant, this is during the night-time when the electrolyser is not in use. When these numbers are removed from the graph it becomes more readable.

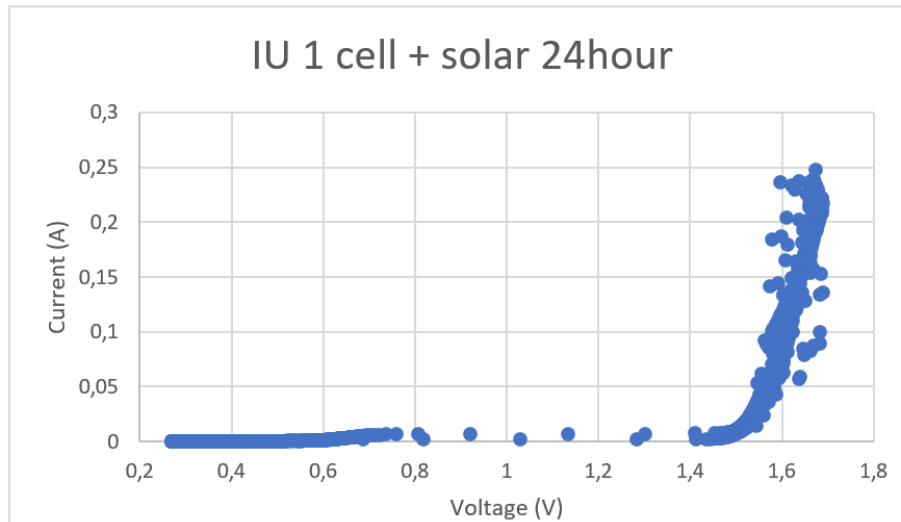


Figure 43: Full day experiment 2 IU characteristic

The second part is when the electrolyser is in its working area. These data points are acquired during the initial power-up of the electrolyser and during the daytime. From the beginning to the 400th minute in the experiment. The endpoint was chosen at 400 because then the limit of 0.08A was reached and the electrolyser is powered down. Pointed out as the red line, the same curve with its distinct curve at the top can be found. This is the second time this curve can be found so this is clearly the specific IU characterisation of this electrolyser module.

The justification of the form of the curve is the same as the last test. The loop can be explained by the rise temperature of the panel in the second part of the day. As well as the solar panel receiving different wavelengths of light due to filtering. However, the large spread of data points in the area of the curve is unlike the previous experiment. The most significant difference is the presence of clouds during the day at given intervals. These data points are most likely the reaction of the electrolyser to the change in the solar panel because of passing clouds. As said before the solar panel reacts differently when exposed to filtered wavelengths of light as well as a temperature difference. It can also be a delayed effect of the electrolyser regarding previous possibilities having an abnormal rise in current or voltage as result.

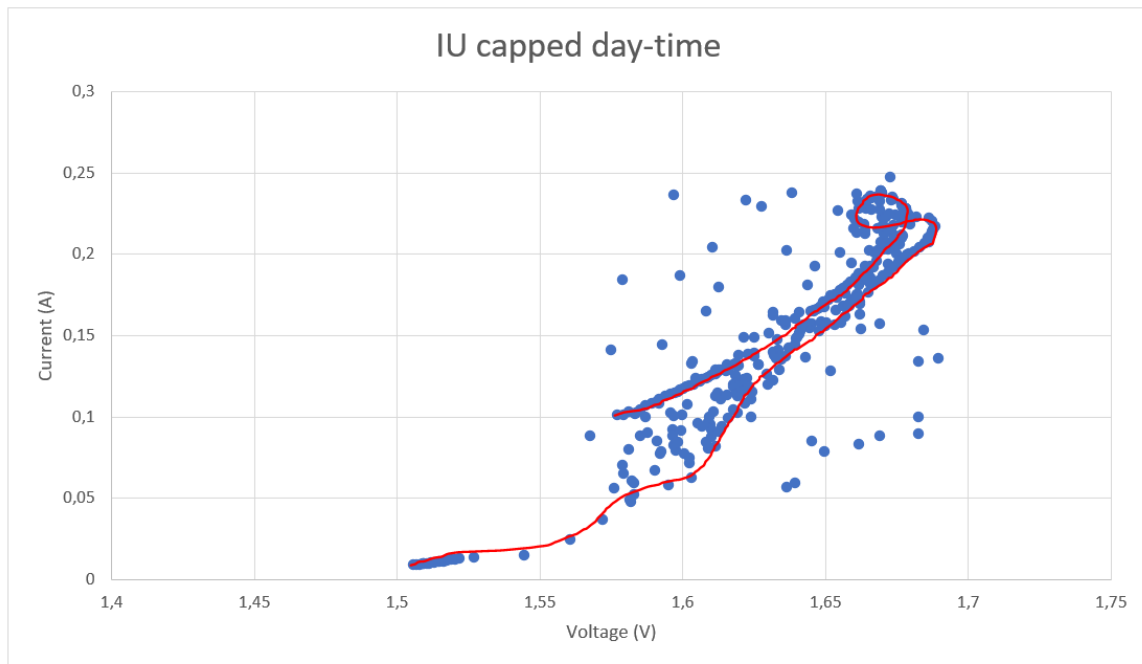


Figure 44: Full day experiment 2 IU characteristic capped

The last part is actually the data from the night and the restart of the electrolyser of the third day. This is again similar to the first day experiment. The curve behaves quadratic until it is at its gas production and operation current, from there it should go linear but the 24h of the experiment ended. The sudden jump is to be expected. In all tests when the electrolyser is started up there is a steep incline or jump to its working point when the gas production starts.

The scattering of data points in the upper part of the curve can be due to some water on the membrane of the hydrogen side? This is known to cause irregularities.

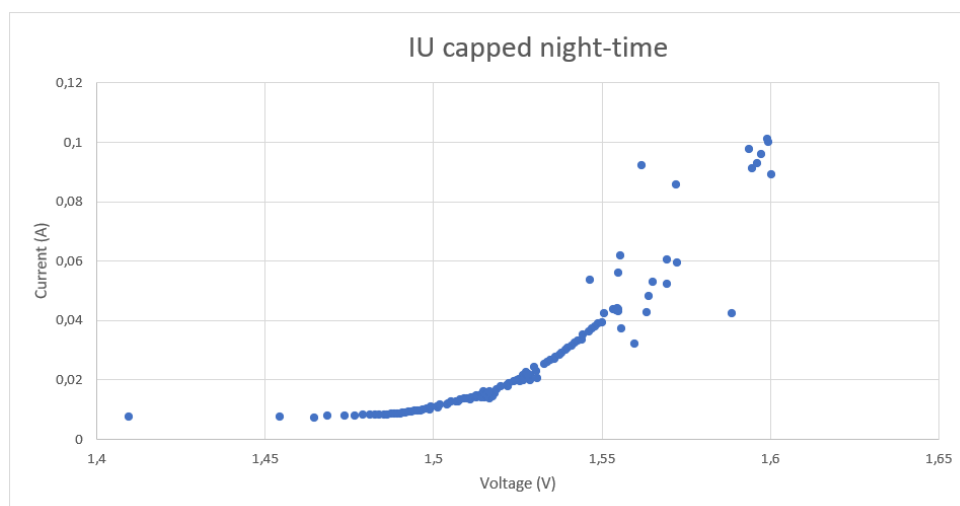


Figure 45: Full day experiment 2 IU characteristic capped night

After discussing the intricate IU graph a description of the current-time (IT) curve will be given. The general form of the curve is similar to the IT graph in the previous day test. Apart from some serious disorders that did not occur in the previous experiment. These disorders are caused by the absence of sunlight at that time, in other words clouds moving over. This causes the current to drop dramatically and temporarily halts the gas production. Furthermore, we see the yet familiar steep incline and decline in the beginning and end of the curve. This happens when the current reaches 0.05A to then rise to 0.08A in the beginning. The fast drop-off at the end is also around 0.08A to then fall and stay consistent during the dark times. At around two in the afternoon the current reaches its peak. This is when the sun's exposure level is at its maximum. Identical to the previous test. Then lastly the current stagnates just below zero.

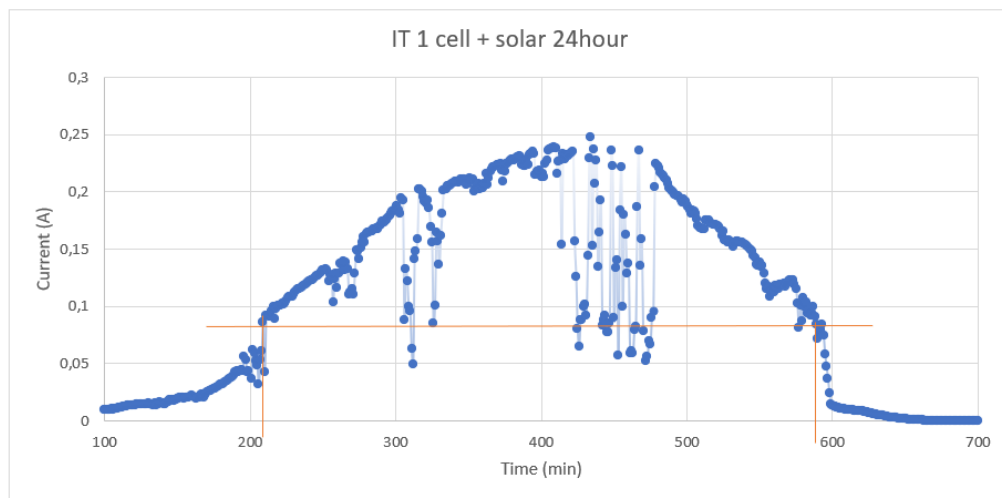


Figure 46: Full day experiment 2 IT characteristic

The orange line on the graph indicates the limit of the interval which is chosen to calculate the rate of volume production. Statistics were once again used to calculate the general average of the current and whether or not presence of peculiar values. The appropriate range in this calculation is [215;586]. This range had to be chosen to the cut-off value of 0.08A. It was a logical choice because then the gas production stopped. This resulted in 24 peculiar values, these were the last values in the range. These values were not excluded in the further calculations because these values were expected and are devoted to the clouds. The results can be found here.

Statistics	
min	0,0490561
max	0,247359
average μ	0,16100748
sigma	0,0490423
$\mu - 2 * \text{sigma}$	0,06292288
$\mu + 2 * \text{sigma}$	0,25909208
values below $\mu - 2 * \text{sigma}$	24
values above $\mu + 2 * \text{sigma}$	0

Table 10: Full day experiment 2 statistics table 1

Average	considering max prod only = graph I>0,8A		
0,1610 A	V		t_full
0,59838275 ml/min	O2	222 ml O2	371 min
1,02425876 ml/min	H2	380 ml H2	
3,71649034 ml/A*min	O2	1,71171171 ratio	
6,36156004 ml/A*min	H2		

Table 11: Full day experiment 2 significant data table 1

To explain these values, we look back and compare with the previous test results. The time in the interval is 371 minutes. The average current is 0.161A. this is lower than before. This is expected because of the number of clouds blocking the sunlight during the day. A total of 222 ml of oxygen gas and 380ml hydrogen gas is produced. The amount of gas produced is 10% lower than the previous experiment. Apparently, the clouds had a great impact on the production of the gasses during this day, but this was also confirmed by the lower average current. The ratio of hydrogen to oxygen equals to 1.712. This more than the previous test and comes closer to the theoretical value of two. Yet it does not achieve this due to inefficiencies in the system.

The oxygen values differ +0.175 ml/A*min and the hydrogen values differ -0.778 ml/A*min. The values for the rate of the volume production are not too far of the specifications, 3.571ml/A*min of oxygen and 7.14ml/A*min for hydrogen. They are also on par with the results found in the short-term experiments. Normal and expected behaviour can be concluded.

A second way of calculating the rate of volume production can be done by using the range determined by the voltage-time graph. In this graph it is shown at what point in time the electrolyser gets enough voltage to start operating and thus generating gasses. As shown in previous examples, the gas production is dependent on the current flowing through the system. Although it brings a different view and more clarity by analysing different graphs. The electrolyser powers up at minute 80. Resulting a rapid rise in voltage. During the whole operation, its voltage does not change very much. A slight rise in voltage happens when the sun progresses over time. Some inconsistencies are seen at minute 200, 300 and between 400 and 500. At these timepoints there were clouds moving over. A dip in voltage can be seen at minute 600 this is when the current drops to almost zero. When it gets too dark, at minute 650, the electrolyser drops the voltage to 0.4V and this state is consistent until the next power-up. Interestingly the voltage and current does not drop at the same moment in time. Anyway, these values give us the range for the second calculation. To maybe find a different outcome.

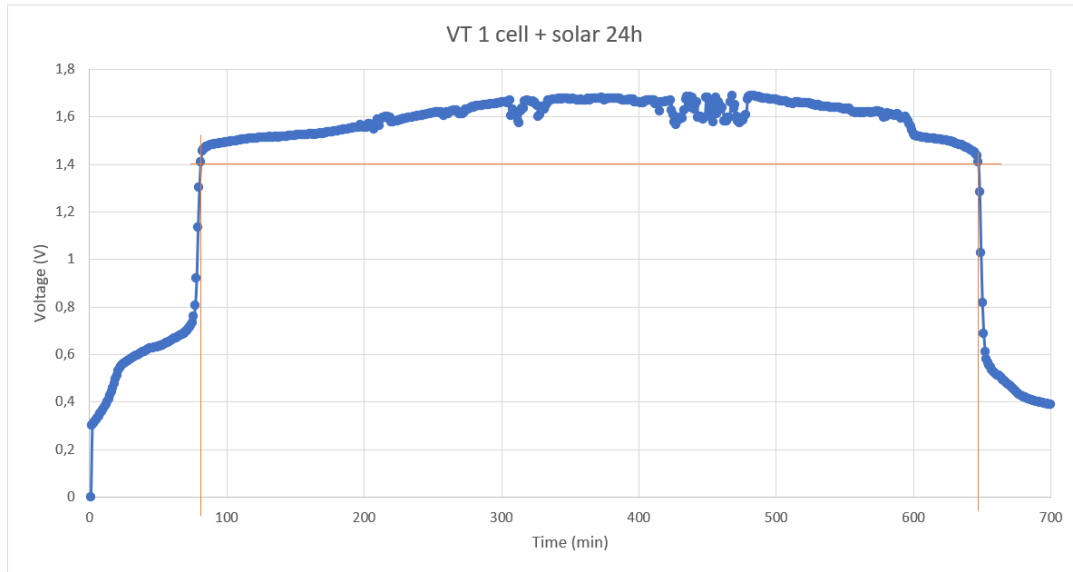


Figure 47: Full day experiment 2 VT characteristic

Statistics calculates the average current and shows no peculiar values. This is because we have a greater range with more low current values thus lowering the chance of values being too low. The calculations with the range considering current values corresponding with voltage values higher than 1.4V are made. An average of 0.113A is found this is 0.05A lower than before. This time we have the range we do not most, but all volume is created. The oxygens rate of volume production is near spec and in line with the short-term experiments. Although being a little lower than the previous method. It is the same case with the hydrogen rate of volume production value. This is to be expected because it takes more low values into account where there is almost no volume production.

Statistics

min	0,0013877
max	0,247359
average μ	0,11302716
sigma	0,0782134
$\mu - 2 * \text{sigma}$	-0,04339964
$\mu + 2 * \text{sigma}$	0,26945395
values below $\mu - 2 * \text{sigma}$	0
values above $\mu + 2 * \text{sigma}$	0

Table 13: Full day experiment 2 statistics table 2

Average	considering light time = VT graph $U > 1,4V$		
0,1130 A	V		t_full
0,39649123 ml/min	O2	226 ml O2	570 min
0,67719298 ml/min	H2	386 ml H2	
3,50792885 ml/A*min	O2	1,7079646 ratio	
5,99141831 ml/A*min	H2		

Table 12: Full day experiment 2 significant data table 2

Testing this different approach of calculating the rate of volume production has proven useful. It is now known that the previous method is more accurate because the values are closer to the specification of the electrolyser and that of the short-term experiment outcomes.

Out of the second dataset the volume production will be studied. Once more, every 15 minutes the volume was manually read together with the current at that point of time to be able to make graphs considering the volume progression. The volume-time graph has the general “S” form and can be seen in both curves. This is exactly the same form as the curve in the previous experiment. Implicating a slower volume production at the beginning and end of the experiment. At the start it can be seen that the volume of the oxygen gas is lower than the hydrogen gas. This is because some bubbles got into the flask during the setup of the experiment. Later this is deducted in the calculations. This is also why for the first 25 minutes the oxygen volume is higher than the hydrogen level. To conclude, the curve has a gradual and predictable development with a slower progression at the start and end.

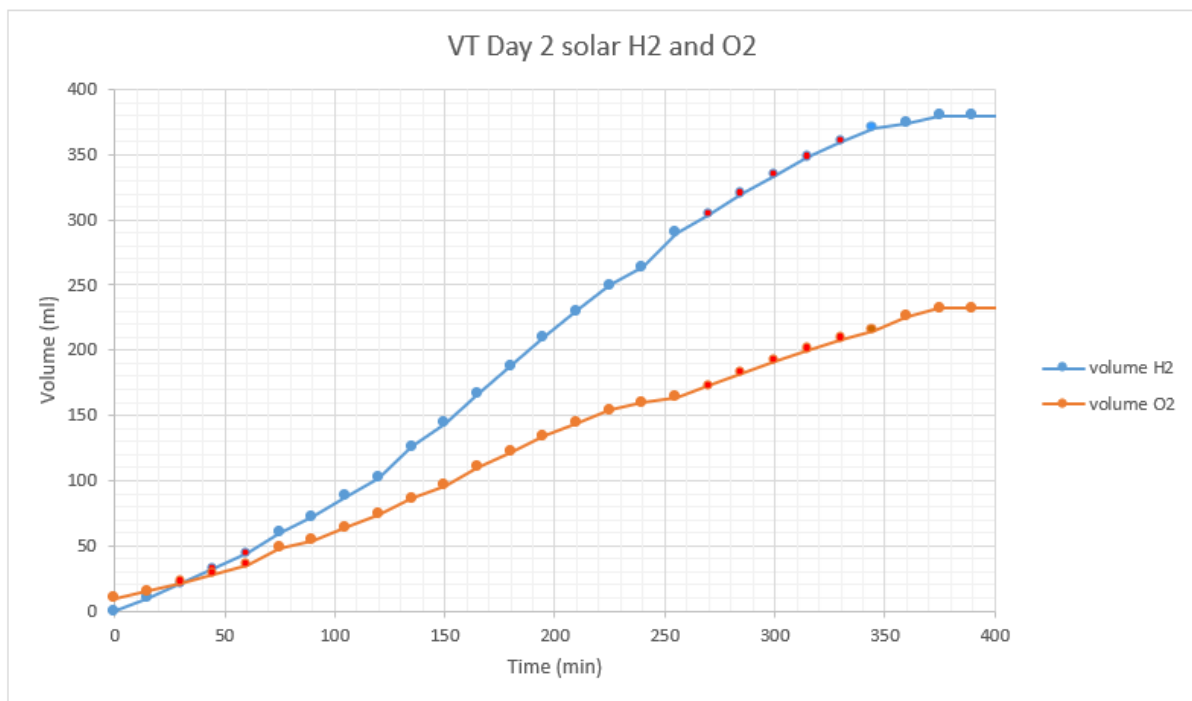


Figure 48: Full day experiment 2 VT characteristic combined H2 and O2

The next graph is the current-volume (IV) characteristic. Here it can be seen that the slope of both curves is steep in the beginning and end. It means that there is little gas production but a fast rise in current. The curve starts and ends at 0.1A this is when the gas starts to flow, as seen in previous tests. The current data, which is used, is the average of the current during the 15-minute interval. To get more accurate data and prevent a high clouded interval with one point of intense light to then be measured at the high point, giving an incorrect low volume production at a high light intensity point. Furthermore, it seems that the hydrogen graph is more spread out but not twice as long as the graph of oxygen, because the ratio is not 2. Once again, the progression of the sun moving can be seen by the gradual rise and decline of the current until it drops when the intensity does not suffice anymore. In contrast to the test the day before, the data points on the curve are very irregular. Two big dips in the curve can be seen. This can be explained by the presence of the clouds. They block the sunlight

therefore restricting the power output of the solar panel and lowering the current and volume production.

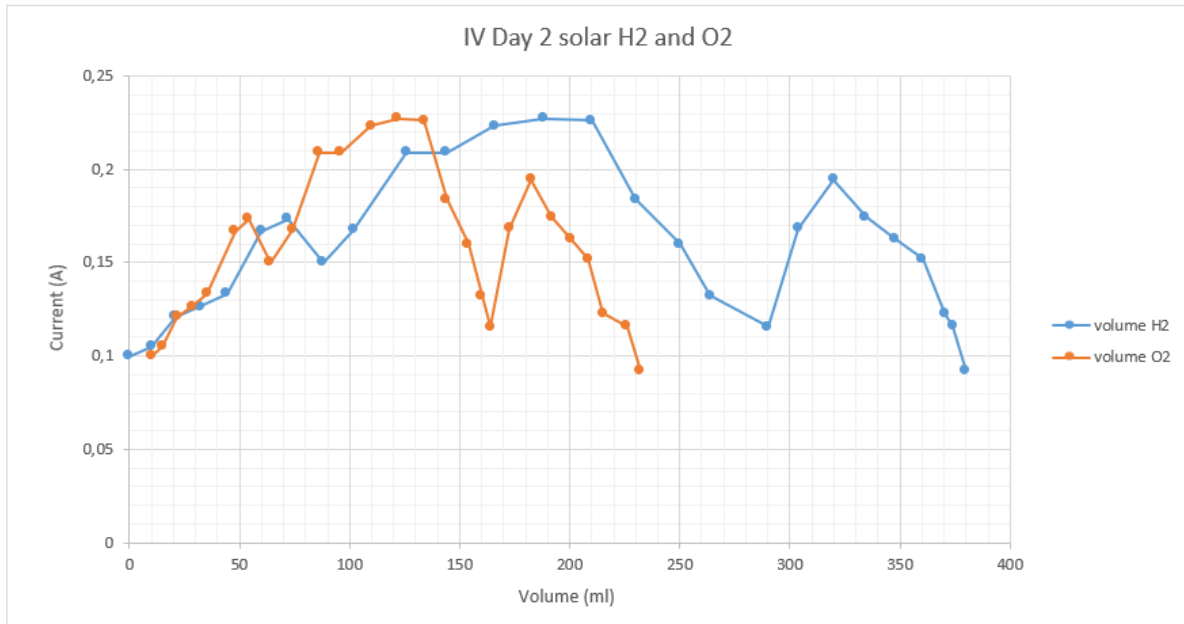


Figure 49: Full day experiment 2 IV characteristic combined H₂ and O₂

3.4.8 Conclusions electrolyser

The total volume produced will give a perspective on the range of the catamaran. The 0.1A is the threshold for producing hydrogen and clouds have a negative effect on the gas production. With a maximum of around 0.25A in this configuration. As soon as there is direct sunlight hitting the solar panel, the electrolyser will hold a stable voltage of 1.5V. Peak power is achieved at midday and amounts to 400mW. Hydrogen production values are accurate regarding the datasheet, close to 7ml/A*min. The results will be used to dimension the power system for the model catamaran.

These full day experiments give more insight into the actual development of the system in two different scenarios. It is interesting to see an ideal day compared with a more realistic day, regarding some clouds. This caused some inconsistencies which are explained in its appropriate part. The study of the voltage-current (VI) graph was unexpected and educational. As well as the current-time (IT) diagram providing important data about the start and end point of the gas production. It is now known above which values the current must be to start producing hydrogen and oxygen. The voltage-time (VT) graph proved to be an interesting second look into the method of determining the range for the volume calculation, however it seemed to be less accurate than the method using the IT graph. The volume-time (VT) graph shows at what rate the volume increases, no surprises here, the "S" shape was to be expected. To finalise the combined current-volume (IV) diagrams showed to be interesting to see the rate of volume production. During the ideal sunny day this was a nice consistent graph but during the cloudy day the change in current showed big changes in the course. At this point the characterisation of the electrolyser mode of the PEM reversible cell is now complete, being provided with all the necessary information to continue further progress in the project.

3.5 Fuel cell practical experiments

This part will describe the characterisation of the PEM-reversible fuel cell in the gas consumption mode or fuel cell mode. The fuel cell is supplied with hydrogen gas and oxygen gas, the cell produces electricity. This must be done to completely understand the functioning of the fuel cell in the operation conditions it will be exposed to. As well as finding its maximum production values and limitations. This is an important step for determining the conversion efficiency later.

The goal is to make the current-voltage (IV) curves and power curves to compare against each other and combine them. Comparing the graphs to a theoretical form of the curve and the specifications on the datasheet. Many tests will be conducted with altering parameters to find the optimum, more in particular, to find the optimal pressure to be supplied to the fuel cell. Curves from the same setup will be combined in an easy-to-read graph and conclusions will be drawn.

There are two fuel cells available, supposedly with the same specifications, they will be compared to each other. The characteristics will be made by using a variable resistor to accurately track the behaviour of the fuel cell. In further experiments the resistor will be replaced by an electrical motor. Therefore, the motor curves and characteristics must be made as well. The motor power curve and fuel cell power can be combined to then calculate the working point of the system.

After calculating the operating point, it can be verified by doing the practical experiment, attaching a motor to the fuel cell while supplying the gasses. The characterisation of this process can be noted and compared. The experiments will be conducted using different pressures to find the optimal working condition. Or to find if the pressure is relevant at all. These experiments can then be repeated for the second fuel cell and compared. If the power is sufficient, two motors in parallel can be connected to the circuit instead of one. The results of these experiments will give more insight on the behaviour of the fuel cells under different loads and supplied gas conditions.

3.5.1 Graph comparison

To get a better idea about the shape of the curves, research has been done to find similar experiments. Figure 50: Polarisation curve 2 [29] comes from a study researching polarization and the power density curves of the 1kW class PEM fuel cell 20-cell stack, written by Kap-Seung Choi [27]. Providing a good starting point to compare the test results from upcoming experiments. On the other hand, Kap-Seung Choi researched powers far greater than this experiment, for example their maximum power goes up to 1KW where these experiments do not exceed 1W. Because this experiment is also using PEM fuel cells it can be presumed that the general shape of the curve will match the shape of the curve in Figure 50: Polarisation curve 2 [29], similar to the one seen in the theoretical background.

The graph shows two curves, one is the IV curve demonstrating the relation of voltage and current of the fuel cell, the other is the PI curve or the power curve. The power curve visualises the power in relation to the current while also locating the maximum power point. Kap-Seung Choi repeats these results one time by using pure hydrogen and oxygen gas, the other time using air instead of oxygen gas. This will be replicated once in the following experiment because at low power this gives worse efficiency.

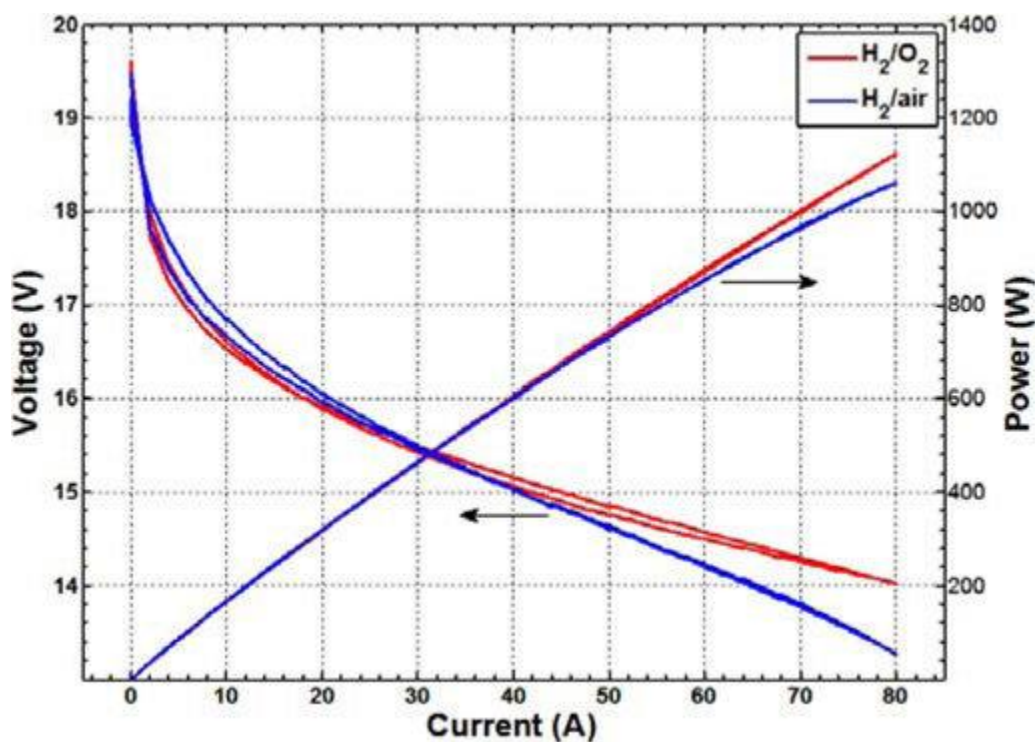


Figure 50: Polarisation curve 2 [29]

3.5.2 Fuel cell characterisation with potentiometer

To characterise the fuel a variable resistor will be used to slowly range through the power curve. While doing this the current and voltage will be measured. Later the variable resistor will be replaced with a motor to simulate the eventual load on the system. The goal is constructing the IV-curves and the power curves to then compare the results and determine the best operating pressure. Also equate the results with the curve in Figure 50: Polarisation curve 2 [29].

3.5.2.1 Setup

Show below is a schematic of the setup as it was built in the lab. Two bottles, hydrogen gas and oxygen gas were connected to the ports of the fuel cell, each has its dedicated regulator. To note, hydrogen needs a special regulator because of the special nature of the gas. It is a much thinner gas eager to escape. Furthermore, a variable resistor was connected to the electrical output of the fuel cell in combination with a voltmeter and a current meter. For this purpose, the Keithley 2601 Source Meter was used to acquire the current data and the Agilent 34401A multimeter is used for measuring the voltage. Both lowest gas-ports of the fuel cell were blocked off, but if needed the one on the oxygen side could be removed to release piled up water or vapor. Water in one of the chambers can negatively affect the efficiency of the system.

Schematic:

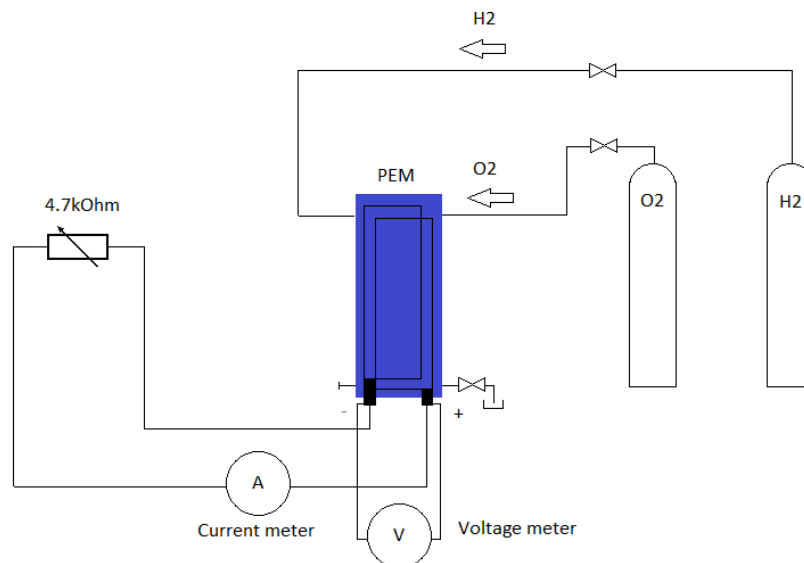


Figure 51: Fuel cell characterisation schematic

3.5.2.2 IV curve

The first graph to construct is the combined IV-curve graph. Nine similar tests were conducted by gradually adjusting the pressure of the hydrogen and oxygen glasses. The first curve was made by only connecting the hydrogen gas tube, as it seems, this is far less effective than using both gasses. Looking for maximum power both gasses will be supplied further. The maximum voltage from the fuel cell is 1V and the maximum power is 180mA. There is some difference compared to the datasheet, voltage

wise it is quite similar 600mV is what the datasheet describes. The current on the other hand is rather low, the datasheet describes 300mA of current. The shape of the curves is similar to the shape of the experiment from Kap-Seung Choi, which is good. It can be seen that when there is a sufficient amount of gas molecules the curve behaves similarly and there is not much difference between them. The curves are negatively linear, when the resistor value increases the voltage goes down and the current goes up. The test pressures range from <0.25bar to 2bar. Not exceeding any further to protect the membrane from damage and preventing the fittings from coming loose.

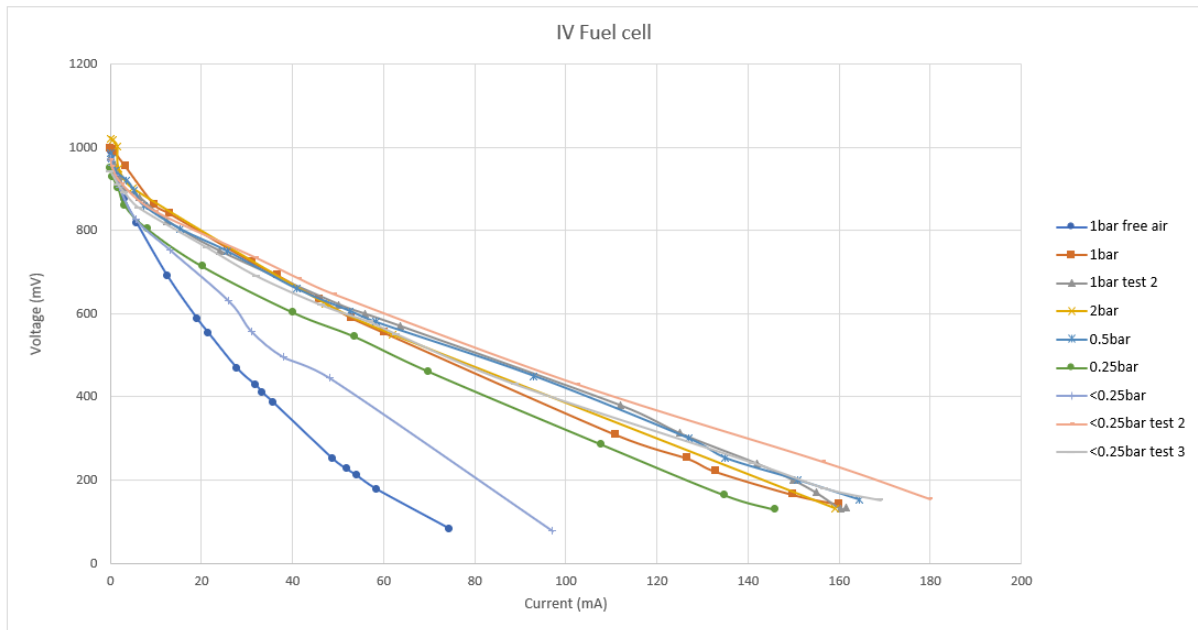


Figure 52: Fuel cell IV characterisation

3.5.2.3 Power curve

Next is the power curve, this is important to find out what load can be powered. It shows the maximum power point as well as the corresponding current values. This curve will also be used to calculate the operating point of the system once a motor is added as a load. The power curve is in relation to the current. The nine experiments were performed in the order as shown in the legend next to the graph. The shape of the curves is for the first part equal to the curve of Kap-Seung Choi, the part after the maximum is left out in the graph of Kap-Seung Choi. Comparing the results to the datasheet, the power is rather low with just 45mW at best. Normally the maximal power should be 180mW. This can be an indication that the fuel cell is not performing optimally at the end of its life.

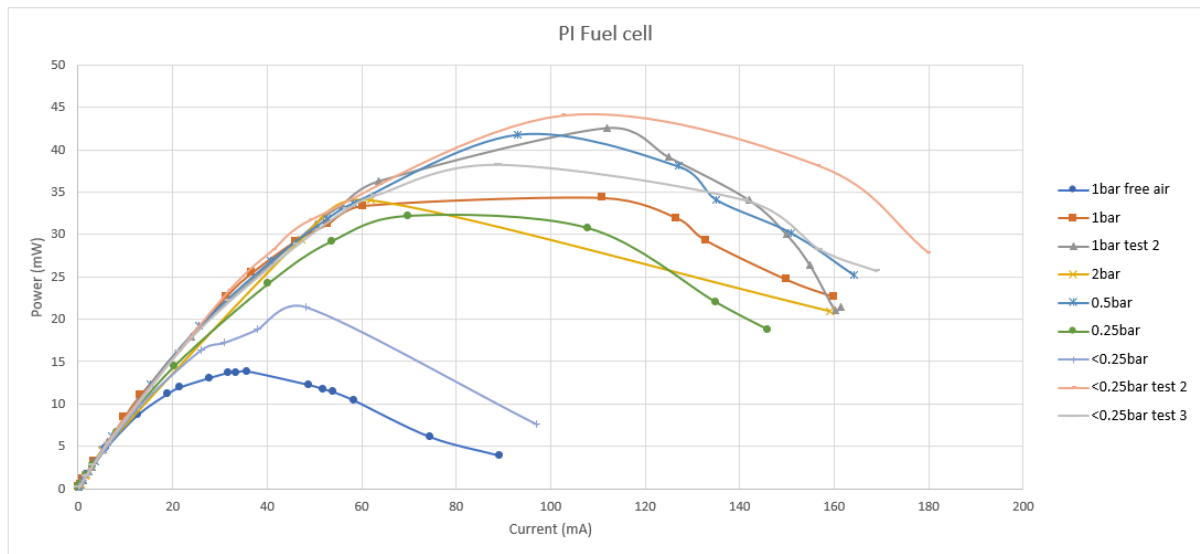


Figure 53: Fuel cell PI characterisation

The individual results will now be discussed. The first test is done with just hydrogen and no oxygen tube attached. This resulted in the lowest curve concerning the power output. This is because air has only 21% oxygen therefore lowering the efficiency. Then the oxygen is attached, and the experiment is repeated, this gives better results. After that, the pressure is increased to two bars and lowered to find the minimal pressure where the fuel cell will produce electricity. It can be seen that by increasing the pressure there is not necessarily an increase in power, on the contrary. While trying to find the minimal pressure there were some difficulties in regulating the pressure. Below 0.5bar it is difficult to read the indications on the gauge, which progresses in increments of 1bar.

The second lowest curve is the threshold value for a stable operation, the pressure was minimal a small puffing noise could be heard if the end stops were removed. The next day this experiment was repeated with the same setting, this time reaching the best values. This explains the phenomenon that saturation of the membrane with water, lowers the efficiency. The <0.25 test 2 was the first test thus using a completely dry membrane.

To conclude it is important to have enough hydrogen and oxygen gas molecules reaching the membrane, not necessarily under a high pressure. Secondly the best performance is achieved when the hydrogen membrane is as dry as possible. This can be achieved by not operating at the maximal current or ventilating once in a while.

3.5.2.4 Combined curve

The IV curve and the power curve are combined in one graph. The example below is the best scenario from before. In this graph the voltage and power can be seen in relation to the current. This makes it possible to see the corresponding current and voltage values at a given point on the power curve.

This graph can be compared to the graph from Kap-Seung Choi. It is very similar in the case of the shape of the graph. There is a sharp decline in the beginning of the IV curve to then progress more linearly. The power curve has a more parabolic evolution. They cross each other in the middle before the maximum power point.

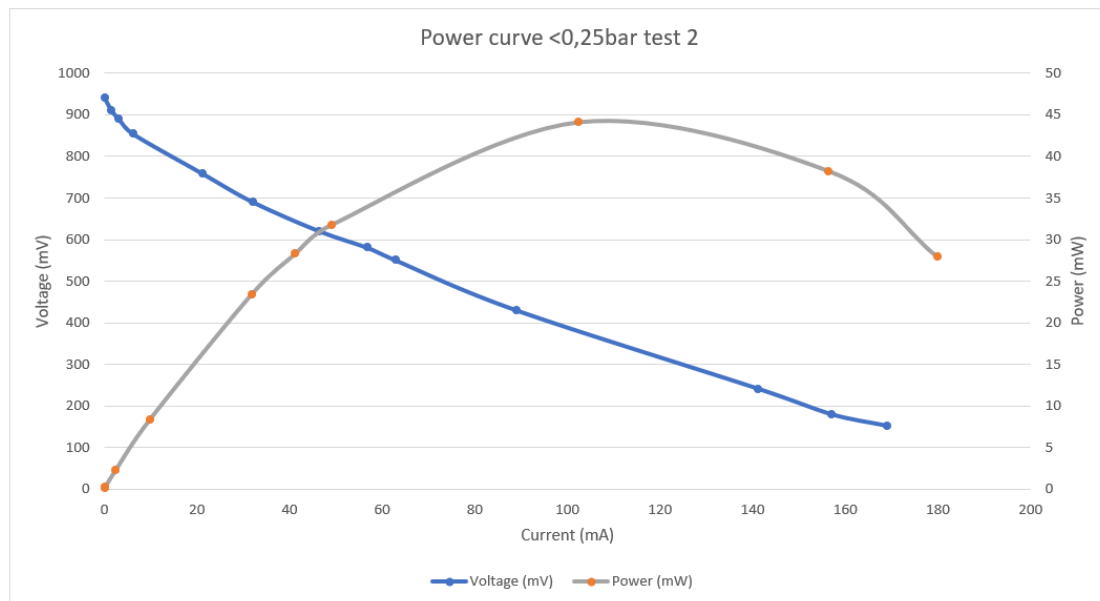


Figure 54: Fuel cell power curve

3.5.3 Second fuel cell characterisation with potentiometer

Since a second fuel cell was available it was interesting to repeat this experiment with the other one. All previous experiments were done using the first fuel cell because the second fuel cell proved to be less reliable. Therefore, testing the characterisation would help to explain the differences.

3.5.3.1 IV curve

Just as before, the first graph to construct is the IV curve. The shape of the curve is similar to the first experiment, this is normal. Taking a look at the values, the voltage is the same, but the current is much higher. A current of 650mA is a lot compared to the 300mA max current the datasheet describes. Despite this, all curves lay close to each other even though the pressure ranges from <0.25bar to 2bar.

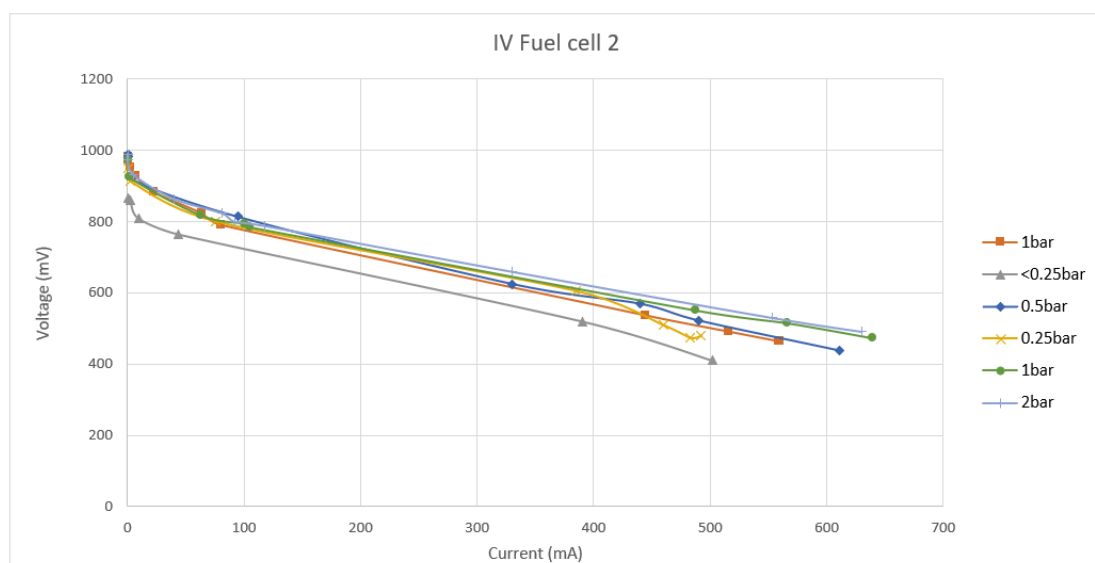


Figure 55: Fuel cell 2 IV characterisation

3.5.3.2 Power curve

The shape power curve is close to the one seen in the research from Kap-Seung Choi. This time it was not possible to get information about the further progression of the curve due to the limited range of the variable resistor and also the unreliability of the fuel cell. The values of the power curve exceed the maximal values of the datasheet quite a lot, the datasheet describes a maximum power of 180mW in this experiment the maximum power is more than 300mW. This aside, the advancement of the curves lay close to each other despite the range in pressure. At the end there are many curves crossing each other so it is difficult to draw conclusions. What can be said is, in this case a higher pressure has the advantage regarding the maximum power. On the other hand, there were many problems with the cell at this point.

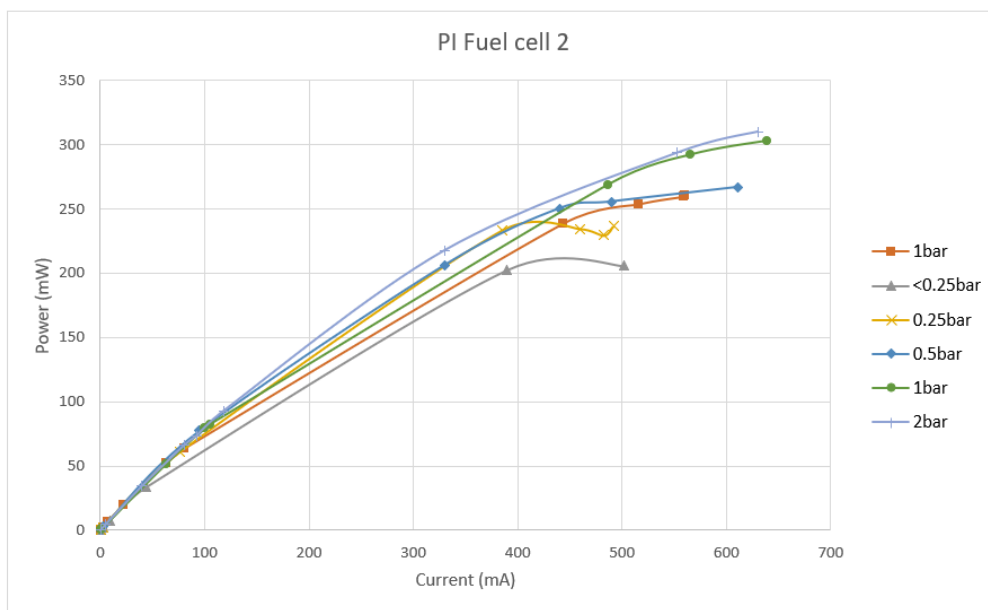


Figure 56: Fuel cell 2 PI characterisation

This time when attempting the measurements, it was hard to get consistent data because many of the fuel cells warmed up a lot and fogged up the hydrogen membrane chamber. When this happens, the power drops drastically and the experiment data is useless, normally this side stays dry. Before reattempting the experiment, the fuel cell has to cool off and be dry. This is a sign that the fuel cell is at the end of its life and needs to be replaced. This can also be deduced by the abnormal high values seen in the current and power, far exceeding the datasheet. But the most obvious giveaway is the unreliability of the cell. This makes the cell not usable for further advancements.

3.5.3.3 Combined curve

The graph made here looks again similar to the Kap-Seung Choi's graph as well as the previous experiment with the other cell. Despite the values for the power and current exceeding the maxima in the datasheet this still fits the shape well. This time the dataset from the experiment using 1 bar is used because it has the most data points near its maximum.

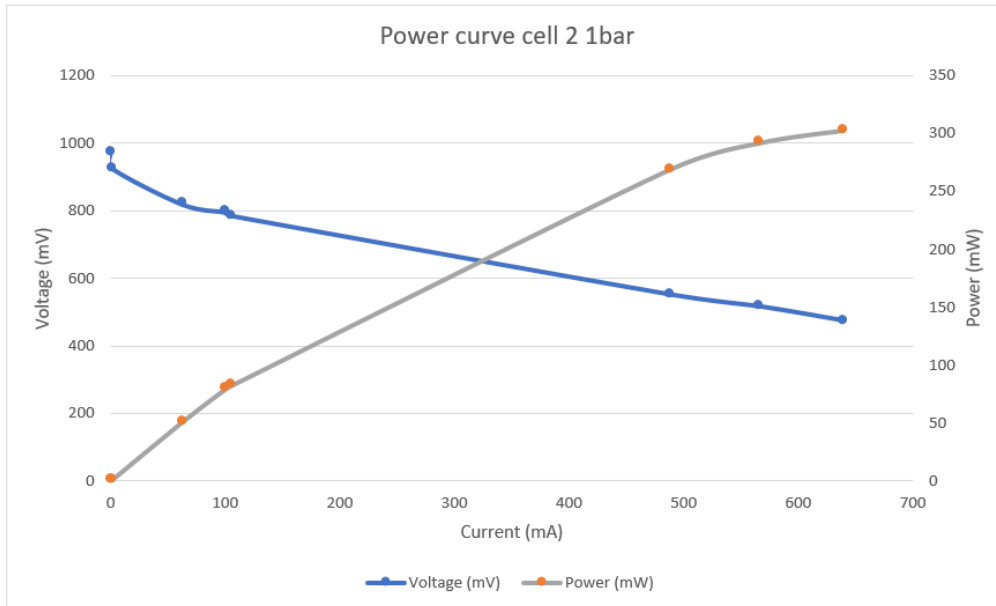


Figure 57: Fuel cell 2 power curve

3.5.4 Fuel cell characterisation using the motor

Instead of the variable resistor a more practical load will be applied. Since the model ship has to be propelled in some way there is the need for a motor. Therefore, the next experiments will be executed using a small brushless DC motor. First the motor will be characterised. When this is done it is possible to calculate the operation point for a given pressure. This can then be taken into practice and connect the whole circuit to carry out the experiment. Alongside the operation point a load will be applied to the motor by braking on the shaft to study the effect on the power. The relevant graphs will be made and explained in the following sections. In case the power is sufficient the effect of two motors will also be investigated. Following experiments will be carried out on the first fuel cell.

3.5.4.1 Motor characterisation

The motor is characterised by connecting it to a power source and slowly increasing the resistance with a 4.7kOhm variable resistor. Meanwhile measuring the current and voltage with the Keithley 2601 Source Meter and the Agilent 34401A. The values were written down to calculate the power in each point, by connecting these points the power curve for the motor is constructed for the motor running without a load on the output shaft.

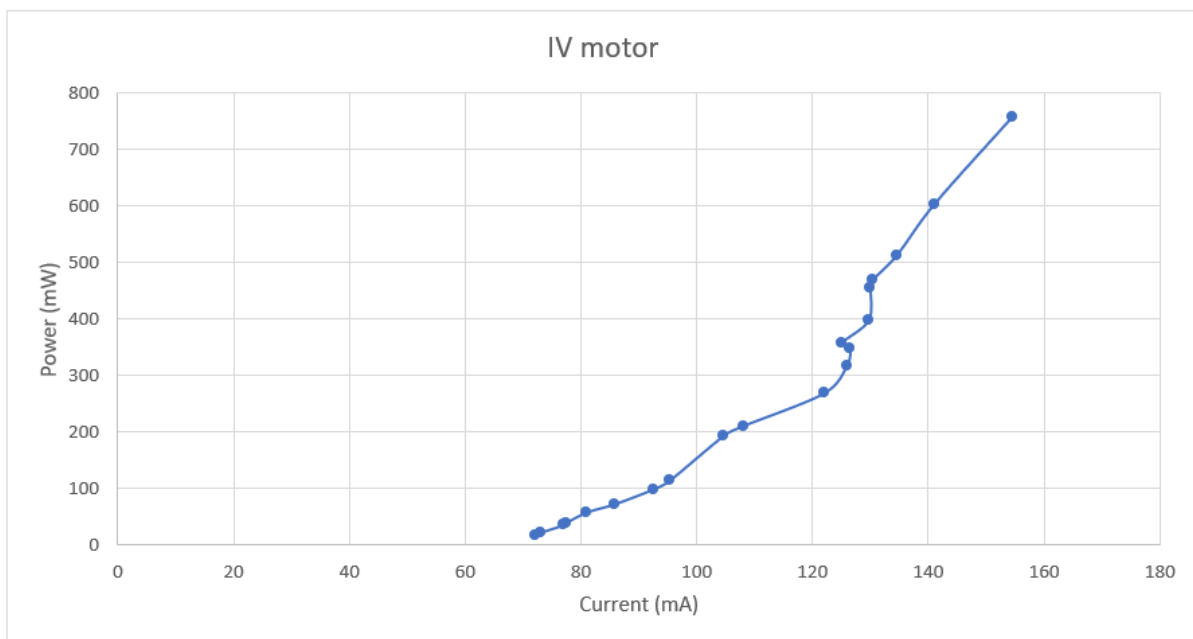


Figure 58: Motor IV characterisation

3.5.4.2 Operating point

The operating point of the system consisting of the motor and the fuel cell is the point where both curves cross each other. Both curves have been put together and can be seen in the graph below. This is the theoretical calculation of this point and will be checked later by a practical experiment.

The operating point for the motor spinning without load is calculated at 40mW and 80mA. The power curve used for the calculation is measured at 0.5bar with supplied gas.

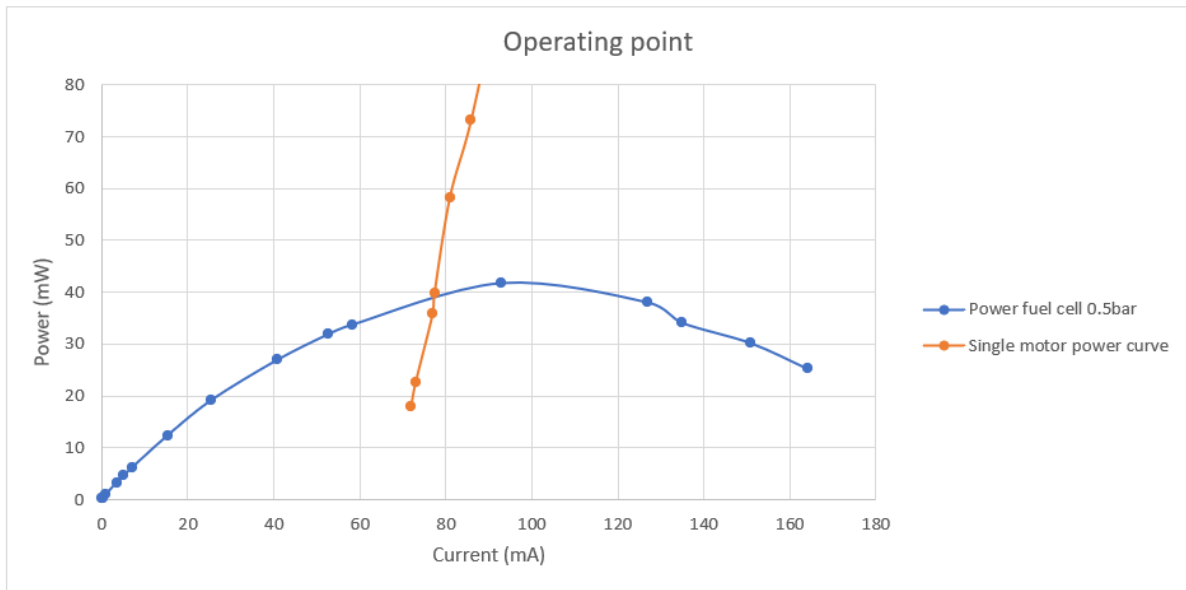


Figure 59: Motor operating point

3.5.5 Fuel cell and motor testing

The next step is to combine the motor and fuel cell in one circuit and study its behaviour and compare it to the calculated operating point. The image below shows the circuit. The two bottles of gas are connected to the fuel cell which is directly connected to the motor. Voltage and current are once again measured by the Keithley 2601 Source Meter and the Agilent 34401A and manually written down.

Schematic:

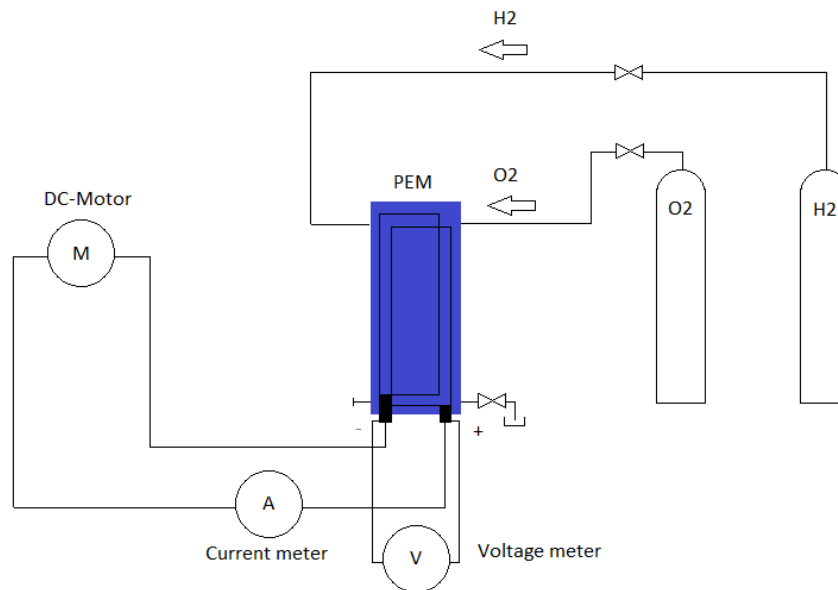


Figure 60: Fuel cell and motor schematic

This time it is the goal to see if different pressures give different outcomes regarding the power of the motor. To once again look for the optimal operation pressure for the system. The IV curve and PI curve will be constructed and compared. The best curve will then be used to find the operating point.

The pressure is gradually increased to analyse the effect of it. Seven tests were performed. Since leaving the motor running at a set speed would not give any beneficial information except for the operating point without load, the motor shaft was slowed down by applying a braking force until the motor stalled. This is what can be seen on the graphs below.

3.5.5.1 IV curve

The first graph consists of the IV curves with the voltage over the motor starting around 500mV and decreasing to 300mV. As well as the current drawn in the system starting at 80mA and increasing to 140mA. This is a common behaviour for dc motors to drop voltage and rise in current when a load is applied.

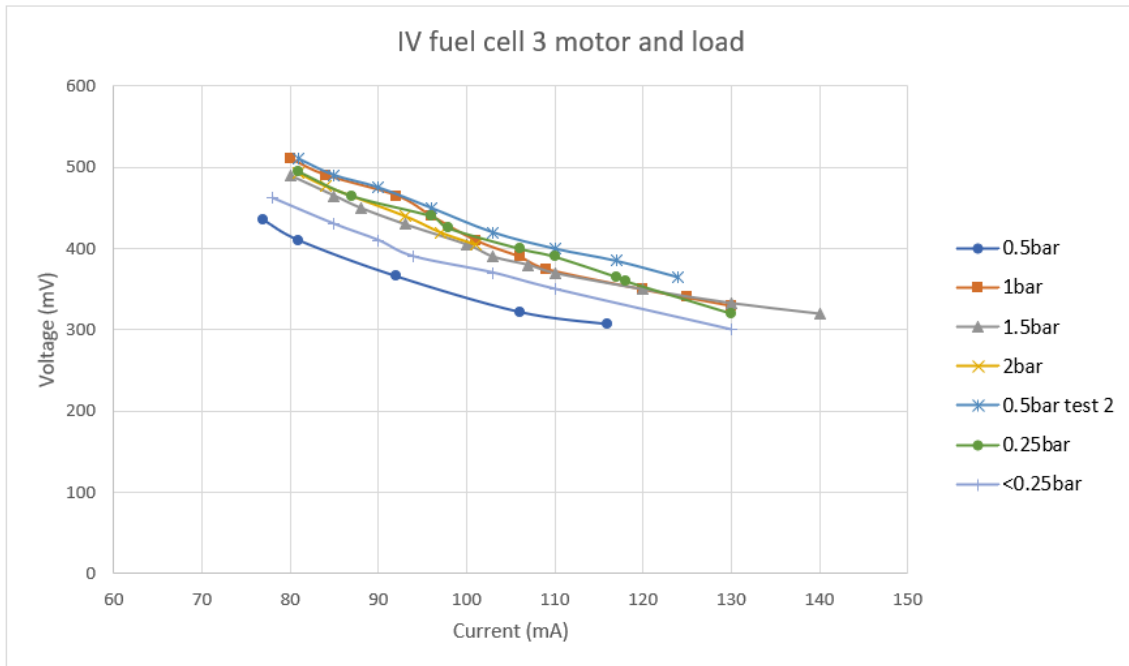


Figure 61: Fuel cell and motor IV characterisation

3.5.5.2 Power curve

The second graph is the power consumed by the motor in relation to the current through the circuit. As found before and now confirmed once again, increasing pressure does not necessarily equal more power. The optimal result in this test is the 0.5bar second test. The explanation for this curve to be higher than the first test is the hydrogen side of the membrane was drier than the first test thus having a better efficiency. The second 0.5bar test was performed after letting the fuel cell sit for some time.

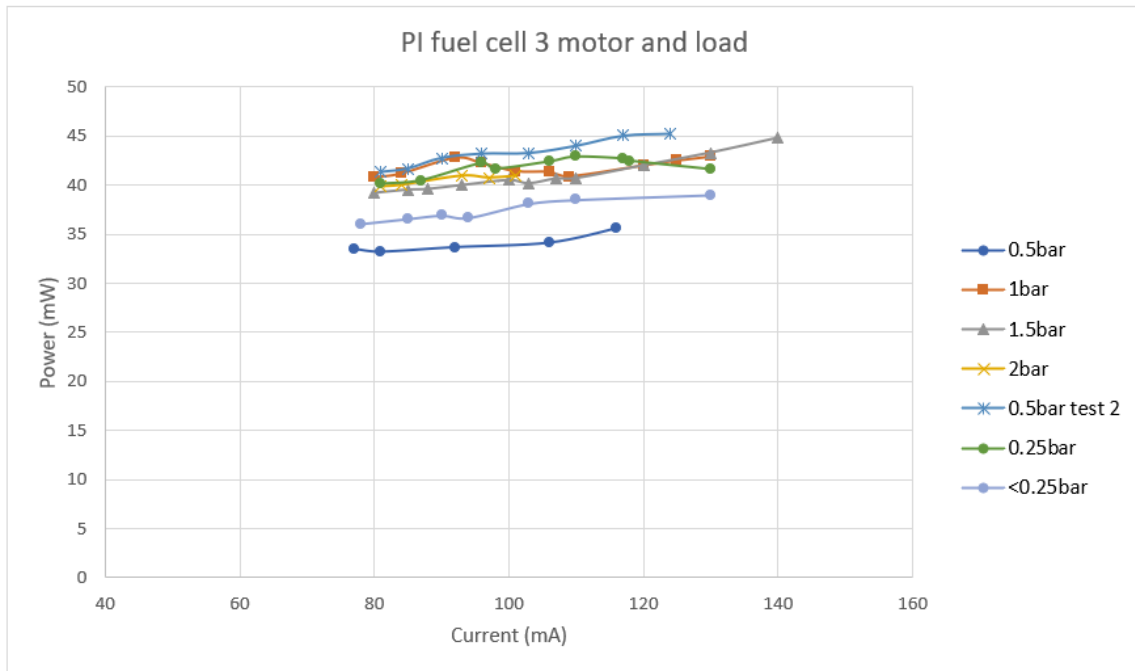


Figure 62: Fuel cell and motor PI characterisation

3.5.5.3 Combined power and IV curve

Focusing on the best performing curve, this graph shows a steady 40mW power curve on the same graph as the IV curve. The graph visualised the voltage drop over the motor while the used power remains constant.

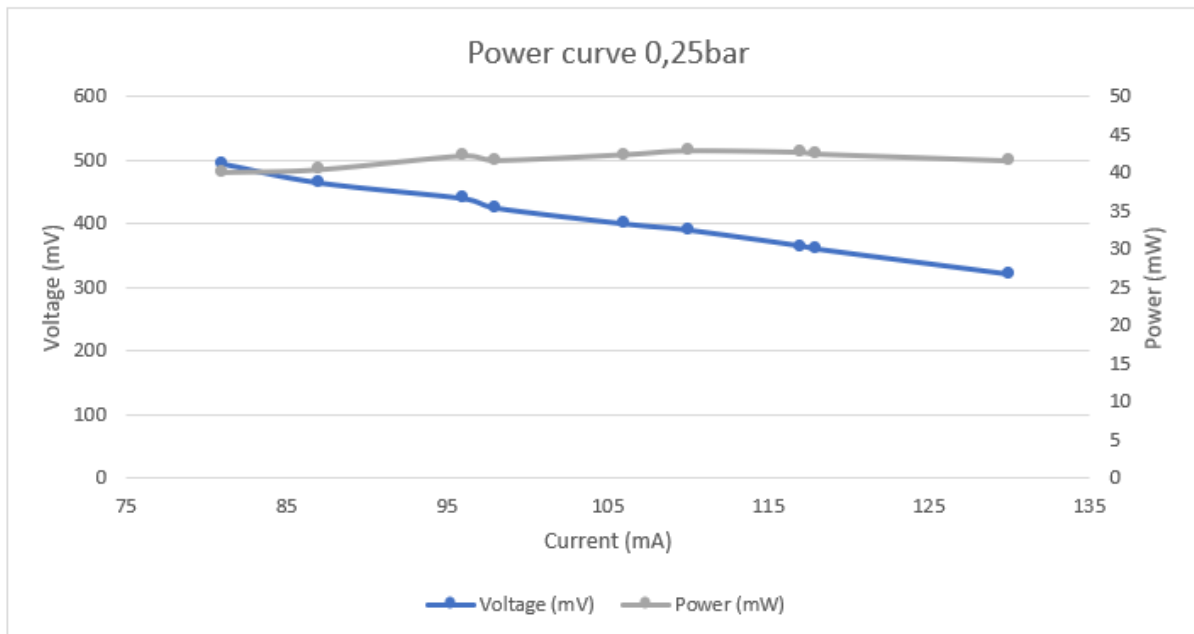


Figure 63: Fuel cell and motor power curve

3.5.5.4 Operating point complete graph

Combining all data from the previous tests, this is the complete graph of the power curve and its operating points. The power curve of the best performing pressure is chosen, they were all close together but +0,5 bar proved to be optimal.

As seen before, the dark blue curve crossing the orange curve gave the theoretical operating point. The light blue curve is the practical experiment where the motor and fuel cell are combined in one circuit and the orange curve is the motor curve of a single motor. The starting point of this graph is equal to the calculated operating point without load. This is rather close thus assumably correct. The further progression of the single motor power curve is when a load is applied to the shaft. As presumed, this curve follows the power curve from the fuel cell. Except the end of that curve is slightly different, this can be expounded by small variations in testing conditions.

Because the provided power by the fuel cell was sufficient, a second motor was added in parallel. All previous tests done with the single motor were repeated with the second as well, below is the summary. As expected, the current doubled as seen on the grey curve, this is the dual motor power curve. Again, the predicted operating point is where the dark blue curve crosses the grey curve.

The yellow curve resembles the dual motor power curve measured at 0.5bar. Values lay close enough to the theoretical operation point that this can also be assumed correct, the small deviations can be dedicated to minor variations in testing conditions. The yellow curve follows the dark blue curve as well when a load is applied and the operating point shifts forwards.

The table below the combined graph resembles the data where the graphs from before are put together with. The numbers colour coded with its corresponding curve.



Figure 64: Fuel cell and motor operating point

D fuelcell 3 + pot 251120 (page 7 +0,5bar) fuel cell 0,5bar - no load			D motor charac 251120 motor - no load		D motor + fuelcell 251120 (page 5 0,5bar) fuel cell + motor + (load)		
Voltage (mV)	Current (mA)	Power (mW)	Current (mA)	Power (mW)	Voltage (mV)	Current (mA)	Power (mW)
153,4	164,3	25,20362	108	210,924	510	81	41,31
200	151	30,2	104,6	193,51	490	85	41,65
253	135	34,155	95,3	114,6459	475	90	42,75
300	127	38,1	92,5	99,16	450	96	43,2
450	93	41,85	85,9	73,1009	420	103	43,26
580	58,2	33,756	81	58,32	400	110	44
606	52,6	31,8756	77,4	39,7062	385	117	45,045
660	40,8	26,928	77	35,882	365	124	45,26
750	25,6	19,2	73	22,484			
803	15,35	12,32605	72	18			
860	7,23	6,2178					
895	5,18	4,6361					
920	3,55	3,266					
943	0,99	0,93357					
972	0,23	0,22356					
986,9	0,1829	0,18050401					
			D DUAL motor charac 251120 motor - no load		D dual motor +fuelcell 3 +0+5bar fuel cell + motor + (load)		
			Current (mA)	Power (mW)	Voltage (mV)	Current (mA)	Power (mW)
			311	1478,183	280	140	39,2
			265	927,5	263	143	37,609
			158,8	121,482	244	152	37,088
			142	59,924	230	158	36,34
			130	30			

Table 14: Fuel cell and motor significant numbers for calculating the operating point

3.5.6 Second fuel cell characterisation using the motor

Although this fuel cell is unreliable, it is interesting to see how the fuel cell would perform attaching one or two motors to the output. The same tests as in the previous experiment were executed. Below is the graph combining all data, this is the complete graph of the power curve and its operating points. The power curve of the best performing pressure is chosen, in this case 1bar proved to be optimal. The dark blue curve crossing the orange curve gives the theoretical operating point.

The curve for the practical experiment where the motor and fuel cell are combined in one circuit could not be made because the fuel cell heated up quickly and interrupted the experiment. The orange curve is the motor curve of a single motor.

This fuel cell offered significantly more power than the other one, so a second motor was added in parallel. The previously failed test done with the single motor was repeated with the second motor. The current doubled by adding the second motor, as seen on the grey curve, this is the dual motor power curve.

The predicted operating point is where the blue curve crosses the grey curve. The yellow curve resembles the dual motor power curve measured at 1bar. Values lay very to the theoretical operation point. The yellow curve follows the blue curve when a load is applied and the operating point shifts forwards. The small deviations can be the result of minor variations in testing conditions.

This fuel cell remains very impractical in use but when the experiments succeeded, the results were useful and confirmed the findings that were built on the results from the tests on the first fuel cell.

The table under the combined graph contains all data points used for constructing the graph. Values are colour coded to make it visually easier to connect the data with its corresponding graph.

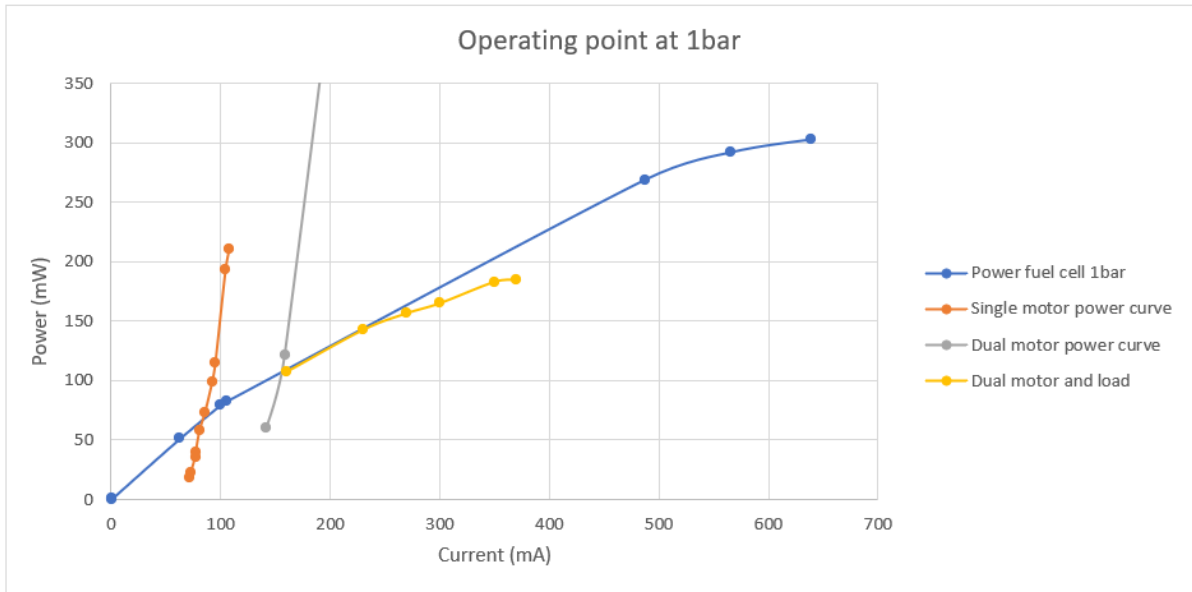


Figure 65: Fuel cell 2 and motor operating point

D fuelcell 2 + pot 251120 (page 7 +1bar) fuel cell 1bar - no load			D motor charac 251120 motor - no load		D dual motor +fuelcell 2 motor - no load	
Voltage (mV)	Current (mA)	Power (mW)	Current (mA)	Power (mW)	Current (mA)	Power (mW)
		0	108	210,924	311	1478,183
474	639	302,886	104,6	193,51	265	927,5
516	566	292,056	95,3	114,6459	158,8	121,482
552	487	268,824	92,5	99,16	142	59,924
785	105	82,425	85,9	73,1009	D dual motor +fuelcell 2	
795	100	79,5	81	58,32	fuel cell + motor + (load)	
818	63	51,534	77,4	39,7062	Current (mA)	Power (mW)
926	1,21	1,12046	77	35,882	160	107,2
973	0,182	0,177086	73	22,484	230	142,6
			72	18	270	156,6
					300	165
					350	183,05
					370	185

Figure 66: Fuel cell 2 and motor significant numbers for calculating the operating point

3.5.7 Additional fuel cell characterisation

A third, additional fuel cell will be characterised to evaluate its performance in comparison to the reversible one. Results should be similar because the same technology is being used and the fuel cell comes from the same manufacturer. This fuel cell has an output power of 270mW, output voltage of 0.6V (DC) and an output current of 0.45A.

The fuel cell is characterised in a similar way than before. Hydrogen is supplied and stored in the container under light pressure. Then the voltage and current are measured while ranging through a 4.7kOhm variable resistor.

3.5.7.1 Setup

In the schematic below can be seen how the circuit is constructed. Hydrogen is supplied from the storage and connected to the fuel cell. A purge valve is added to get rid of the air in the unit before testing. Electrically, the resistor is connected to the positive and negative terminals and a voltage and current meter is added to measure the quantities.

Schematic:

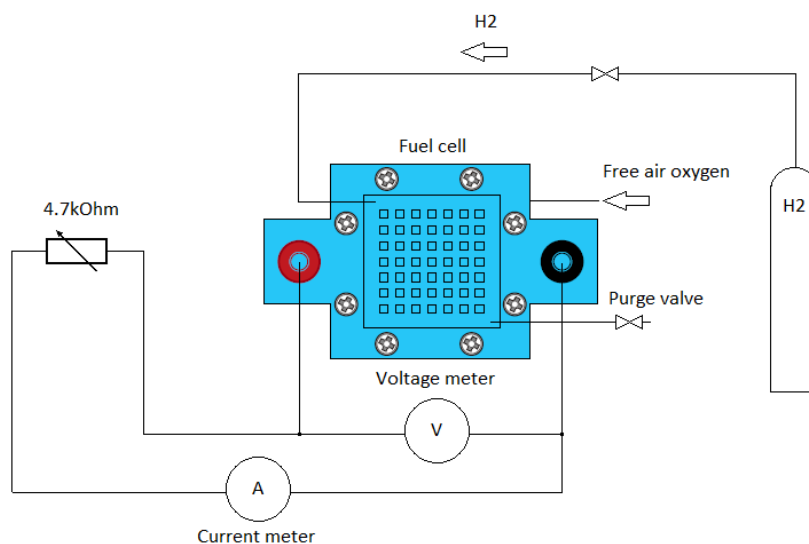


Figure 67: Additional fuel cell schematic

3.5.7.2 Iv- and power curve with a 4.7kOhm variable resistor

The IV curve and the power curve are combined in this graph. In this graph the voltage and power can be seen in relation to the current. This makes it possible to see the corresponding current and voltage values at a given point on the power curve.

This graph can be compared to the previous one. It is very similar in the case of the shape of the graph. There is a decline in the beginning of the IV curve to then progress more linear. The iv-curve starts at 950mV and at 300mV, this is equal as before. The current goes up to 400mA in contrast to the 180mA before.

The power curve has a more linear evolution with a kink in the middle. They cross each other in the middle before the maximum power point which is the last measured point. The power curve has a maximum in this configuration of 120mW this is much better than the 45mW maximum of the old fuel cell.

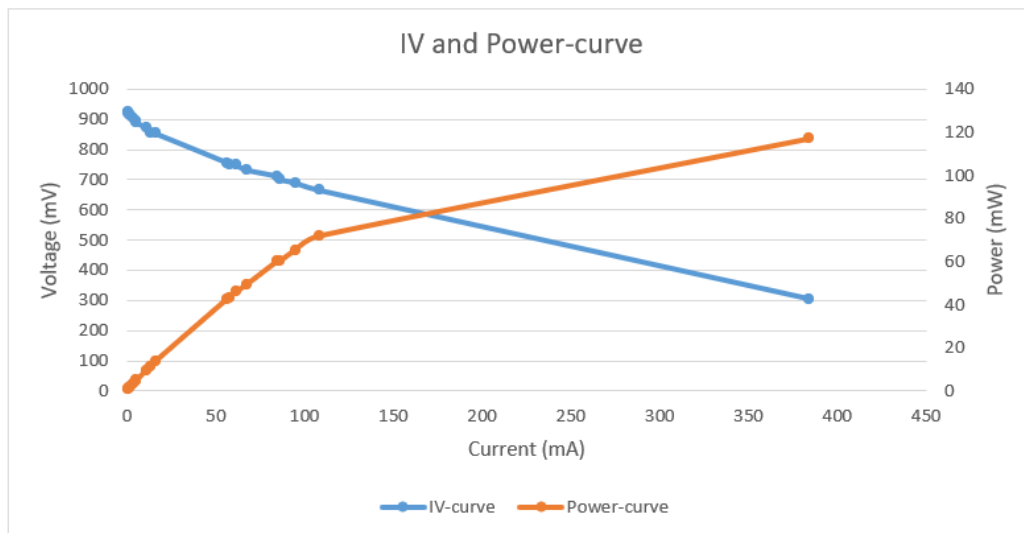


Figure 68: Additional fuel cell IV – and power curve

3.5.7.3 Iv- and power curve with a motor

In the next experiment the variable resistor is replaced by the motor, this motor is slowed down to by hand at the output shaft. Maximum used power is now 160mW while previously only 40mW was possible. This is not yet the 270mW as the datasheet describes, a higher load has to be found to test the fuel cell to its limits.

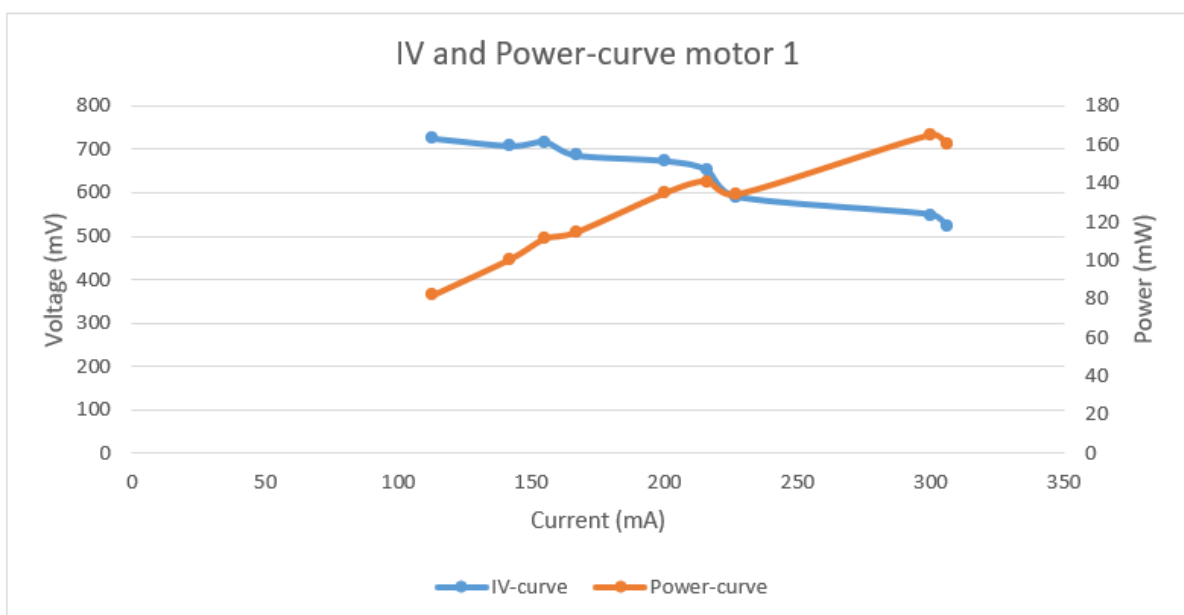


Figure 69: Additional fuel cell IV – and power curve motor 1

3.5.7.4 IV- and power curve with the second motor

When the fuel cell was bought a different motor was also in the purchase, this one is now attached to the circuit. This motor has a gearbox attached to it to reduce the shaft speed thus requiring more torque. Measurements were difficult to take because of some play in the gearbox and therefore the voltage and current jumped around sometimes, this can be seen in the graphs where the data points sometimes surpass themselves.

In this test the maximal power of the fuel cell is reached, the last point is close to 300mW and the current is 450mA. This motor in combination with the new fuel cell is a better choice than the previous motor and will therefore be chosen to power the model ship.

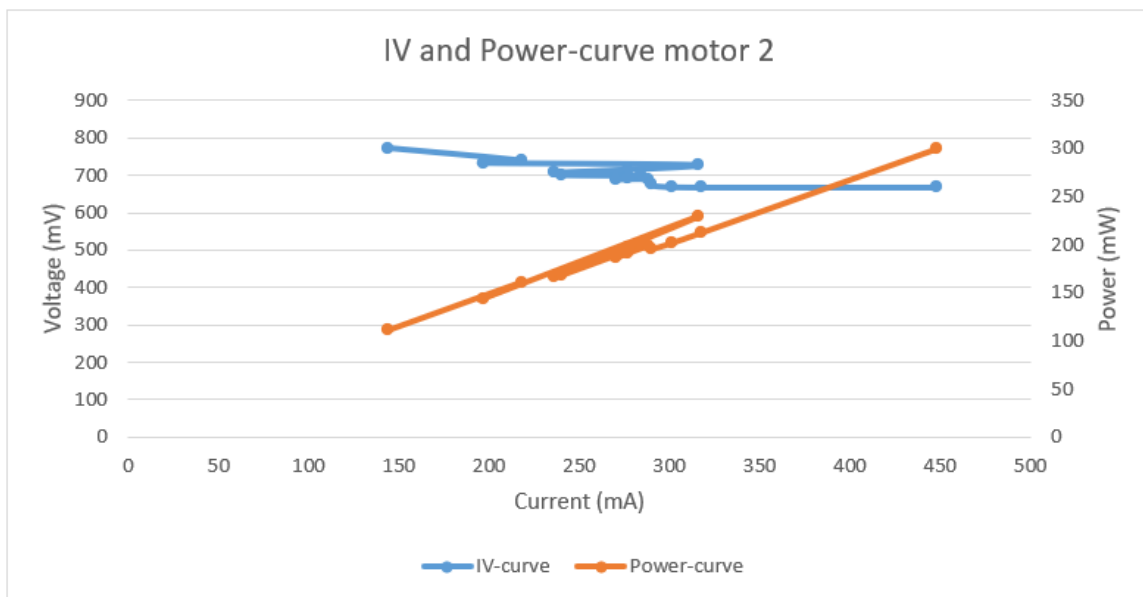


Figure 70: Additional fuel cell IV – and power curve motor 2

3.5.7.5 Efficiency

The efficiency of the hydrogen circuit is an important part of the energy matter. Therefore, in this part the energy efficiency and loss of energy will be discussed. There are many factors that have an effect on the performance of the electrolyser and fuel cells. These consist of the material, design, temperature, pressure, and corrosion. Also, each component in the circuit has a certain power loss. Studying these individual parameters into detail would lead too far as the main interest is to find the overall efficiency of the system. Therefore, the energy calculation will be made by comparing the used energy for generating one container of hydrogen to the energy used by using this one container of hydrogen. This includes all the individual losses and focuses on the bigger picture. On the next page the table with calculations and comparisons can be found.

The energy production calculation will be made using the acquired data from previous tests. For the energy usage calculation, three different conditions will be analysed namely, low load or idle, medium load and high load where the motor nearly stalls. Results can be compared and the optimal condition regarding efficiency can be determined.

Using a 10ml container with a balloon to keep the hydrogen pressurised. Charging the container is done by running the gas production station, this is the fuel cell connected to a power supply. The gas production station is connected to the container and can be closed off with a valve. While charging the container the power is monitored. These values are needed to calculate the energy used for a full container which will be used later.

An average current of 0.2A if its powered by the solar panel and a voltage of 2.3V is needed to achieve a flow rate of 7.284ml/A*min. The volume is known thus the time can be calculated to fill the container, this is 6.9 minutes. If for example a current of 0.7A is supplied as the datasheet describes the time to fill up the container is only 2 minutes. The power is voltage times current which equals 0.460W. multiplied by the time the gas production station runs, this is the used energy, is 189.46J for the process.

The container is then disconnected from the charging station and is now powering the circuit. Three scenarios are tested low medium and high load to see what impact this has on the results. More specifically, low is without load at 88mW, medium is halfway the power curve at 221mW and high is when the motor almost stalls, this is at 254mW. Accordingly, the runtime is shorter when the load is higher, this equals to 7; 6 and 5.5 minutes of running the motor before stalling. The calculations are done in the same manner and the used energy is respectably 37.1J, 79.5J and 83.9J.

3.5.8 Fuel cell conclusion

Now the values are known for generating the 10ml of hydrogen and the output energy after using the hydrogen. The highest load gives the best efficiency for the system namely 44.3%, secondly 42.0% and lastly 19.6%. These values are very plausible considering friction and heat losses and other losses. PEM fuel cells generally have an efficiency of 50-60% [28]. The best efficiency is reached at the highest load this is normal because at low load the majority of the power is used to overcome friction. The friction losses are in essence constant in regard to the load. Therefore, at higher loads friction takes up a smaller part of the overall efficiency.

Looking at the figures, the best option for the catamaran is the last fuel cell and motor two. In combination with the second motor, it produces 300mW of power which is up to 3 times better than the first results. If the fuel cell is supplied with a minimum amount of pressure it will deliver adequate and stable power. Therefore, the simple way of storing the hydrogen in a balloon is sufficient. These results lead to choosing the storage medium, the motor, and the fuel cell which will be implemented in the design of the catamaran.

Efficiency**Storing hydrogen**

<u>av flow rate</u>	<u>ml/A*min</u>	<u>ml/W*min</u>			
	7,284	3,642			
<u>volume</u>	<u>ml</u>				
	10				
<u>current</u>	<u>A</u>	<u>power to fill</u>	<u>W</u>	<u>Energy needed</u>	<u>J</u>
	0,2		0,460		189,46
<u>voltage</u>	<u>V</u>	<u>time to fill</u>	<u>min</u>		
	2,3		6,9		

Using hydrogen

<u>current</u>	<u>A</u>	<u>power to empty</u>	<u>W</u>	<u>Energy used</u>	<u>J</u>
lowest	0,139	lowest	0,088	lowest	37,130
mid	0,291	mid	0,221	mid	79,513
max	0,400	max	0,254	max	83,952
<u>voltage</u>	<u>V</u>	<u>time to empty the balloon</u>	<u>min</u>	<u>ml/min</u>	<u>runtime</u>
lowest	0,759	no load	7	1,43	∞
mid	0,700	med load	6	1,67	46
max	0,636	high load	5,5	1,82	27,1

Table 15: Fuel cell and motor efficiency calculations 1

Efficiency

no load	19,6
med load	42,0
high load	44,3

Table 16: Fuel cell and motor efficiency calculations 2

3.6 Series and parallel tests combining solar panel, electrolyser, and motor

During the daytime there is a lot of electrical energy available from the solar panel, probably enough to run the motor and produce hydrogen at the same time. In the following experiments this hypothesis will be looked into. The effects of combining the motor and the fuel cell in parallel or in series will be studied as well as gas production that happens simultaneously. The goal is to determine what is the most optimal situation using the available power. Gas production and power of the motor are important factors in this experiment as well as using as much power as possible that the solar panel provides.

3.6.1 Setup series circuit

The Xunzel solar panel is used as power supply and placed into direct sunlight in the laboratory. At the time, the sun was shining brightly, and the sky was clear. The PEM module is set up as usual with its two gas outlet ports coupled to the containers. These containers are filled with water at the start and fill up with gas when the experiment progresses. A water supply is added to the inlet port of oxygen side of the module. The PEM module is connected in series with the brushless DC-motor. The cell used for these tests is the first fuel cell. Both voltages of the motor and electrolyser were monitored with the use of the Agilent 34401A and the National Instruments DAQ 9174 Ni 9129 Card Equipment. The latter is connected to the computer and controlled by the same program used in the electrolyser characterisation experiments. This means that every minute a measurement is taken. The Keithley 2601 Source Meter is used to accurately measure the current going through the system. The voltage of the solar panel can be calculated by applying Kirchhoff's voltage law.

Schematic:

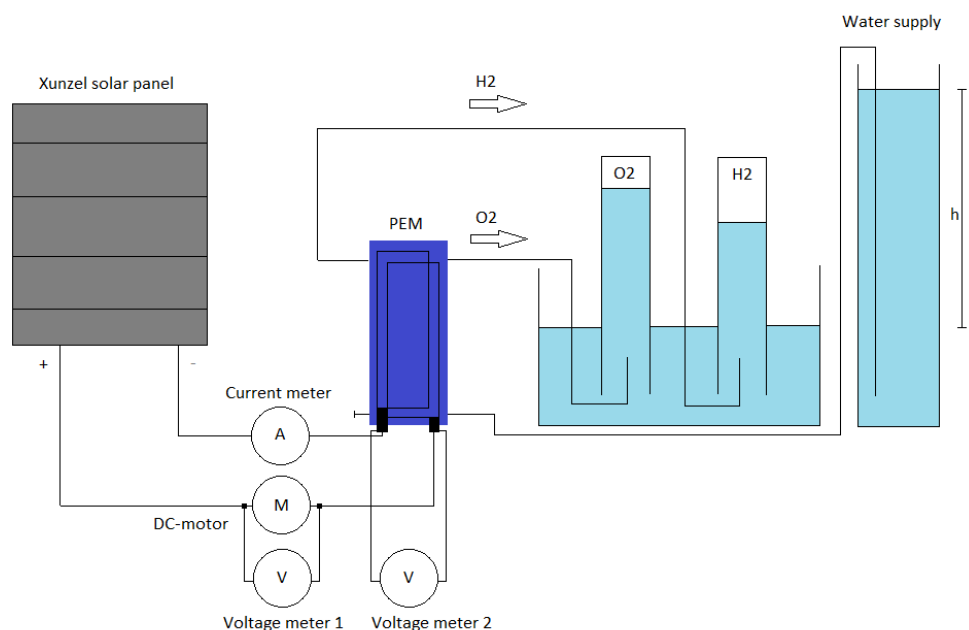


Figure 71: Series experiment schematic

3.6.1.1 Control test

To have a good baseline before comparing results the electrolyser is first tested without connecting the motor in series to it. Good operation of the cell is tested, the results were as expected and similar to the results from the electrolyser tests. Also, on par with the values of the manufacturer's datasheet. Apart from the power consumption, which is written to be 2V and 0.7A so 1400mW. However, the experiments where the electrolyser was tested during a whole day the maximal consumption was around 400mW when tested in combination with only the solar panel. The power curve shows a constant development of the power during the time it takes to fill the 10ml volume.

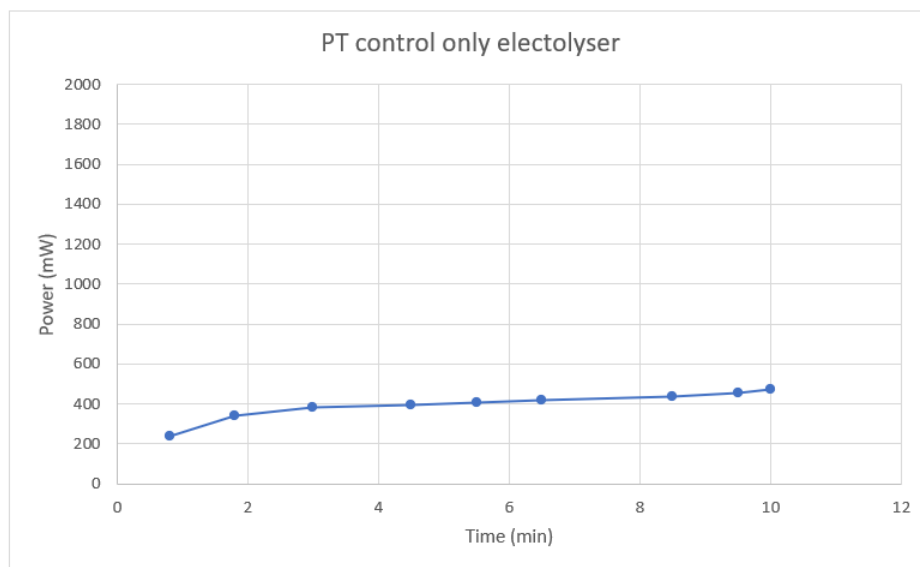


Figure 72: Series control experiment PT curve

The graph above visualises the power curve of the electrolyser. Below, the table with the significant values can be found from the control test. The electrolyser takes up 500mW while producing a steady amount of hydrogen and oxygen gas. The numbers given in the table are the average current, the time it takes to fill up the volume of hydrogen and oxygen gas, also the average voltage over the fuel cell is given. Calculations are then made to determine the flowrate of the gasses as well as the flow rate per amp, this makes comparing to other tests more convenient.

I av (A)	V H2 (ml)	V O2 (ml)
0,1782	10	5
Time (min)	ml/min	ml/min
8,5	1,18	0,59
V av (V)	ml/A*min	ml/A*min
2,290	6,601	3,300
	7,14	3,35

Table 17: Series control experiment significant data

3.6.2 Series experiment

One motor is now connected in series with the solar cell and the fuel cell. The current through the circuit is measured as well as the voltage over the motor and electrolyser. In the graph below it can be seen that the power consumption of the electrolyser is similar to the result of the control test, namely 400mW. The motor uses 1400mW of power. This adds up to 1800mW in total and can be seen in the power curve of the solar panel, this is the supplied power. At this point the solar panel can provide sufficient power, the motor has a decent rpm, and the hydrogen production time is still reasonable with 12 minutes. The control test takes 10 minutes to fill the same volume with gas.

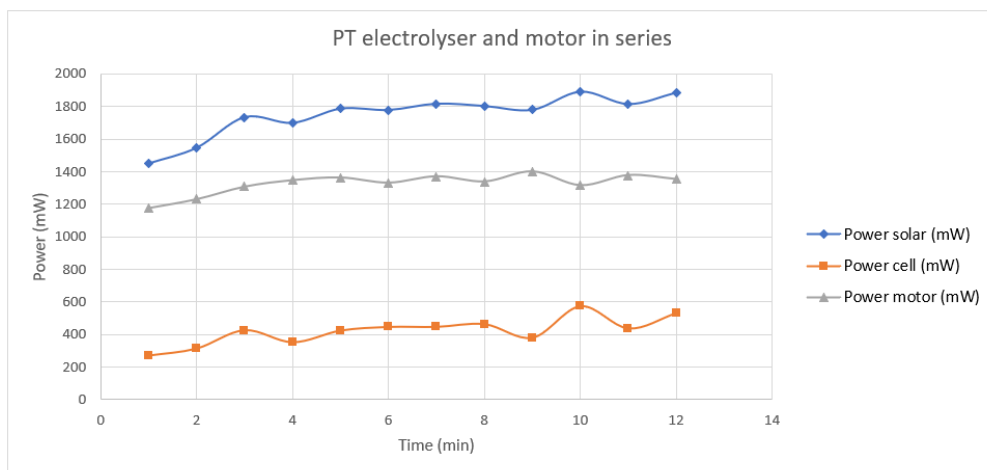


Figure 73: Series experiment 1 PT curve

The values of the measurements can be seen below, the voltage over the electrolyser is equal to the control test and stays constant. The voltage over the motor is 7.1V, therefore the solar panel's voltage is set at 9.4V. This is not yet the optimal operating point for the solar panel, this setting is located more to the left in the graph than at the possible maximum. The maximum power point is at 15V which can be found in the datasheet and in the solar panel characterisation graph below. better power performance can be expected at the maximum power point, but the solar panel produces enough power for now.

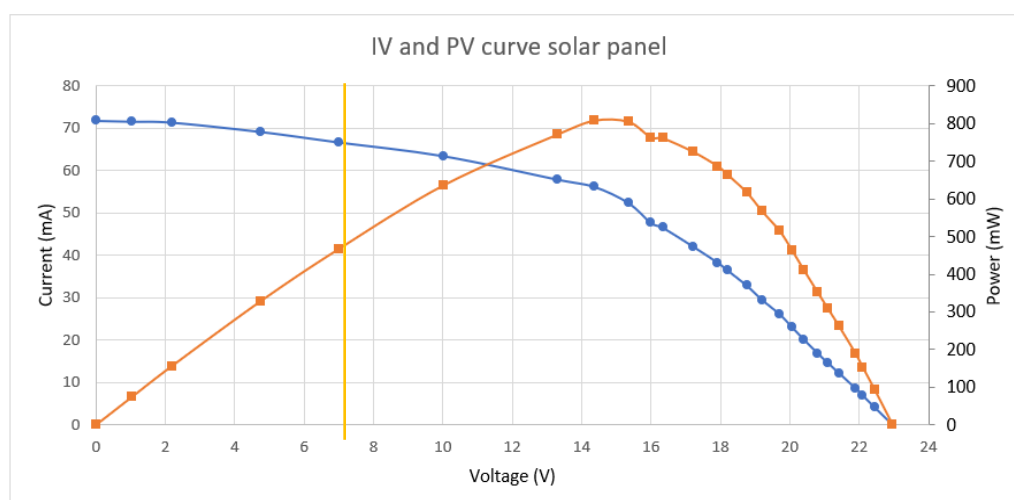


Figure 74: Series experiment 1 IV- and PV curve

Important to note is that the efficiency of the electrolyser is decreased, now only producing 4.4ml/A*min of hydrogen instead of the 6.6ml/A*min. This phenomenon also happened in the small-scale tests when the current was too low and the time to fill the container increased as well.

Vpem av (V)	I av (A)	V H2 (ml)	V O2 (ml)
2,305	0,1889	10	7
Vmotor av (V)	Time (min)	ml/min	ml/min
7,092	12	0,83	0,58
Vsolar av (V)		ml/A*min	ml/A*min
9,396		4,411	3,088
		7,14	3,35

Table 18: Series experiment 1 significant data

To conclude this test in this configuration it is very acceptable to be running the motor in combination with the fuel cell producing hydrogen. Over time and depending how long the solar panel is exposed to the sun, this allows for a significant volume in hydrogen which can be used in times of no sun to provide power. This will be discussed later in the project.

3.6.3 Series experiment 2 motors in series

In this second experiment another motor is added in series to raise the total voltage in order to come closer to the maximal power point of the solar panel which is located at 15V. The updated setup can be seen below, this time the voltage is measured over both motors and the electrolyser.

Schematic:

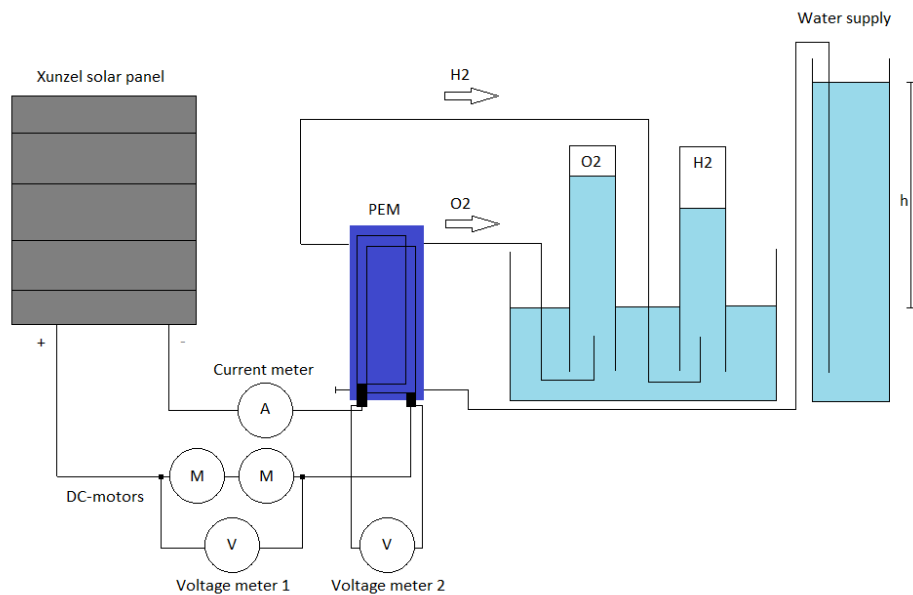


Figure 75: Series experiment 2 motors in series schematic

The motor rpms were noticeably lower during this experiment but there was sufficient power to start them without problem. The used power by the electrolyser was again around 400mW. The motors use a combined 1800mW of power this is 900mW each, this is noticeably lower than 1400mW as before and explains why the rpm is lower. All powers combined give a total of 2200mW produced by the solar panel.

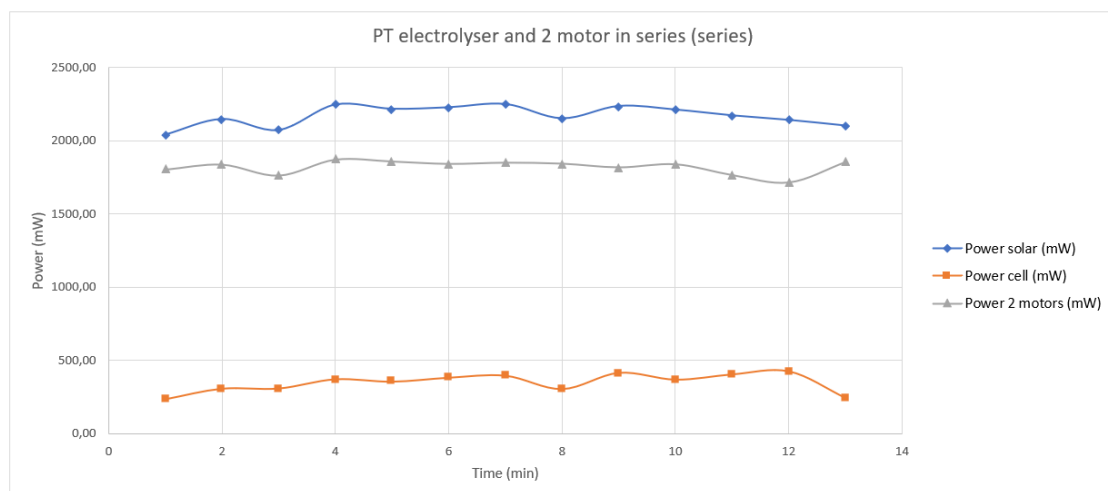


Figure 76: Series experiment 2 motors in series PT curve

The time it takes to fill the gas container has increased by one minute but the values for the flow rate stay constant. The increase in time is because the current was slightly lower. The voltage value for the electrolysis is again similar to the previous tests. The voltage over the motors is 11.4V that makes 5.7V each motor. Furthermore, the total voltage is now 13.5V this is closer to the 15V maximum, as a result of this increase the operating point is moved more to the right on the solar characterisation curve and an increased power of 2200mw could be provided by the solar panel, which was expected.

Vpem av (V)	I av (A)	V H2 (ml)	V O2 (ml)
2,181	0,1601	10	7
Vmotor av (V)	Time (min)	ml/min	ml/min
11,374	13	0,77	0,54
Vsolar av (V)		ml/A*min	ml/A*min
13,555		4,804	3,363
		7,14	3,35

Table 19: Series experiment 2 motors in series significant data

After the second experiment it can be concluded that increasing the voltage requirement is beneficial for the system. To optimise 15V would be ideal and will put the operating point at the maximum power point of the solar cell. As a result, the current dropped slightly this caused the hydrogen container to fill up slower but looking at the ml/A*min flow rate, it was slightly better than a single motor test. This is still sufficient after some time to have enough hydrogen in storage to generate the power needed for propelling the ship after the solar panel does not produce electricity anymore.

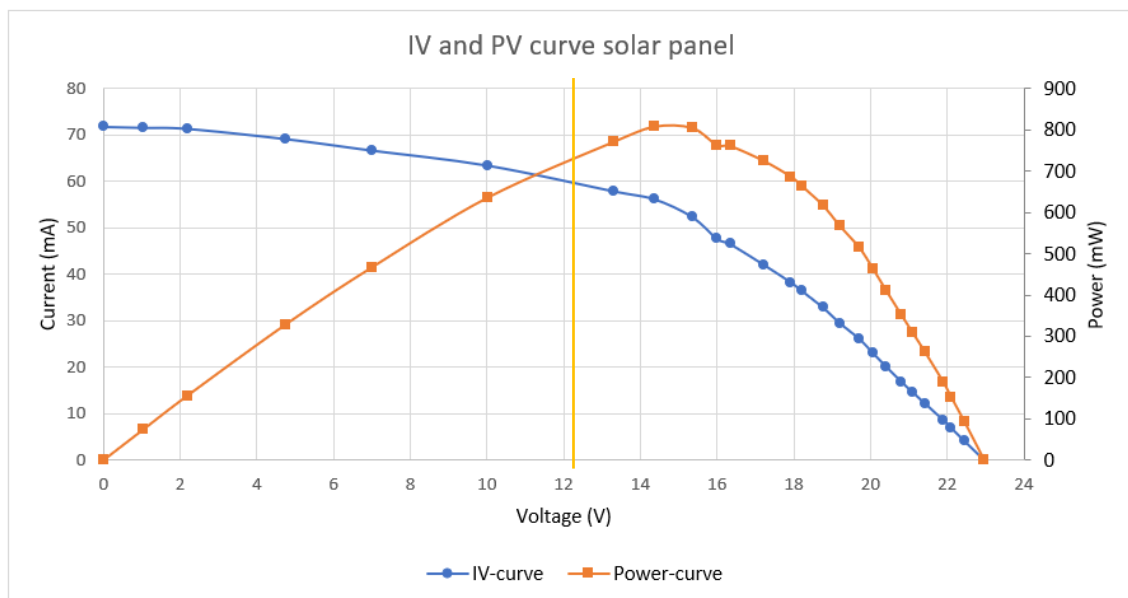


Figure 77: Series experiment 2 motors in series IV- and PV curve

3.6.4 Series experiment 2 motors in parallel

After exploring the two motors in series, it might be interesting to see what will result connecting the two motors in parallel to each other. A lower power output can be expected because the solar cell will be operating further from its optimal operating point regarding the voltage. Below, the setup for this experiment can be seen which is similar to the one before only with the two motors in parallel instead of in series with each other.

Schematic:

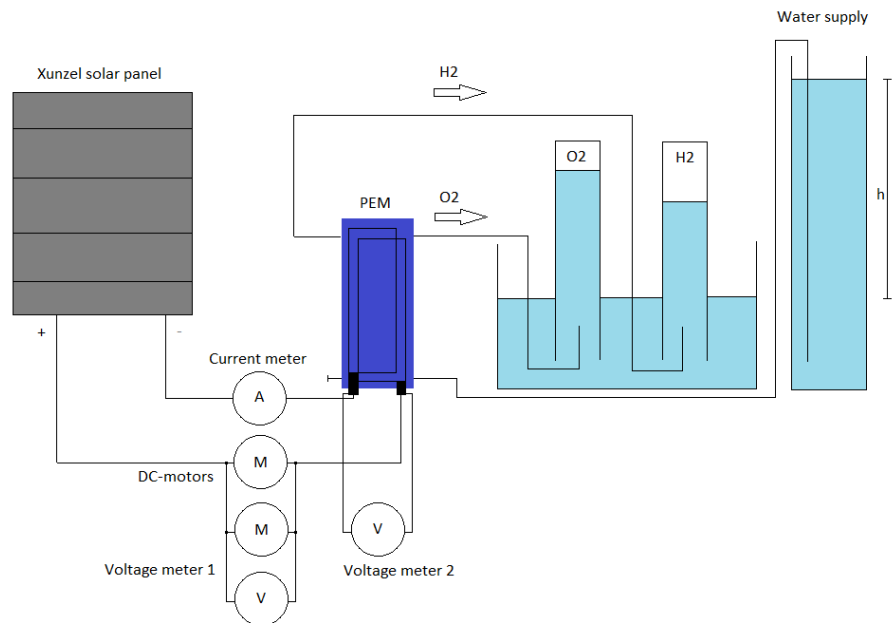


Figure 78: Series experiment 2 motors in parallel schematic

The power used by the fuel cell is now slightly higher than before, around 500mW. Both motors run slower and their power usage is also far less than before this time only using 400mW in total. This brings the total delivered power to 900mW which is far less than before.

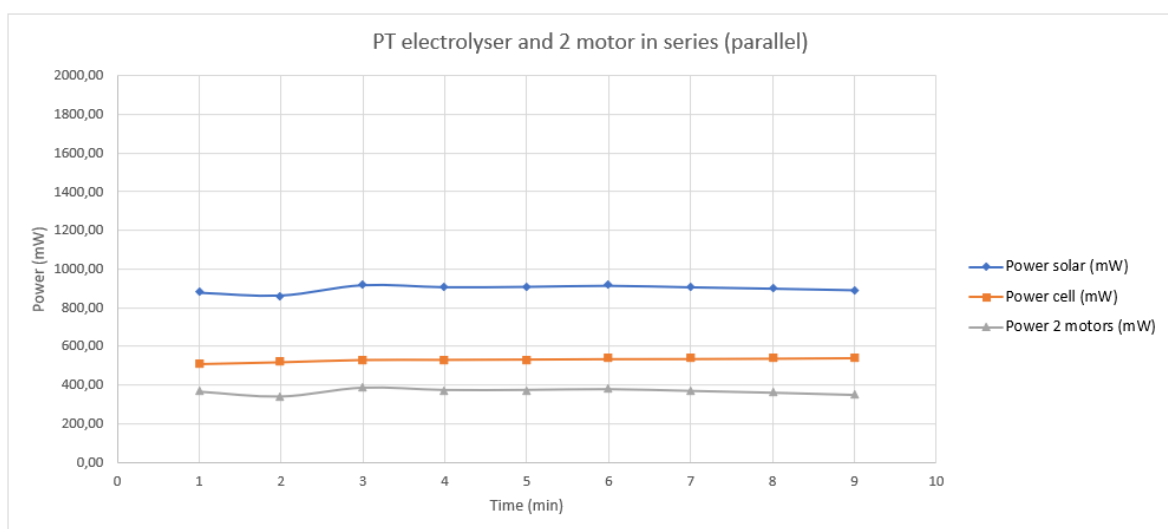


Figure 79: Series experiment 2 motors in parallel PT curve

The reduction in power was expected because the operation point is now very much to the right in the solar characterisation curve. The cause of this are the motors having the same voltage over them which is 1.661V and the electrolyser using 2.411V, a total of 4.072V which is far from the optimal 15V therefore providing only a fraction of the power. A higher current of 0.2204A is drawn by the system.

Vpem av (V)	I av (A)	V H2 (ml)	V O2 (ml)
2,411	0,2204	10,5	5,8
Vmotors av (V)	Time (min)	ml/min	ml/min
1,661	9	1,17	0,64
Vsolar av (V)		ml/A*min	ml/A*min
4,072		5,293	2,924
		7,14	3,35

Table 20: Series experiment 2 motors in parallel significant data

The upside of this configuration is that the hydrogen and oxygen production values are higher than the other tests, producing an adequate 5.3 ml/A*min of hydrogen gas and 2.9 ml/A*min of oxygen gas. In general, this was not a good configuration because the operating point is too far from its optimal thus losing too much of its potential power output.

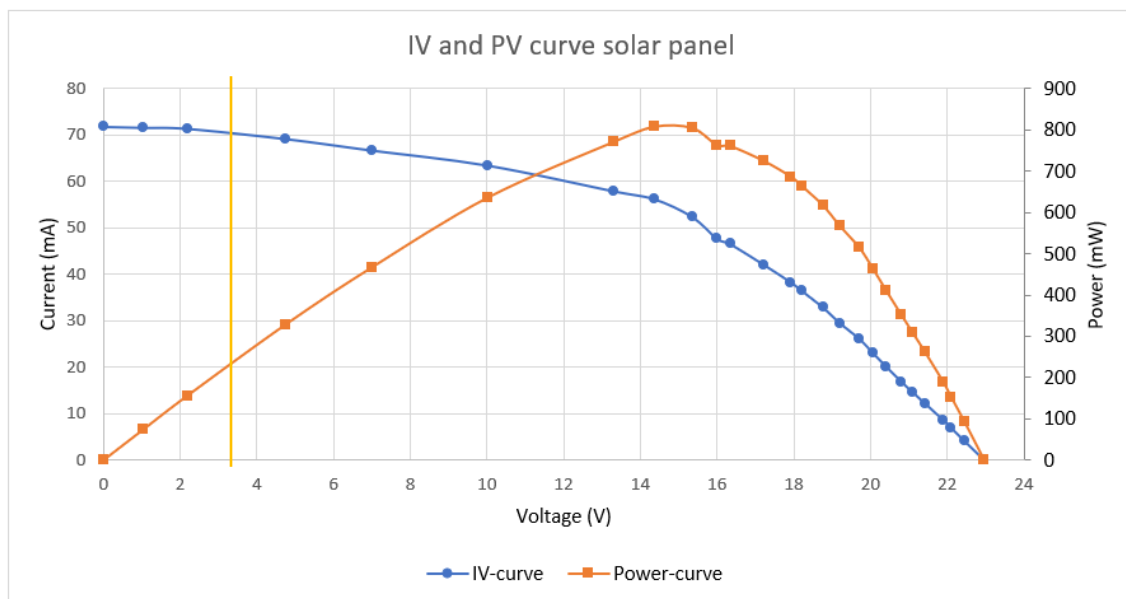


Figure 80: Series experiment 2 motors in parallel IV- and PV curve

3.6.5 Parallel experiment

In this case is the electrolyser connected in parallel with the motor in order to study the behaviour in this configuration. The voltage will now be equal over the electrolyser and the motor, but the current will differ. In the next diagram the connections are visualised.

Schematic:

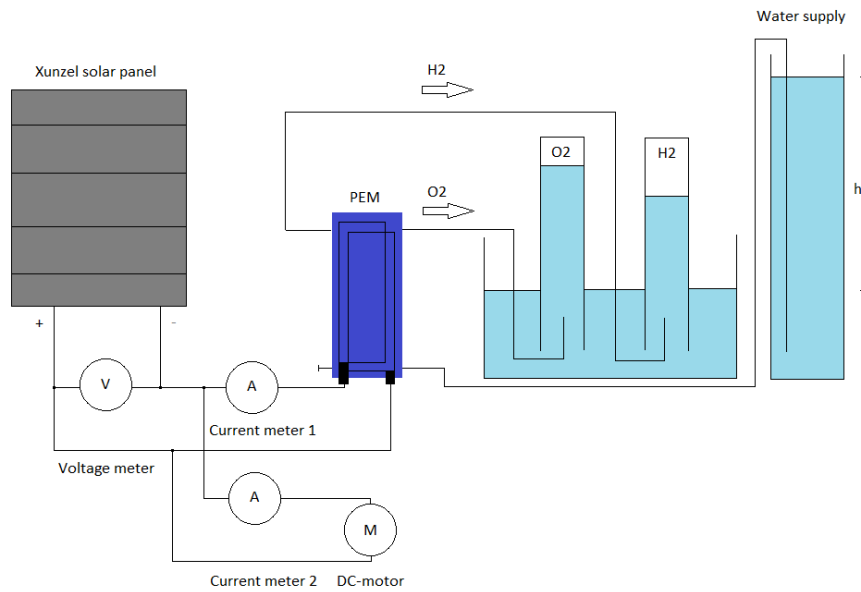


Figure 81: Parallel experiment schematic

Performance is poor, the rpm is rather low. This is because the voltage over the motor and fuel is only 2.58V. As well as the hydrogen and oxygen production, with a flow rate of only 1.846 mlH₂/A*min and 1.477 mlO₂/A*min. This is not enough for a stable operation. The current drawn by the electrolysis is 0.0944A which is few in comparison with the 0.170A the electrolyser consumes during the full day tests.

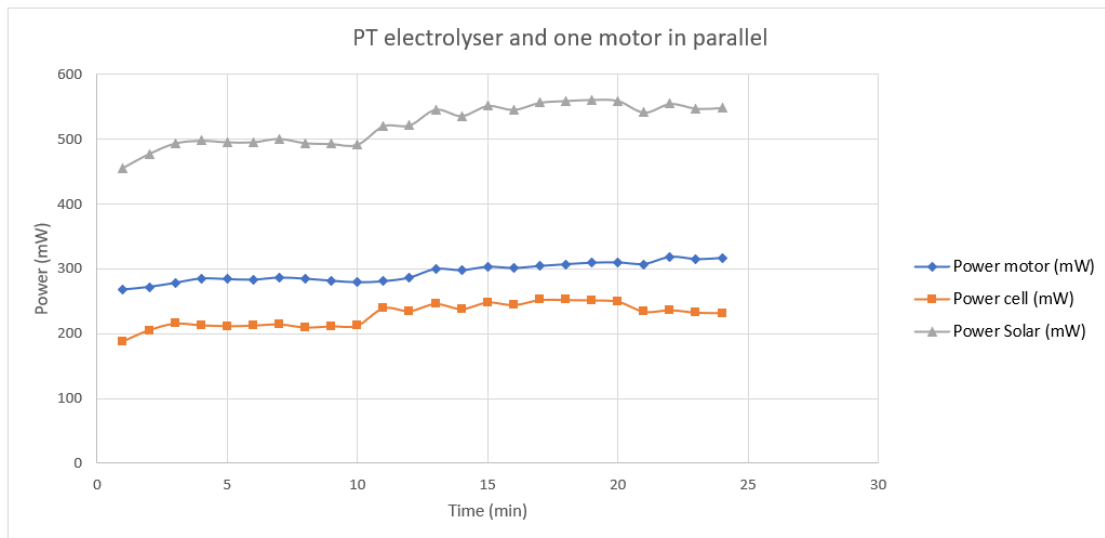


Figure 82: Parallel experiment PT curve

The maximal power this time is 550mW produced by the solar panel. The electrolyser uses 250mW of the total which is low compared to the 400mW usually. Therefore, it produced less hydrogen. The total time to fill the gas container is 25minutes which is long as it normally fills in around 10 minutes.

I_{pem av} (A)	I_{av} (A)	V H₂ (ml)	V O₂ (ml)
0,0944	0,2167	10	8
I_{motor av} (A)	Time (min)	ml/min	ml/min
0,1223	25	0,40	0,32
V_{solar av} (V)		ml/A*min	ml/A*min
2,5793		1,846	1,477
		7,14	3,35

Table 21: Parallel experiment significant data

Since it is a parallel circuit the voltage over the motor is equal to the voltage over the electrolyser, the total voltage is only 2.58V. This is very much in the beginning of the power curve of the solar characterisation. Therefore, wasting a lot of potential power which could be pulled from the solar cell. This setup is not desirable. There is no point of continuing these tests with two motors in parallel as the power would be insufficient.

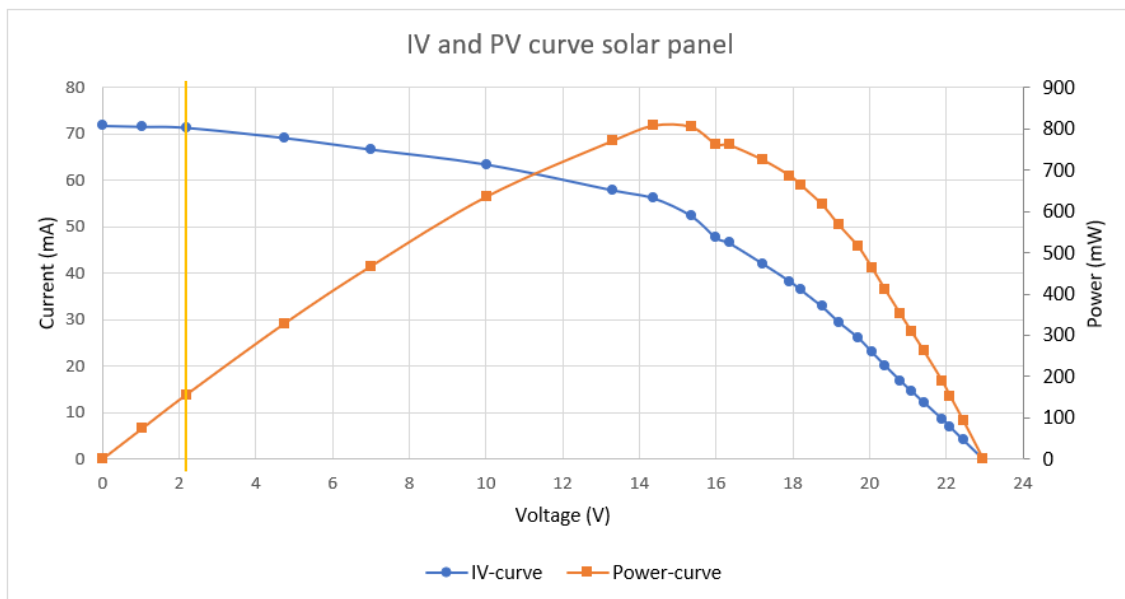


Figure 83: Parallel experiment IV- and PV curve

3.6.6 Circuit conclusions

The most important factor to get the highest power is the voltage at the operating point of the solar panel. Ideally this should be 15V. As seen in the series test the best result of 2200mW was achieved with a voltage of 13.5V, connecting two motors and the electrolyser in series. Therefore, a parallel circuit is not beneficial because the voltage is too low, not being able to progress far enough in the power characterisation curve of the solar panel and delivering too little power.

The solar panel is capable of delivering enough power to continuously power one or two motors while also powering the electrolyser. The electrolyser is collecting hydrogen gas for when the solar panel is not lit enough and a switch in power supply has to happen.

With these insights it is now possible to dimension a circuit which will optimise the power generated by the solar panel. This will be further explored in Power system integration since the design of the catamaran will impact which motor configuration will be most viable.

3.7 Additive manufacturing

In this part the additive manufacturing process will be discussed. First will be the material choice and what to look for, along with its advantages and disadvantages as well as some other techniques that can be used. Then the setup of the 3D printer with the choice of the slicing software will be investigated as well as the calibration. It is also important to take a look at the build-up of the machine, regarding its frame and print head layout along with its implications. Fine tuning the software and hardware to optimize printing quality is next. The changes brought will be verified by doing practical test prints. To then finalise with constructing the catamaran and all its challenges.

3.7.1 Material choice

Previously model boats were mostly made by hand using various materials such as wood, pottery, metal, ivory or plastic. [29] In recent years technology has advanced and the term additive manufacturing has come to light. Additive manufacturing uses 3D models made with computer aided design (CAD) to direct hardware to deposit material layer upon layer. Additive manufacturing adds material to form a structure. In contrast to the more traditional way of shaping models, material is removed by machining, milling, carving, or cutting. [30]

There are many types of additive manufacturing materials. The most popular one and used in this project are thermoplastics. There are still a lot of options that fall into this category, each with its pros and cons to explore. For example, acrylonitrile butadiene styrene (ABS), polylactic acid (PLA), polycarbonate (PC), nylon, acrylonitrile styrene acrylate (ASA) and polyethylene terephthalate (PET) are the most popular ones.

Firstly, ABS is a UV resistant material, good for outdoor use, strong but rather hard to print. The printer needs to be enclosed to print reliably and it tends to come loose from the bed and warp in the corners. The bed must be heated. This is the same case for PC and nylon, these materials are even stronger and heat resistant but harder to print. This strength is not needed for a model which will not be under much load. Also, the added heat resistance is not of much use because most of the ship is going to be submerged in the water and requires a very high print temperature where the used type of hot end is not capable of. PET is a good option, it combines the positives of ABS and PLA which are the ease of printing, its toughness, it does not have a very high melting point and does not warp easily. Also, PET does not absorb water that much and has good impact resistance. Material wise ASA would be the optimal choice, it has great durability and long-time UV-ray exposure resistance. It does not absorb water and is great material to use outdoors. The material is easy to print, it does not warp but it needs a high build plate temperature like ABS. The biggest con of this material is the rather expensive price. This leaves PLA as the material of choice. It is the most cheap and easy material to print with. This means that the models can be produced quickly, and iterations can be made without a great cost involved. Strength and stiffness are good, but it has a low heat and UV resistance. Water absorption is also not ideal. Therefore, it is not great to use outdoors for long periods of time. But the material was chosen because of its positive properties. The model ship is not to be out on the water for too long on its first sea trials. It is always possible once the final design is made to reprint the model in ASA. [31]

3.7.2 3D printer and setup

The three-dimensional (3D) printer used for the printing of all parts is FlashForge Pro. The Technology used is Fused Deposition Modelling (FDM), this is the most common type of 3D printer. The process of FDM printing is straight forward, a spool of filament is fed to the extruder which then feeds the filament to the heater block. In the heater block the filament gets warmed up until it is approximately 215°C, the filament is fluid now. The extruder feeds the molten plastic through the nozzle which has a reduced hole diameter. By then moving the print head in a determined path, a form can be made. The printhead makes a 2D form by moving in the X and Y direction. The third dimension is added by moving the printed downwards thus giving the machines 3 degrees of freedom. The bed moves down layer by layer. The printhead is equipped with a cooling fan to cool down the extruded filament so it hardens after it sticks to the previous layer.

3.7.2.1 Cartesian type 3D printer

The FlashForge Pro is a cartesian type 3D printer, this is also the most common type of printer found on the market. The name is derived from the cartesian coordinate system found in mathematics. This implies that there is a printhead which moves in the X and Y direction and a print bed that moves in the Z direction. Another configuration of the cartesian type printers is a printhead that moves in the X direction and moves up and down in the Z. With the print bed staying at the same height but moving in the Z direction. Generally, the printers from the first type can move faster because they do not need to accelerate the bed fast. The printer at hand is as the first type describes.

The printer is completely encapsulated that means that the temperature can be kept consistent. This is great for printing materials prone to detaching from the print bed, for example Acrylonitrile butadiene styrene (ABS). For the more frequently used Polylactide (PLA) this is not needed.

3.7.2.2 Extruder setup

Another important configuration factor is that the FlashForge Pro is equipped with the direct drive extrusion type. There are two types of extruder configuration used with these printers, each with their respective pros and cons.

3.7.2.2.1 Bowden type extruder

The first type is the Bowden tube setup, the extruder is hereby mounted on the frame of the printer. The filament is fed through a hollow polytetrafluorethylene (PTFE) tube by the extruder to then reach the heat block and get melted.

The advantage of this configuration is that the printhead is now much lighter because the weight of the extruder and stepper motor is not mounted on it. This results in a faster print speed regarding quality. This is because the weight of the extruder does not have to be accelerated and decelerated when the printer is in operation and moves the printhead. Another advantage is the easier disassembly of the printhead in case of a blockage in the nozzle. In the other case, the whole printhead must be disassembled, now the Bowden tube can be disconnected, and the nozzle unscrewed, and the problem can be resolved.

The disadvantages of using this system are firstly, stringing issues because of the stretch in the long filament cable when the filament is retracted. Stringing is when the print looks hairy, in fact this is filament that has dripped out of the nozzle when moving the printhead. Secondly, it is hard to print flexible material for example thermoplastics polyurethane (TPU). Also because of extreme elasticity and the long path the filament must travel after being extruded to reach the nozzle, causing knots or blockages through bucking in the extruder or in the tube. Flexibles perform best with a direct path. Thirdly, abrasive materials are also more difficult because they wear out the Bowden tube more quickly.

3.7.2.2.2 Direct drive extruder

The second, and in this case used type, is the direct drive extruder. The extruder along with its stepper motor is mounted on the print head, just above the heated block. This makes the travel path of the extruded filament as short as possible. The advantages of this system are less chance of blockages, better stringing performances which is an aspect of print quality. Also, the option to use more difficult filaments such as flexibles or nylon.

The disadvantages on the other hand are the increased weight of the weight of the print head. This means the printer is prone to ringing. Ringing or ghosting are small ripples seen next to a feature in the print, mostly resembling the feature a few times like waves in the water. This happens due to the acceleration and jerk of the print head while speeding up and slowing down. The printer has a rigid frame, but this is not enough to counter this effect. This is a common problem with direct drive extruders.

3.7.2.2.3 Dual extruder print head

The FlashForge Pro is equipped with a dual extruder print head, this means that there are two extruders and heater blocks attached to the moving printhead. This is a complex addition to the printer allowing for dual coloured or dual material prints. Configuring this dual print mode is a challenge and will be discussed later. The advantage of this system is that multipart models including colour of material changes can be manufactured. Also changing the filament can be labour intensive. With a dual extruder type printer, it is simply selecting the other extruder in the slicer software. When a print has a lot of support structures it makes sense to print the supports in a lower cost material. Some support materials dissolve in water, making the removal more convenient if printed in this material without affecting the structural part. The disadvantages of this system are the added weight. This makes the print head rather heavy because it is combined with the direct drive

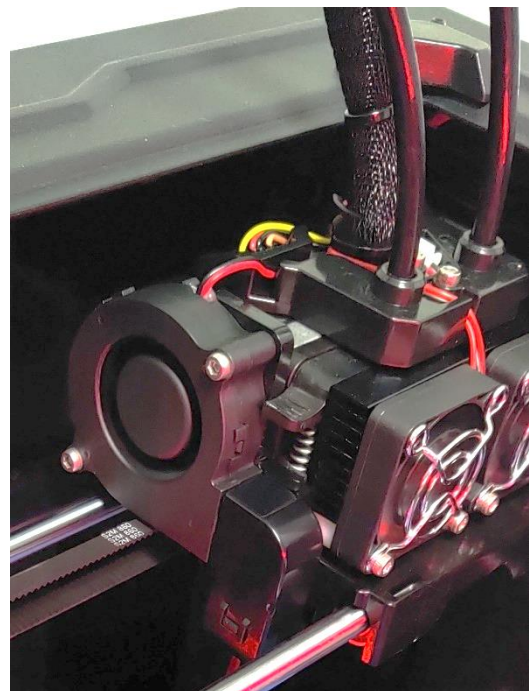


Figure 84: Dual extruder print head

system. Consequently, the print speed is reduced to avoid loss in quality and effects of ringing, to counter the effect of the weight.

3.7.2.3 Slicer and profile configuration

The chosen slicer software is Cura 4.8.0. A slicer software enables the user to convert their 3D cad-model into gcode. Gcode is the required format for 3D printers and CNC machines to operate, it is an instruction-based programming code. Cura is an open-source software developed by the company Ultimaker with the help of the 3D printing community. Cura is chosen because it is easy to use and it has a wide range of usable features. A lot of parameters can be adjusted which is good for making a new printer profile and fine-tuning the settings later on. Based on experience it delivers good quality.

3.7.2.3.1 Single extrusion mode

Because Cura is not the native software of FlashForge there are no fast configuration files available. The printer must be manually added and configured. Program files were added to the software so the printer could be recognised. It is now time to design a custom profile for the specific setup and material choice. It is good practice to do this for each material and colour because these behave slightly differently compared to each other. This is done the experimental way by changing parameters in the software, printing a test model, evaluating, and then repeating this process. Print speed, retraction settings, wall thickness, temperature, fan speed, infill, etc. were adapted until the quality of the printed model was satisfactory. Approximately 75 settings were defined on the current profile. This was done for both extruders because the left extruder is equipped with white PLA, the right one is equipped with translucent blue PLA. Luckily, most of the settings can be applied on both because the material is equal.

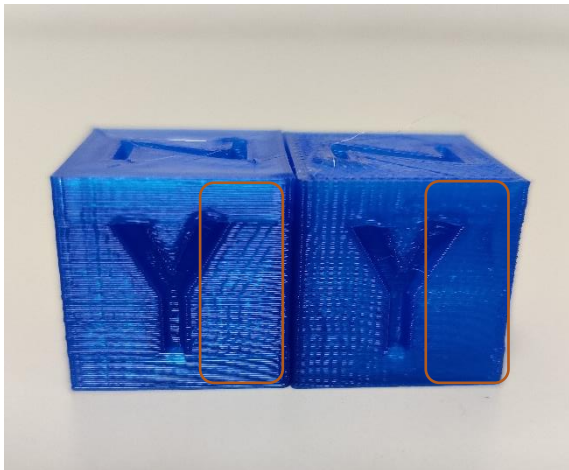


Figure 85: Xyz cube before-after tuning: ringing

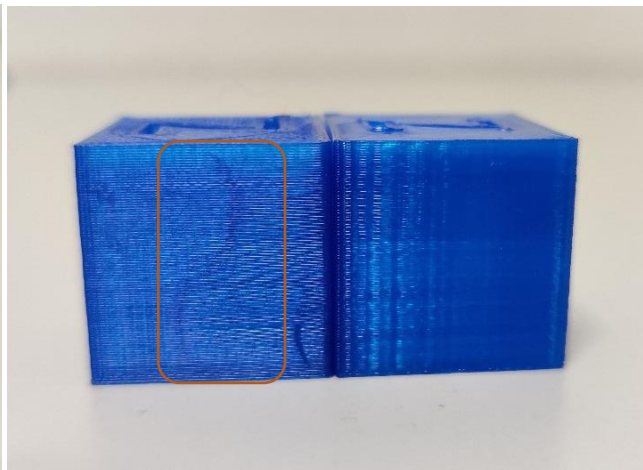


Figure 86: Xyz cube before-after tuning: outer wall error

For example, in this picture it can be seen that there is a lot of ringing. Also, the gyroid infill can be seen through the outer wall. These are the clearest errors which can be fixed by changing the parameters. The outer walls were increased to three walls, this means the thickness of the model now is three lines instead of two. The acceleration and jerk were reduced to reduce ringing. This limits the printhead from acceleration and stopping to fast inducing the ripples. The print speed was also reduced for the same reason. Reducing the print speed has a negative effect on the total time the

printer needs for completing the model. Therefore, the trade-off must be made between speed and quality of the print. In an attempt to further improve the quality, the belts were checked and tensioned if needed, the guiding rods and Z-axis spindle were greased. All these efforts resulted in a better quality of the print. Lastly reducing the layer height is the most effective way to have a higher quality print but this has a direct effect on the print time reducing a 0.2mm layer height to 0.1mm effectively doubles the time needed to print the model.

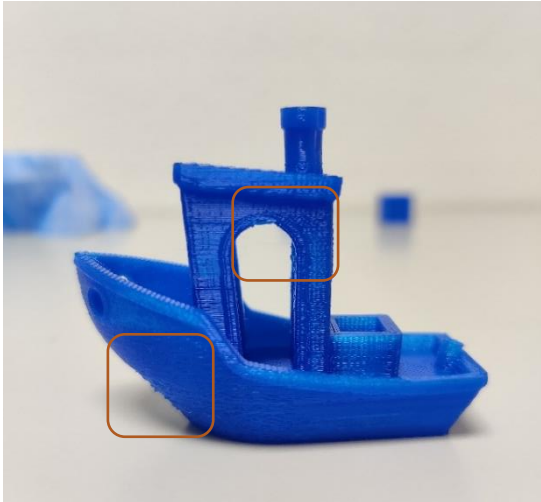


Figure 87: Benchy sideview

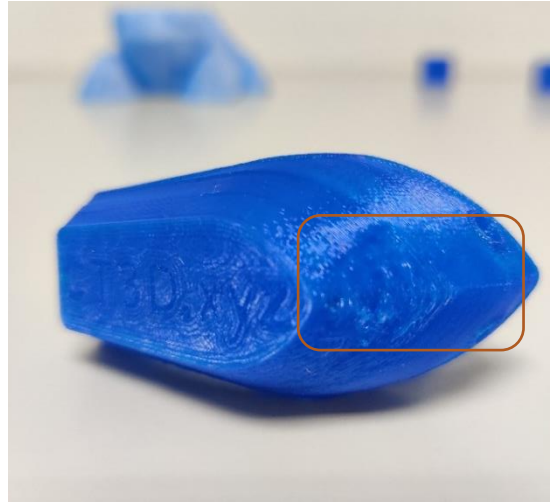


Figure 88: Benchy bottom view

This print is a general print for testing many aspects of the printer. On the bottom and back there are letters which must be readable. The sides must be smooth. The cabin is a good test for overhangs and ringing, there is a little to be seen. The chimney is excellent for testing cylindrical prints and its accuracy. The bow is also prone to inducing ringing. From these tests it can be seen that the hull of the benchy suffers from cooling problems. The plastic did not have time enough to cool down and this is caused by the cooler blower fan. There is only one of these mounted on the opposite side. Taking this into account, the problem would be resolved by rotating the model so the hull would be in the direction of the fan. Apart from this last issue, this test print turned out good. This means that the printer is fairly well set up and the software is tuned.

3.7.2.3.2 Dual extrusion mode

The configuration for the individual extruders is done. The more challenging configuration can begin for the simultaneous working of both extruders. Both extruders must be enabled in the software. Then a model can be printed to inspect the relative position of each extruder to the other. This is done by looking at the transition and position between the two colours. The results were rather good, little adjustments were made in the printer configuration in the software.

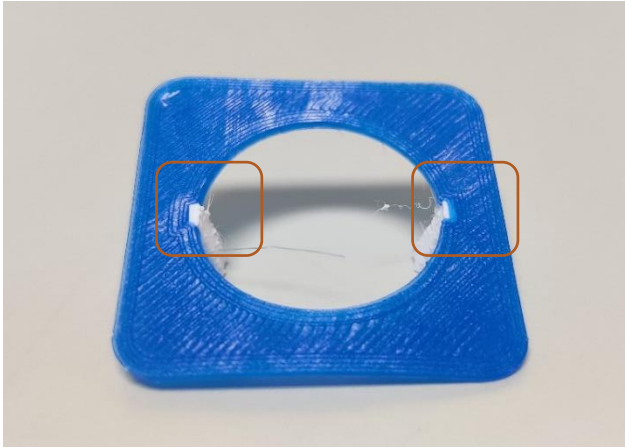


Figure 90: First picture: alignment of the two nozzles



Figure 89: Second picture: complete dual colour cone

A full dual coloured print could now be attempted. A prime tower and ooze shield were enabled to prevent artifacts on the print. The prime tower is a small cylindrical tower printed next to the model, where the print head will change colour and will ensure a sufficient pressure build up in the nozzle. The ooze shield is printed closely around the model. This is one line and printing a layer is altered between the two extruders. The ooze shield prevents blobs of melted plastic leaking from the inactive extruder from hitting the model. This is rather effective seeing the majority of artifacts caught on the shield.



Figure 91: Prime tower



Figure 92: Ooze shield

After a couple of successful prints, a very complex model could be printed to fully use the dual extrusion mode and test the accuracy and capabilities of the printer. The chosen model is a frog with multiple colour changes throughout each layer. It also has a steep overhang, to also test this quality of the printer. To ensure optimal quality, the prime tower and ooze shield were enabled. This model takes 16 hours to print.



Figure 94: Complex dual colour frog 1



Figure 93: Complex dual colour frog 2

The printer did a phenomenal job, all the features are well defined. There are barely any artifacts on the print. The colour transitions are good. The overhang is also fine. The ooze shield did its job and as seen on the back side, a lot of artifacts were caught. Some negative points, there is some stringing to be seen on the print where the print head moved in and out the boundaries of the model. This means that the retraction settings could be improved furthermore. Also, there are traces of under extrusion in the white parts, this can be due to a clog in the nozzle. This can be remedied by replacing the nozzle or removing and cleaning the nozzle. The flowrate can also be adjusted if the problem is not cured by replacing the nozzle.

This concludes the setup and testing of the printer. Now the printer is configured and ready to print the catamaran model.

3.8.1 Tolerance

In designing the parts for the ship, tolerances have to be taken into account because of inaccuracies of the printer. After some tests it became clear that a total tolerance of -0.3mm has to be used for anything that has to slot together. This results in a light press fit. If a firm press fit is needed, then -0.15mm is to be used. A loose fit is achievable with a total tolerance of -0.4mm .

3.8.2 Complete model

Before exploring each individual component, the completed model in CAD is shown in the rendering below.

It consists of:

- Solar panel on top.
- Blue coloured hull.
- White hull top covers.
- Rudder assembly in the back containing the rudder, rudder support bracket and the steering arm.
- Propellor assembly in the middle containing the motor coupling, the shaft, the shaft support bracket, and the propellor.
- Deck with the power unit, - mount, and the electrolyser on top.
- Solar panel risers

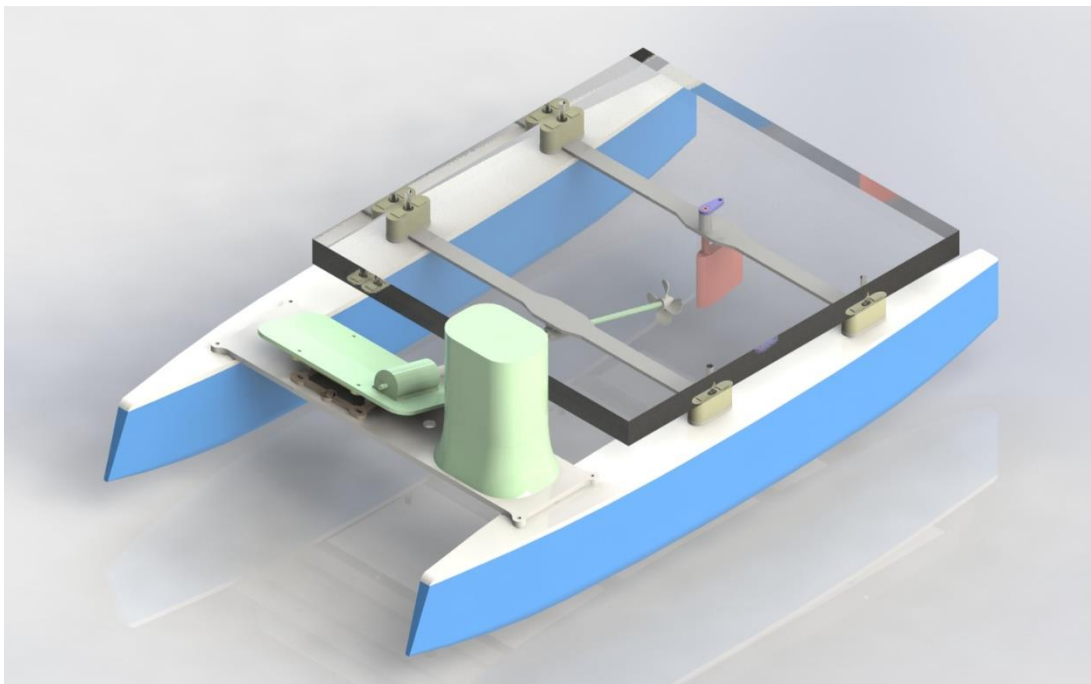


Figure 96: Completed catamaran in CAD

3.8.2.1 Hull

The first part which has to be designed is the hull construction. First the solar panel and the power unit were measured because these are the largest parts of the ship and the hull has to accommodate them. The length of the hull is 800mm long and 75mm wide. Four reinforcements were placed in the hull.

These will hold the screws and pins for connecting the deck and the solar panel. They also keep the sidewalls of the hull together, stiffening the structure. Dividing the hull in several compartments also has the benefit of keeping the boat afloat if one of the compartments is structurally damaged and flooded, the other unbreeched compartments will prevent the boat from sinking.

The technique used for shaping the hull is to define several cross-sections to then loft the sections together resulting in an even outer surface which is hydrodynamic. The features of the bow and aft are inspired upon the design of the Alinghi 5 catamaran. Because of a necessary amount of displaced water volume, the hull looks proportionally bulkier than the Alinghi 5. Since that boat was purely designed for racing and was made out of ultra light materials it is no surprise that when the scale is reduced and equipped with a relatively heavy solar panel on the model ship, proportions will have to be altered.

In order to print the hull, it is split into four parts and afterwards glued together. This is done to fit the hull on the build plate.

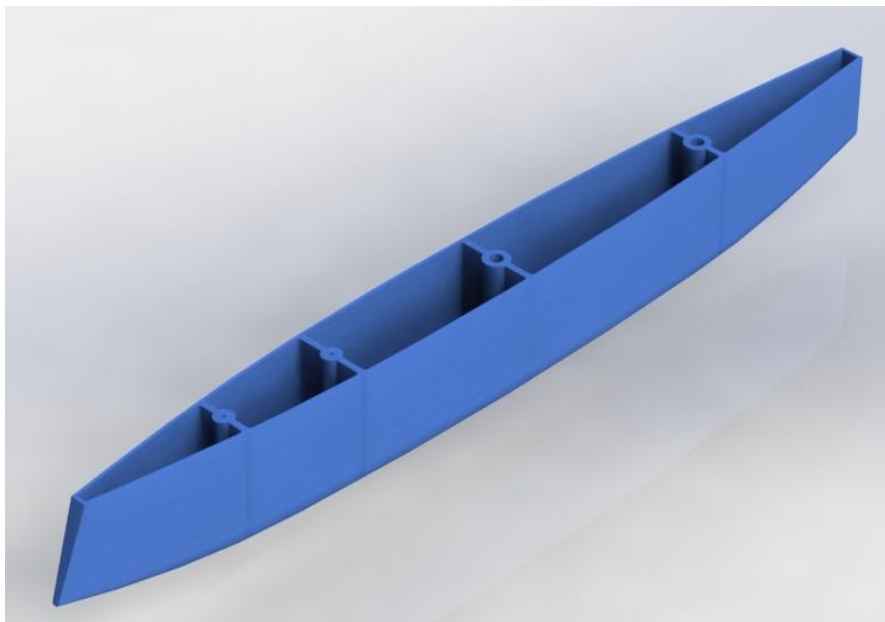


Figure 97: Hull

3.8.2.1.1 Buoyancy

Naturally, a boat has to be able to float, therefore some basic buoyancy calculations will have to be made. The mass of the loading capacity will now be calculated. The net force on the hull must be zero in order to be static, therefore the Archimedes principle is valid. Then the sum of the buoyancy force and the boat's weight can be made. The formula to calculate is as follows:

$$F_{net} = 0 = W - F_b$$

$$F_{net} = 0 = m * g - \rho_{fluid} * V_{displ} * g$$

$$m = \rho_{fluid} * V$$

W Is the weight of the object. F_b Is the Archimedes force also known as the buoyancy force. ρ_{fluid} Is the density of the fluid, in this case water. The density of fresh water is used to ensure buoyancy in salt as well as is fresh water. g Is the gravitational force. V_{displ} is the displaced or submerged volume, considering the extreme scenario where the boat is at its maximal weight, the V_{displ} is the total volume of the hull. This can be calculated through the “mass property” function in SolidWorks.

When filled into the equation:

$$m = 1000 \frac{kg}{m^3} * 0,003530085m^3 = 3.53 \text{ kg}$$

A single hull of the ship has a capacity of 3.53kg, a catamaran has a double hull therefore the maximal mass of the ship can be 7.06kg including the build material of the ship as well as all the components which will be added.

3.8.2.2 Hull top cover

In order to protect the internal components and close the open hull structure, a flat cover is designed to be put on top. This cover will be screwed down and will also be the attachment point for the deck. The cover has several holes going through it to accommodate for the pins of the solar panel and the deck screws. As well as the hull, the cover is split into three 200mm long pieces to fit the printer. The individual parts are connected to each other by the use of a dove-tail design. This will interlock the pieces and prevent them from loosening.



Figure 98: Top hull cover

3.8.2.3 Servo control housing

Because the ship will be remote controlled for steering, there has to be enough room to house the receiver and servo motor. Therefore, a special bracket for mounting the servo is made and placed on the back of the hull. The remaining components can be stored in the next compartment.

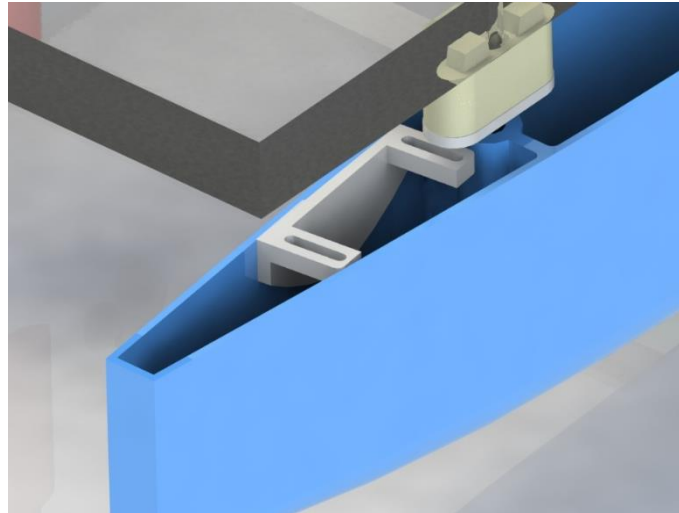


Figure 99: Servomotor mount

3.8.2.4 Rudder assembly

From the servo there will be a connecting rod to the rudder in order to be able to steer the boat. The rudder assembly consists out of the bracket which is supporting the rudder and held in place by the pins of the solar panel, the steering arm, which is connected to the servo with the connecting rod and connected to the rudder with a screw, and lastly the rudder itself.

The function of the rudder is to develop a transverse steering force on the aft end of the ship, using the reaction force of the water flowing along the ship and over the water. The rudder is located in the waterflow after the propeller and is shaped in such a way that the water flow is deflected as effectively as possible in combination with minimum resistance. These criteria are satisfied by giving the rudder a cross section of a wing profile. The rudder can be seen as a vertical wing on which a lifting force is generated by the waterflow. The drag should be as low as possible. The rudder force gives a turning moment around the ship's centre of displacement and rotates the ship. [32]

The chosen rudder is a spade-type rudder, this type of rudder is mainly used for ferries and other high-speed ships. It offers the advantage to be well balanced and to allow high rudder angles. For large ships however, it is becoming very heavy and prone to damage.

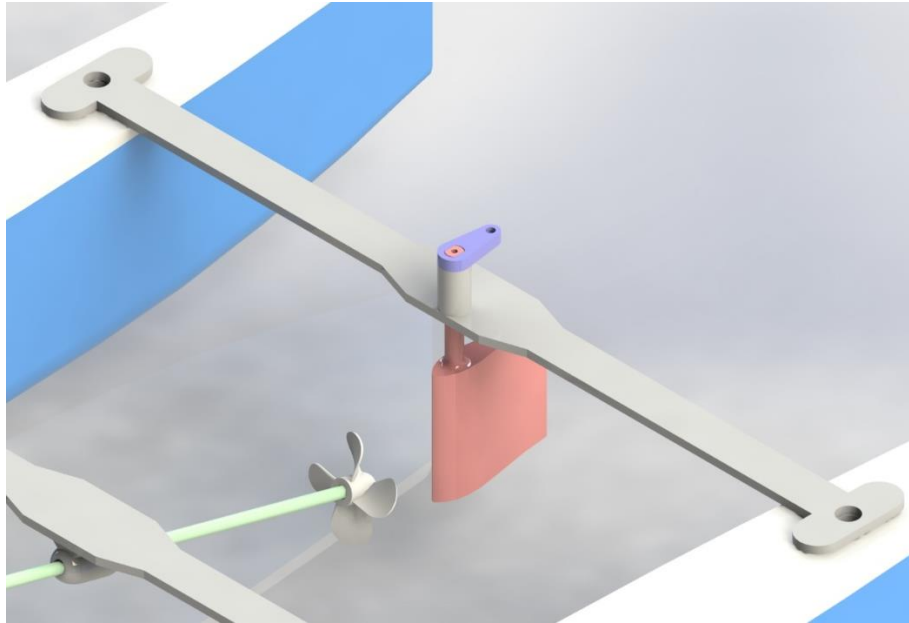


Figure 100: Rudder assembly side view

The typical double rudder used on catamarans was not chosen because of a more complex design using linkages and, more importantly, because it is more efficient to place a rudder directly after the propeller generating a stronger waterflow.

The bracket is equipped with reinforcement beams in order to increase stiffness and reduce sag. The bracket is split in three pieces with dovetail connections to fit the print bed, later they will be glued together.

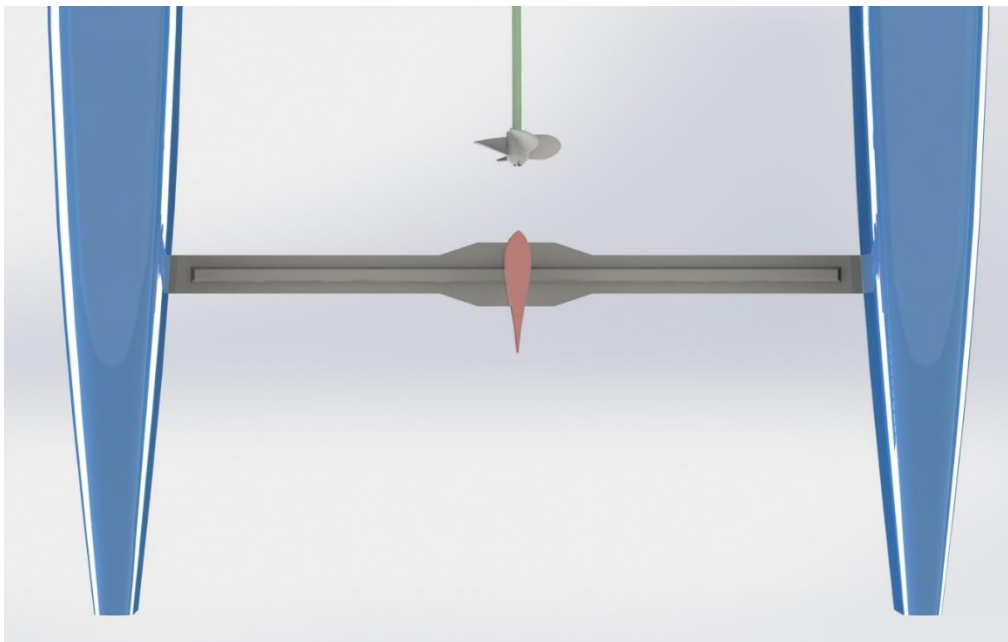


Figure 101: Rudder assembly bottom view

3.8.2.5 Propeller assembly

The electric motor is the driving force of the catamaran. To convert electrical energy into thrust exerted by the propeller it has to be coupled to the shaft. This is done by the motor coupling. The motor coupling is a tube which connects the 2mm motor output shaft to the 4mm stainless steel propeller shaft. The coupling is made from PLA and connects two shafts together via a press fit.

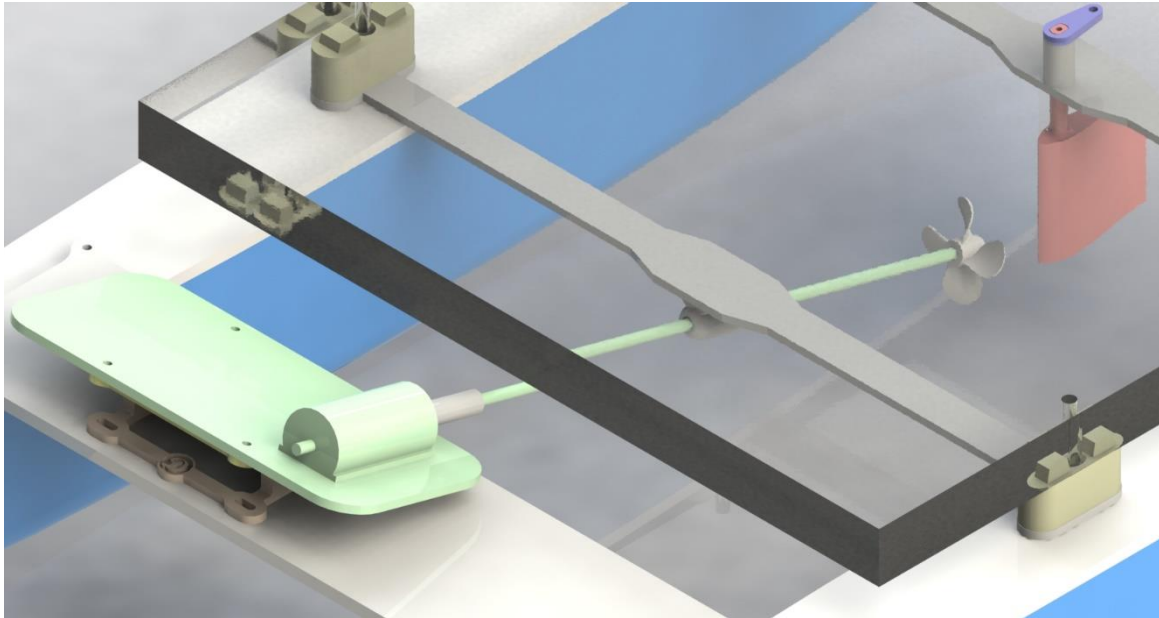


Figure 102: Propellor assembly top view

To continue, the stainless-steel shaft is supported by a bracket. The shaft spins freely in the through hole of the support feature. This bracket is held in place by the pins used to support the solar panel. Also, the rudder bracket is reinforced with reinforcement beams to increase stiffness and reduce sag. The bracket is also split up in three sections, connected with each other by the use of dovetails and glued together after printing. [32]

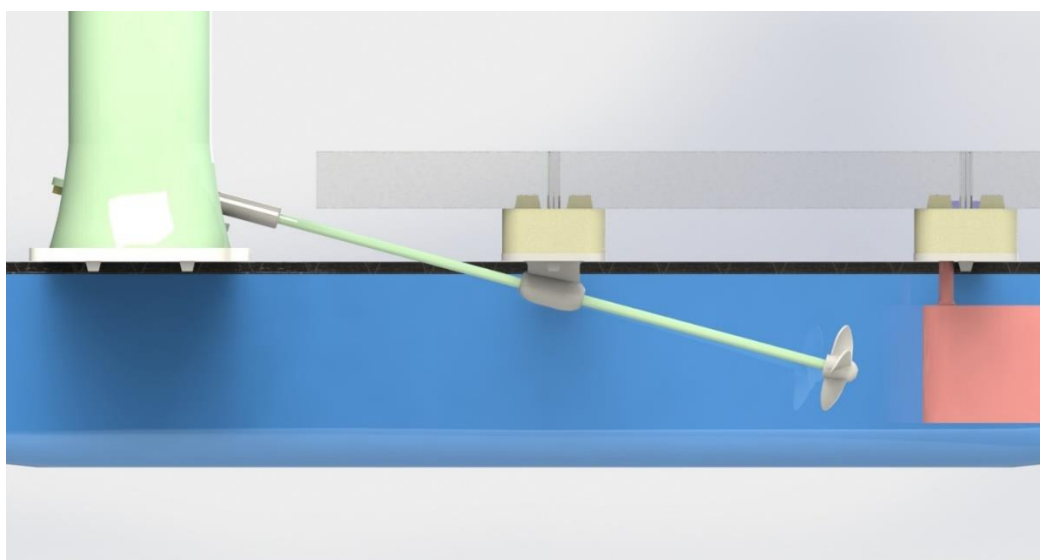


Figure 103: Propellor assembly side view

The motor, shaft, and support feature are tilted to a 20° angle to submerge the propeller underwater. The angle is kept as low as possible to maximise forward thrust. The decision made to tilt the motor has the advantage that the electric and hydrogen components are placed at a safe distance from the water. In addition, it makes the viewer see the process of hydrogen production and storage which are the key features of this project.

The disadvantage of tilting the motor, instead of mounting the motor in the hull, is the long shaft. A long shaft in combination with meagre tolerances regarding centricity of the printed parts induces an imbalance with wobble as result. This wastes some of the power but is outweighed by the advantages previously mentioned.

3.8.2.6 Propeller

For a ship to obtain a certain speed, a force needs to be exerted on the ship. The magnitude of this force depends on the ship's resistance at that speed. The force that moves the ship comes from an outside force that comes from a propulsion system. The propulsion system consists of an electric motor driving a propeller via the shaft. The propeller holds an important place in the design of the propulsion system because its efficiency and the power consumption are related directly. Efficiency depends on the flow field of the propeller which depends on the shape of the underwater body, the delivered power, the number of blades on the propeller, rotations per minute, diameter, surface smoothness, and the ship's speed. [32]

The highest efficiency in propulsion is achieved when the largest possible quantity of water is displaced with the smallest acceleration. This means that the configuration must result in a minimal excess speed of the wake produced by the ship. For the propeller this means it should be as large as possible with as low as possible revolutions per minute. Most small ships use a 4-blade propeller, while 5-blade propellers are more common on bigger ships with more power to decrease vibration. 3-Blade propellers are used on twin screw vessels and ships with a high revolution count. [32]

Trying to design an appropriate propeller is difficult on this small scale. Large diameter propellers would result in installing the motor which has little power. Consequently, multiple propellers are printed with differing diameters to assess the effect on the ship. The propeller is printed, and press fitted on the shaft, that way different propellers can easily be swapped for testing purposes, later the propeller can be glued down if necessary.

3.8.2.7 Power unit mount

The power unit consists of the electrolyser, fuel cell, hydrogen storage and the electrical motor. For the reasons mentioned before, it is tilted under a 20° angle. A special bracket is designed to hold the power unit in place. It consists of two pieces which can be slotted together. Both pieces are provided with through holes. The top part is screwed onto the bottom of the power unit, the bottom part screws down into the deck. The lower part is given slot holes to allow for alignment.

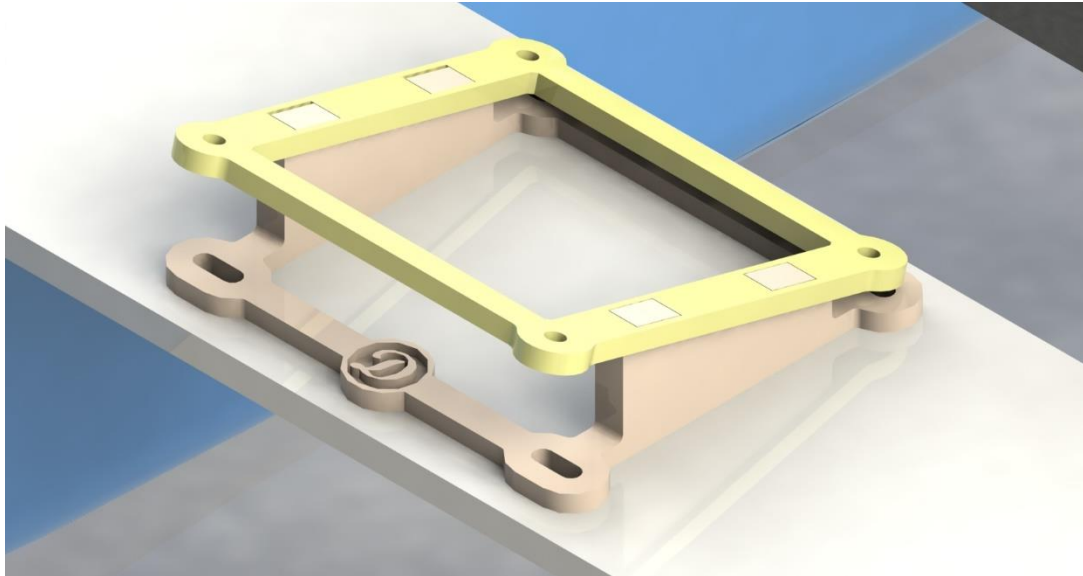


Figure 104: Power unit mount

3.8.2.8 Deck

The deck is used to mount the power unit, - mounting system, and the electrolyser. It is screwed down through the top covers and into the hull which has dedicated mounting structures, this can be seen in Figure 97: Hull. The bottom side of the deck is equipped with reinforcing beams to make the deck stiffer. A hole is made in the centre to allow for neat cable management of the electrolyser. The deck is also split into two pieces and joined with dovetail connections for printing purposes. Afterwards, both pieces are glued together.

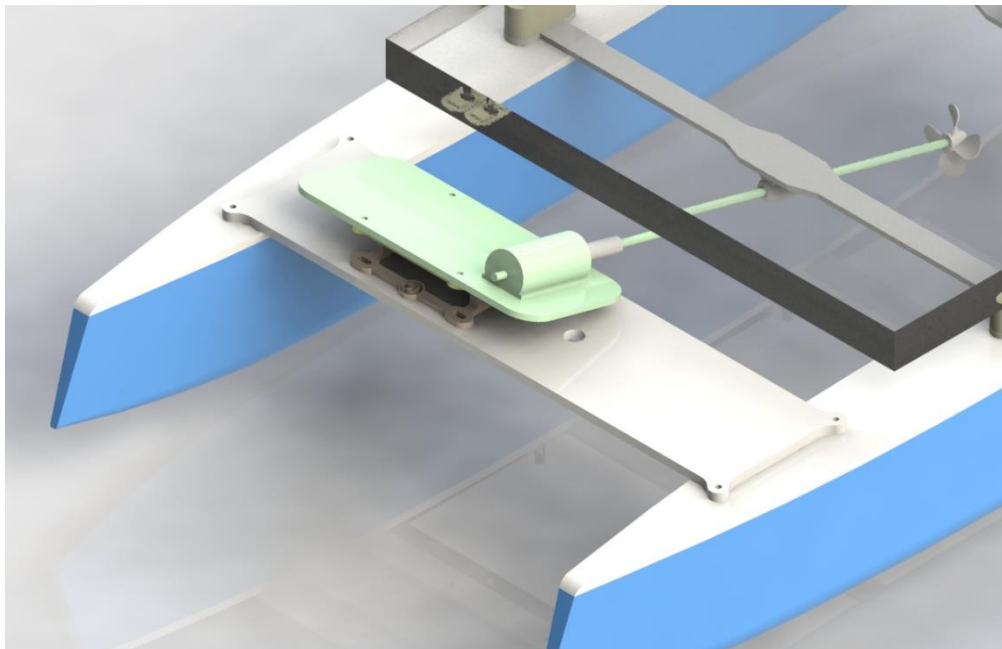


Figure 105: Deck

3.8.2.9 Solar panel risers

The last printed parts are the risers for the solar panel, they lift the solar panel nearly two centimetre in order to accommodate the propeller shaft which is angled down and would hit the solar panel otherwise. This is illustrated in Figure 103: Propellor assembly side view. Furthermore, these risers have a hole in the middle so they can be slid over the pins of the solar panel. They also have small extrusions which slit into the aluminium frame of the solar panel, so they do not rotate. The risers are mounted on top of the brackets for the rudder and propellor shaft.

3.8.3 Print settings

The settings for each part are dependent on the overall shape and size of the part and is sometimes different with materials which are being used, namely, PLA and ABS. Some settings are general and regardless of the material used. This will be explained in the sections below.

3.8.3.1 Layer height

Layer height is the first setting which will be adjusted which is of equal importance with ABS or PLA. The layer height has a direct effect on the surface quality of the part as well as the time to complete the print. Large, less detailed parts can be printed as high as 0.26mm layer height, a good example here is the hull. The hull does not have a difficult geometry and is large, therefore it is more appealing to have a faster printing time than a higher surface quality. On the other hand, a low layer height of 0.12mm is used to print the propeller. This is done because the blades are thin, the propeller is small, and the geometry is complex.

3.8.3.2 Wall line count

This is the thickness of the shell of part. In other words, the number of lines printed before the infill starts. Normally this is left at 3 lines or a thickness of 1.2mm but in some cases where there is a feature that has to be strong, it can be increased. For example, the dovetail slots for connecting the top covers. The wall line count is increased to 7, rendering the connections solid plastic. In general, the strength of the parts increases up to a line count of 8, more than this is not beneficial anymore, disregarding infill percentage.

3.8.3.3 Top and bottom layers

These are the number of layers printed before the infill is printed, basically the same as the wall line count but horizontally. By default, this is put at 4, but at large prints sometimes decreased to 2 or 3 in order to reduce printing time. This brings the risk of being able to see the infill pattern.

3.8.3.4 Z-seam alignment

The start and ending point of the layer is called the z-seam. This is not aesthetically pleasing therefore this feature is put on "hide seam". The slicer program will put the z-seam in a corner where the line is

less visible. The seam also unsettles the tolerance slightly, therefore when printing round parts, it is set to “random” starting and ending each layer at a random point.

3.8.3.5 Infill

This is the percentage of the volume of the inner part which is filled. Most parts do not need to be solid, 100% infill. The infill ensures an internal support structure for the top layers to rest and adhere to. Most parts get their strength from the wall line count, therefore 5% infill will suffice in most cases. For example, the solar panel risers, the hull, and the rudder were printed with very low infill but with a higher line count.

Different patterns can be chosen for the infill such as grid, linear, triangles, ... with gyroid being the strongest and therefore chosen for all parts.

3.8.3.6 Temperature

The temperature is very material dependent, PLA is printed at 205°C hot end temperature and 55°C bed temperature. ABS on the contrary is printed at 230°C hot end temperature and 90°C bed temperature. As well as printed in a housing so no heat can escape. Ideally, for every new material, a temperature tower is printed. This is a configuration print to determine the ideal printing temperature where the result is not too brittle and there is no layer separation. The temperature is responsible for fusing the layers together, hence the strength, it is therefore important that the right temperature is chosen.

3.8.3.7 Print speed

Parts printed in PLA are less prone to warping so they can be printed faster, a print speed of 80mm/s is used for large prints and 40-60mm/s for smaller prints or difficult geometries. ABS is more difficult to print and tends to tear off the build plate. Therefore, ABS parts are printed between 20-60mm/s. generally, a lower print speed results in less artifacts on the prints and a better surface quality.

3.8.3.8 Cooling

The cooling feature enables the blower fan mounted on the hot end and blows cold air on the newly printed layer. This ensures the plastic does not stay liquid or sag. The blower fan should only be enabled if PLA is being used and not with ABS. ABS does not share the need of a fan and enabling it would risk layer separation and warping.

3.8.3.9 Support

If needed, support material is printed under the actual model because a 3D printer cannot print in thin air. When this feature is turned on the slicer software shows the support structure in the preview window. Several sub-settings can be adjusted, for instance the maximum overhang angle before placing supports, the support density, pattern, and so on. Supports are mainly used under the hull because the bow and aft are raised. The rest of the parts are designed not to need any support, this saves material and print time.

3.8.3.10 Build plate adhesion

For PLA, the bed adhesion type chosen is a skirt. The printer will extrude five lines in a perimeter around the print to clear the nozzle. PLA normally sticks well to the print bed therefore a skirt is sufficient. ABS on the other hand benefits from using a brim. This is an adhesion type which connects to the model, printing a thin wide film first. Other options are none or a raft, this is a small structure slightly larger than the print but several layers high, this is beneficial if bed adhesion is a big issue. Most prints get away with using a brim or a raft.

3.8.4 Total print time and mass

The total print time and mass is calculated in Table 22: Print time and mass calculations. These calculations are based on the estimated values acquired from the slicer software. Occasionally, the actual values for the print time were higher than the estimates. Generally speaking, the overall print time will be close to the actual print time. Failed prints and duplicates were not taken into account.

<i>Parts description</i>	<i>amount</i>	<i>material</i>	<i>weight (g)</i> <i>pp</i>	<i>total (g)</i>	<i>print time (h)</i> <i>pp</i>	<i>total (h)</i>
Hull		PLA		766		51
bow	2		94	188	6	12
mid bow	2		149	298	10,5	21
mid aft	2		140	280	9	18
aft	2		83		5,5	
Hull top cover		ABS		208		24
bow	2		16	32	2	4
mid bow	2		32	64	3,5	7
mid aft	2		34	68	4	8
aft	2		22	44	2,5	5
Rudder assembly				29		3
bracket out	2	ABS	6	12	0,5	1
bracket mid	1	ABS	4	4	0,5	0,5
bracket reinforcement	2	ABS	3	6	0,25	0,5
rudder	1	PLA	7	7	1	1
Propellor assembly				30		3,3
bracket out	2	ABS	6	12	0,5	1
bracket mid	1	ABS	7	7	1	1
bracket reinforcement	2	ABS	3	6	0,25	0,5
propellor	1	PLA	4	4	0,5	0,5
motor coupling	1	PLA	1	1	0,3	0,3
Power unit mount		PLA		11		1,1
top	1		4	4	0,4	0,4
bottom	1		7	7	0,7	0,7
Deck		ABS		70		7
part 1	1		35	35	3,5	3,5
part 2	1		35	35	3,5	3,5
Solar panel risers	4	ABS	6	24	0,5	2
			total weight (g)	1138	total time (h)	91,4

other components	
hydrogen station	95
fuel cell and electronics	51
servo components	90
prop shaft	26
solar panel	1360
total weight (g)	2760

Table 22: Print time and mass calculations

The total weight of the printed parts is 1138g and the combined print time is 91.4 hours. The total weight of the boat can now be calculated by adding the weight of the remaining components. This equals 3098g. The load capacity of the hulls is 7,06kg, this means that the boat will float with a safety margin of 156%. This is considered in standing water before the hulls are submerged. This margin resulted in the ship being more buoyant thus less risk of making water.

3.8.4.1 Post processing

The parts are not yet ready after printing. When they come off the print bed the skirt, brim, or support material is removed, this can be done by hand or with a knife. The hull top cover needs some sanding for a better finish, this was done with an orbital sander and the dovetail connections were filed to fit well.

The separate parts of the hull were sanded on the faces that would touch and then glued together, this then formed the complete hull assembly. The rudder assembly and propeller assembly were also slightly sanded and filed, to then be glued together as well.

3.9 Power system integration

3.9.1 Functional explanation of the model ship

The model ship consists of 4 key components: solar panel for electricity generation, an electromotor for propulsion, an electrolyser for hydrogen production, and a fuel cell to convert hydrogen back into electricity. The goal is to monogamously combine these components in order to achieve propulsion in sunny conditions as well as in dark conditions.

The way the model ship is set up is, during sunny conditions, solar energy is directly used to power the motor. In addition, hydrogen is produced with the excess energy by the use of the electrolyser and then stored. Secondly, when there is not enough solar irradiation, the stored hydrogen can be used by the fuel cell to produce electricity and on its turn power the motor.

If the ship is docked and there is enough sunlight it is also possible to activate the electrolyser in order to produce and store hydrogen. By the use of pilot switches an operation mode can be chosen. For steering the ship, a servo system is installed which can be remote controlled.

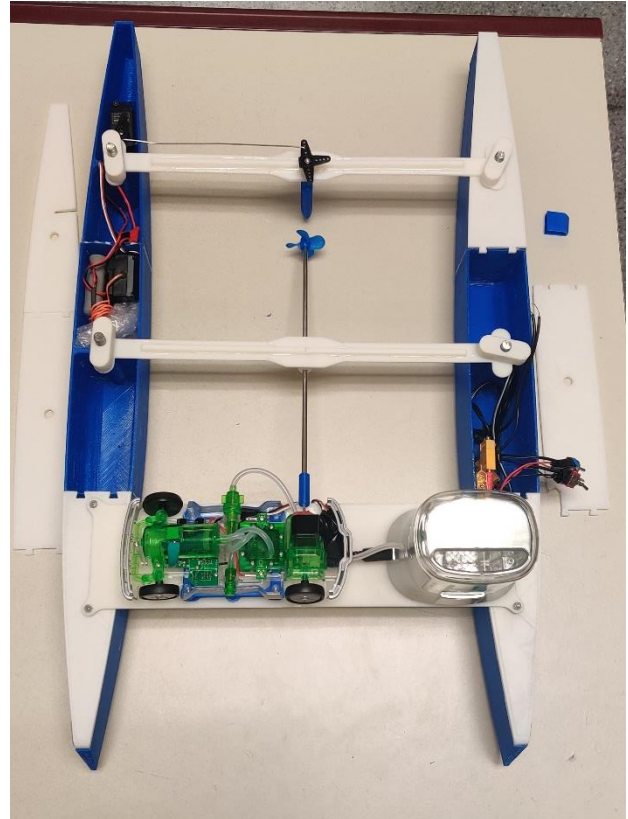


Figure 106: Model ship internals

3.9.2 Assembly

Continuing the build with the assembly of the boat, the printed parts, hydrogen, and the electrical parts will be put together to form an operational model ship. The following paragraphs will explain the assembling process of the boat and the instalment of the power circuit. As well as an explanation of the purpose of the components.

3.9.3 Printed parts

As previously mentioned, the individual parts are glued together and can now be assembled. First, the subassemblies of the rudder and propellor are put together. The rudder is slid through the bracket and the rudder steering arm is screwed down. The propeller is put onto the shaft and also slid through the support bracket. After, the motor coupling is press fitted onto the shaft.

The top electronics mounting plate is screwed onto the bottom of the hydrogen components mounting plate. The bottom electronics mounting plate is bolted on the deck. Which can then be screwed through the hull top cover into the hull with long M3 bolts.

3.9.4 Hydrogen related components

The hydrogen system consists of three important pieces which have to be connected. These components are the electrolyser and water tank, the hydrogen storage, and the fuel cell. The parts are supplied by the company Horizon and came in a kit to make a hydrogen powered car.

3.9.4.1 Electrolyser

The electrolyser comes built into a housing which is also the reservoir for the distilled water. Internally, hydrogen and oxygen lines are connected to the designated ports on the fuel cell. The output tube is a hydrogen line with a valve connected at the end. This will connect with the hydrogen storage. At the backside of the device is a switch located with the options: Off, DC, and solar. For the purpose of the model ship, only off and solar will be used when the ship is in operation. The DC mode would make use of a pair of internal batteries, since the ship will be powered by solar energy it is not needed to use batteries.

The hydrogen station is wired to receive power through the input at the side of the device. The plug connector is wired under the deck and comes through the designated hole in the deck. The wires connect to the internal circuit which is housed mainly in the left hull.



Figure 107: Hydrogen station

3.9.4.2 Storage and fuel cell

Since the hydrogen assembly consists of two parts, the hydrogen station, and the storage – fuel cell station, it is possible to refuel the boat without the need of the hydrogen station on board.

The storage and fuel cell station are connected in the following way. First, the valve for receiving hydrogen is connected via tubing to the fuel cell. Secondly, the fuel cell is connected to the 10ml hydrogen storage balloon. And lastly, the storage balloon is connected to a purge valve. The purpose of the purge valves is to remove all the air from the system when it is first started up.

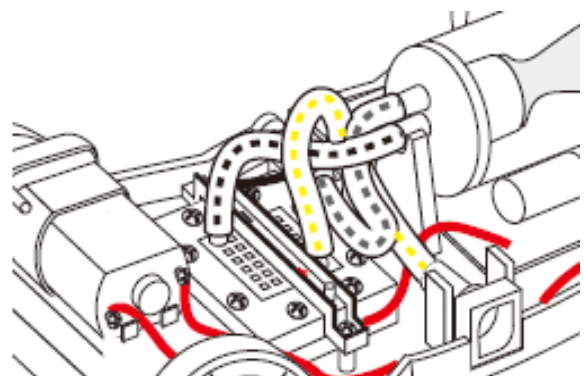


Figure 108: Fuel cell connections

The fuel cell does not need a supply line for oxygen because it simply uses the oxygen from the air. The fuel cell is electrically connected to the integrated circuit, this will be further explained in the following units.



Figure 109: Hydrogen power unit

3.9.5 Solar panel

The solar panel is a crucial element of the power generation as well as for structural rigidity. The solar cells are mounted on a stiff aluminium frame with threaded mounting rods screwed into. This is used as an advantage, connecting the hulls to the frame makes the whole ship sturdy. The threaded rods slide into the supports in the hull. The disadvantage of the aluminium frame is the increased weight. Electrically, the solar panel is connected to the circuit with the use of XT60 connectors. These connectors make assembly and disassembly convenient. The rated current for these connectors is 60A.

3.9.6 Servo and radio control

A remote-control system was chosen to steer the ship. An unused vintage Futaba system was available and could be used for implementation. The systems consist of 5 servo motors, a 35.080Mhz receiver module, a 500mAh battery pack, and a remote control of the same frequency.

The servo motor is equipped with a steering arm with variable positions for the linkage arm. The servo is mounted in the previously designed bracket and connected to the receiver module. The battery pack is also connected to the receiver module and can be activated with a power switch. The remote control and receiver unit is capable of controlling up to 7 servos, in this case only one is used for the rudder.

The components are fitted in the hull of the ship and a cut-out is made in the hull top cover to allow the linkage to actuate freely. The rudder has a turning radius of 100° in its current configuration, this gives the best actuation, but it can be changed by modifying the position of the linkage. With this addition, the ship is now completely remote controlled.

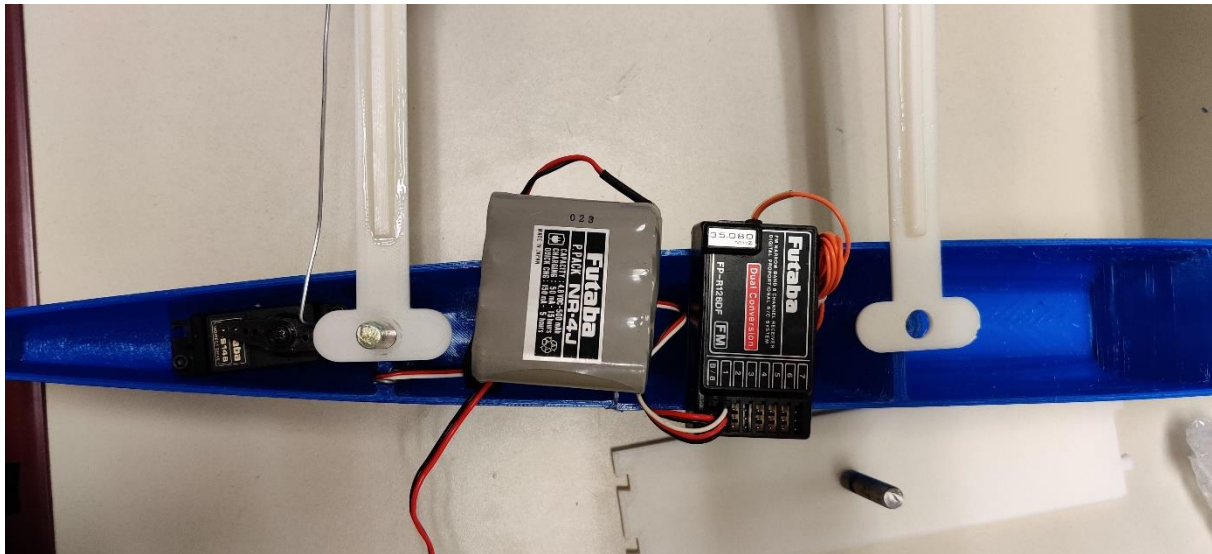


Figure 110: Servo control components

3.9.7 Circuit

A simple electric circuit has to be designed in order to enable the desired functionalities. These functionalities are motor operation in sunlight, motor operation in without sunlight, and just hydrogen production without motor operation.

The kit from Horizon also contained an integrated circuit, this circuit has the following functions. Forward and backwards driving of the motor by the use of a separate remote control. There is also a switch on the bottom to activate a warm up cycle for the fuel cell. This is for the fuel cell to reach operating temperature and is done by shorting the poles. The other positions of the switch are “off” and “on” with obvious functions.

The solar cells and the fuel cell are both separate voltage sources. To protect the components and the integrated circuit from any possible voltage differential, it is chosen to completely separate them while the motor is in operation. It will either be the solar cell powering the motor or the integrated circuit powering the motor. This is done by physically disconnecting both positive and negative leads to the motor by the use of two 2-way switches. There is also a third switch that shorts the motor in solar mode, this way only the hydrogen station is actively producing hydrogen while the boat is stationary.

Below the circuit diagram can be found:

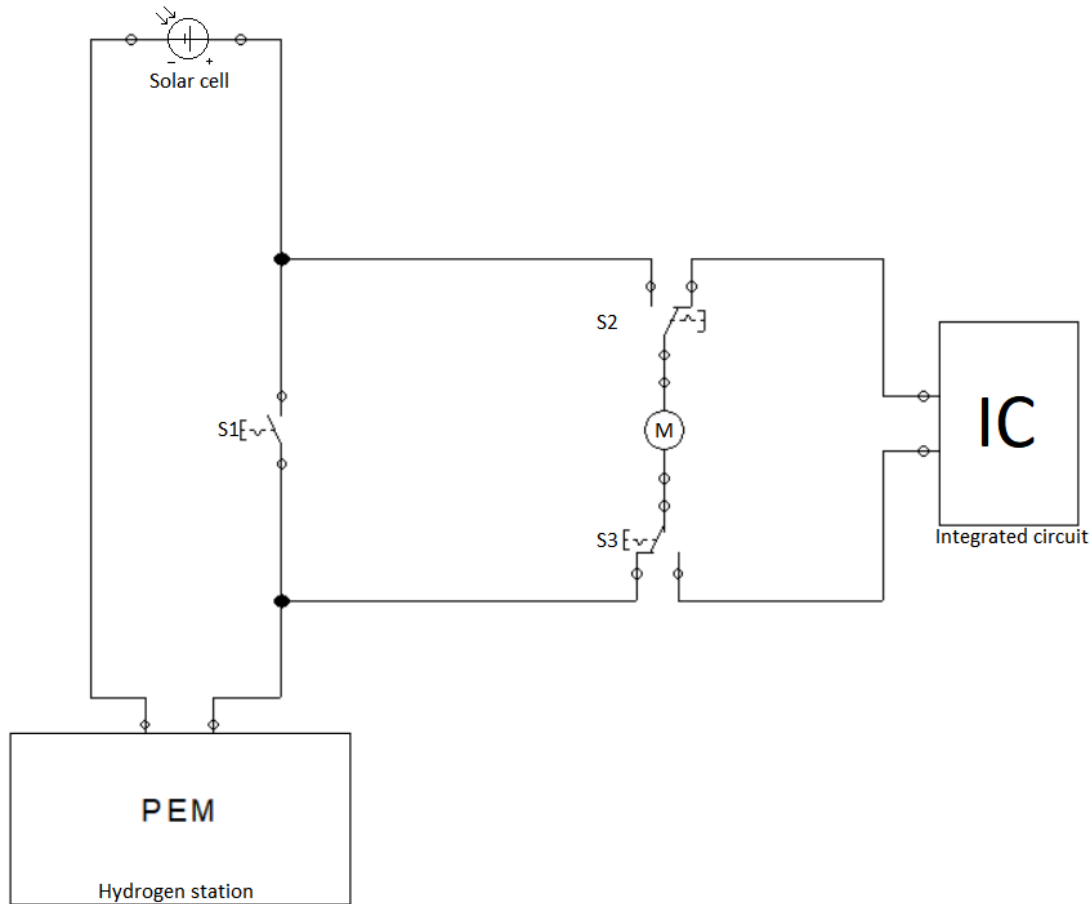


Figure 111: Power system integration electrical circuit

3.9.8 Modes

As previously mentioned, there are three operating modes which are selectable by activating a combination of the switches. First is hydrogen charging mode, S1 has to be closed, the power of the solar cells will go directly to the hydrogen station. This is useful if the ship is docked and the hydrogen tank is not filled completely.

The second one is solar mode, S1 is opened, S2 and S3 are connected to the solar cells. This way the motor is powered by solar energy. The remaining power is being used by the hydrogen station. This mode is useful when sailing during the day when there is an abundance of light hitting the solar panel.

The third mode is used for when there is not enough light to produce sufficient energy. The switches S2 and S3 are then connected to the integrated circuit and powered by the fuel cell. The motor and integrated circuit are completely disconnected from the solar cell circuit. With the remote it is then possible to activate the motor.

Additionally, the hydrogen station can be run on batteries which have to be put in the bottom of the station. However, the goal is to autonomously sail the boat with the power generated by itself.



Figure 112: Mode pilot switches

3.10 Operational performance evaluation of the design

This final section will evaluate the functioning of the model catamaran. The results from previous experiments will be compared with the actual findings. It will discuss the specifications and use of the power modes.

3.10.1 Specifications

The catamaran is equipped with a solar panel capable of producing around 1800mW of power in its current configuration. This is in solar mode on a sunny day. The power is split between the motor, which uses 1400mW, and the electrolyser, which uses 400mW. The electrolyser takes 12 minutes to fill the tank. And the rpm of the motor is high.

In hydrogen charging mode all the energy is used for producing the gas, then it only takes 6.9 minutes for a full 10ml tank. Calculated with an average current of 0.2A. In hydrogen usage mode the motor is driven by the fuel cell which uses the stored hydrogen. Looking back at the efficiency, there were three loads: low, medium, and high which emptied the tank in respectively 7,6 and 5.5 minutes. The actual sailing time in water is on average 6-7minutes which makes for a medium load.

3.10.2 Hydrogen runtime

This also means that if the boat runs purely on hydrogen and the hydrogen charging mode is active, it could run for either: indefinitely, 46min or 27min without having to stop and recharge the hydrogen tank. Calculated with the results on the water it runs for 46min. However, these numbers are highly dependent on the current drawn which range from 0.1A-0.25A. Half of the time this value is 0.2A or higher.

During the sunny full day experiment a total of 420ml of hydrogen is produced when in hydrogen recharge mode. If a larger storage tank could accommodate all the hydrogen, this would result in 11h and 40min of sailing.

3.10.3 Electrical runtime

The minimum for the motor to run is 0.4V and 0.09A. This translates to an operational status as soon as there is direct sunlight hitting the solar panel. This can be seen in the day 2 experiment Figure 46: Full day experiment 2 IT characteristic. If the solar panel is in the shade for example thick clouds pass over, current drops to 0.05A and the motor will stagnate.

3.10.4 Open water evaluation

Putting the catamaran in the water made clear that the balance and stability of the boat was good, and it floats evenly on the water. However, the boat has a loading capacity of 7kg, and this caused the propeller not to be completely submerged. It had a freeboard of 6cm. 1.5kg of ballast was added and the freeboard was reduced to 3cm, submerging the propeller completely therefore making the boat

perform better. The speed of the boat is around 10m/min. The remote controlled steering worked fine although the turning radius is big. This is a point for improvement as the surface area could be bigger.

The motor turned the quickest in direct sunlight in solar mode. All the modes worked as designed. The motor rpm in hydrogen was lower because the power output of the fuel cell is less than the power output of the solar cell. All and all the test runs were positive and resulted in a proof of concept.

3.10.5 Advised sailing mode

In order to have the best performance of the ship it is advised to follow this mode progression. As soon as there is direct sunlight shining on the solar panel it is possible to start sailing electrically in solar mode, this is the yellow area starting at 0.1A. In the meantime, the hydrogen tank is being resupplied.

Once a current of 0.2A is reached it is possible to either keep sailing electrically until the end of the second yellow area, also generating hydrogen. Or switch to hydrogen mode, to generate and use hydrogen at the same time. The blue line indicates the point where there will be more hydrogen consumption than generation, at this point there will be roughly 1h left before hydrogen depletion. After that it is still possible to sail on solar. This option is less desired.

A better option is to keep sailing electrically from the start of the first yellow area until the end of the second yellow area. This way the maximum amount of hydrogen is generated. If hypothetically a bigger tank is fitted that could accommodate all of the hydrogen than it could sail through the night. This is the green area. With the limitations of the current tank, it is possible to sail for 6min into the green area and is indicated with the green lines.

In summary, green is only on hydrogen, yellow is motor driven on solar and producing hydrogen, and optional blue is generating hydrogen and using it at the same time. The combination green and blue gives the longest sailing time.

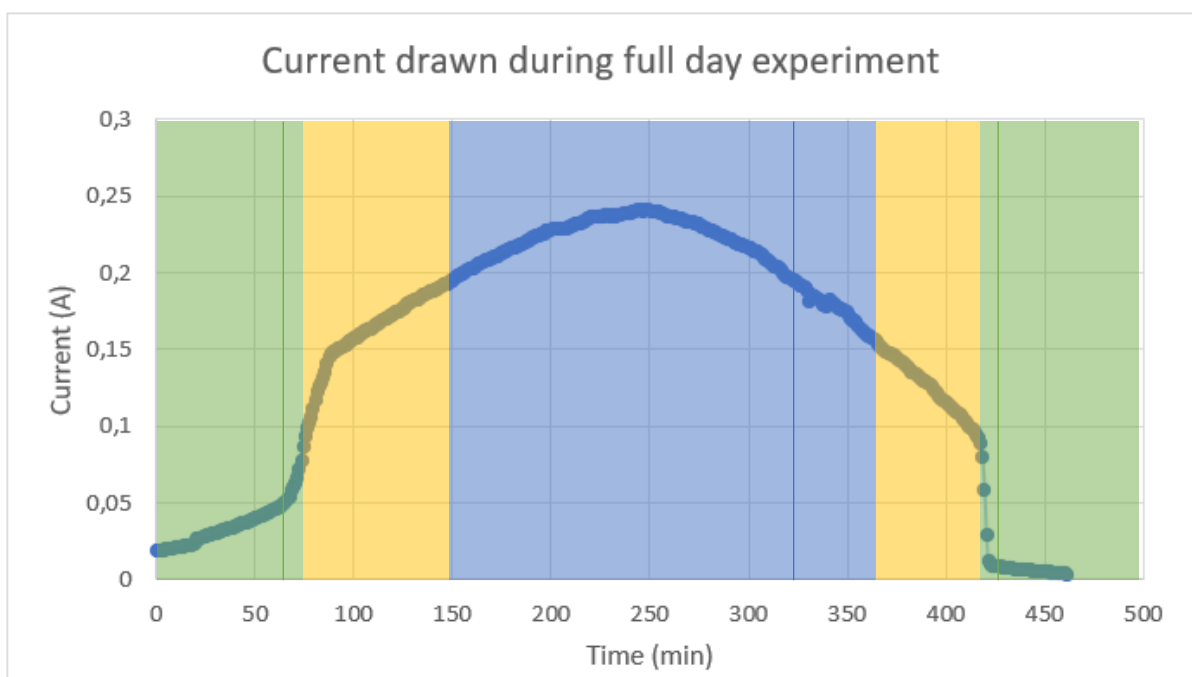


Figure 113: Advised sailing mode

4 BUDGET



4 Budget

After finishing the model catamaran, it is now time to project this proposal to the full size Alinghi 5 catamaran. The goal is to make a rough estimate of the costs involving the retrofitting of the current catamaran in its current state to an operational yacht and the annual expenses once it is done. This will include repairs, maintenance, as well as the cost of new equipment such as the solar cells, electrolyser, fuel cell, storage, and motor.

Since it will be a sustainable and autonomous yacht, the difference regarding fuel costs with regular motor boats and sailboats can be made.

To find the return on investment, a way of income will have to be generated. This can be done by chartering the yacht for periods of time or as transport to nearby islands and calculating the income. This can then be compared to existing options, and in turn provide for a fully sustainable maritime mobility as the first step in eliminating fossil fuels in navigation.

The Alinghi 5 is a large boat which will, after retrofitting, be able to accommodate between 10-12 people. Therefore, upcoming propositions will be compared to similarly sized vessels.

4.1 Energy observer

A good reference point for this calculation is the Energy observer developed by CEA-LITEN. The Energy observer is an experimental research vessel generating and powered by hydrogen. Just like the Alinghi 5 it is a former race catamaran similar in size and it has a similar purpose. Its length is 30m and the technologies used on board are as follows.

The autonomous catamaran emits no greenhouse gas by the use of renewable energies. It has 3 types of solar panels extending over a surface of 130m². This generates a 21kW peak. In addition, the ship has two vertical axis wind turbines generating 1kW each, and 2 electric motors of 41kW. The energy is stored in a lithium battery with a capacity of 106kWh. The ship is also equipped with 1 desalinator, 1 electrolyser, 1 compressor, and 1 fuel cell of 22kW. The weight of the ship is 28 tonnes. This configuration allows the ship to sail with a speed of 8 to 10 knots. [33] [34]

For simplicity and since this catamaran is in operation, it can be determined that components with similar specifications with the same order of magnitude will also work for the Alinghi 5. Price calculations can be done by finding the cost for these components. A more detailed analysis can be made recalculating power necessities, but this would lead too far and therefore is out of the scope of this thesis.

4.2 Solar panels and battery

The energy observer's length is 30.5m by 12.8m. This makes for a surface area of 390.4m². The total surface area covered by solar panels is 130m², which is one third in its current configuration. If the Alinghi 5 is configured in the same way a total of 170m² would be covered by solar panels, as its dimensions are 34m by 15. This would produce 27kW peak.

This solution is from Sunwatts. They offer a 30kW solar system. This package includes 77 solar cells of 390W, 4 inverters, monitoring system and accessories. The monthly energy production is 3,629 kWh AC. The surface area is 150m². This costs € 28100 as a base price. Additionally, a complementing battery pack can be purchased for € 33210. The battery pack has a capacity of 100kWh. [35]

The total cost for this system not including installation is € 61310.

4.3 Wind turbines

Wind turbines on the catamaran are a great secondary source of energy generation when the sun is not shining. It is therefore recommended to implement them on the ship and in this calculation. There is room for 2 turbines on both sides of the boat.

This product comes from Wattneed, they supply a kit including the vertical axis turbines and inverter. The price per turbine is € 1.976 and the inverter costs € 2.137. An additional braking resistor is needed, and it costs € 90.8. [36]

The total cost of this kit not including installation cost is € 6.180.

4.4 Electric motors

Two motors will be placed in the ship, one in each hull. Next solution is not as powerful as the one from the energy observer but will be sufficient because the Alinghi 5 is half as light as the observer (in its unconverted form).

The solution comes from Oceanvolt, it is a dual motor configuration each 20kW, suitable up to 23 tonnes. Included in the system: 2 x 20kW shaft drive motor, 21kWh Lithium battery bank, 22kW DC Generator, 2,8kW Charger, Hydrogenation feature. With fully charged batteries, this system has a range of 20nm. In combination with the 100kWh battery bank this range becomes 125nm. [37]

The price of this complete system equals to €102.280

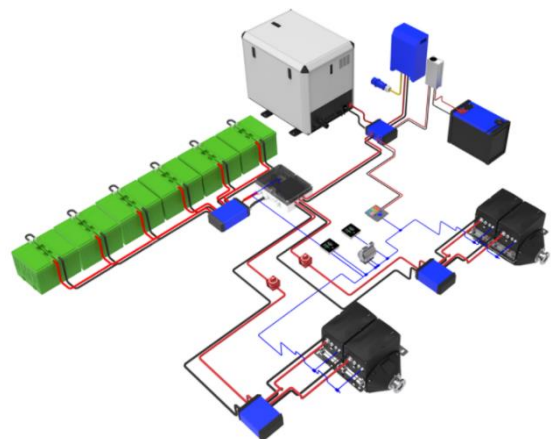


Figure 114: OceanVolt electric motor system [37]

4.5 Fuel cell

In this alternative four 5kW PEM fuel cell stacks will be fitted in the ship. This is one of the bigger expenses of the retrofitting as each stack costs €18.500. The fuel cell is supplied by Fuelcellstore and is made by the Gatechn Team. Hydrogen Consumption is four times 58.3 l/min at nominal power. This specific unit works at 0.06Mpa. [38]

The total cost of this system is thus € 74.000.

4.6 Electrolyser

From a supplier called Pure energy centre, an electrolyser can be bought. The “small scale” electrolyser produces 250 litres of hydrogen per hour and can therefore accommodate the hydrogen need of the fuel cells. The operating pressure can be specified and therefore matched with the fuel cell. The price for this unit is € 46.000. [39]

4.7 Hydrogen compressor and storage

In order to store a bigger volume of hydrogen it can be compressed and stored in a tank. This solution comes from the same supplier, Pure energy centre. A compressor can be chosen to pressurise the gas to 200 bars. The cost would be € 46.000. [40]

They also suggest a 12 pack of 200bar containers, accommodating for 105.6m³ hydrogen under pressure. The tanks cost in total € 6.500. [41]

4.8 Retrofit

The retrofit of the catamaran is going to be the most expensive part of the equation. This is because it requires the most man hours, labour. Starting from redesigning the layout and calculating the capacity to the actual construction and finishing of the ship. It is therefore difficult to assess the cost as it is dependent on many factors. Especially as it is an experimental design and not common practice making a boat autonomous. Building a new catamaran of equal length would cost anywhere from 5-15 million depending on the complexity and luxury required.

The redesign can be estimated not to exceed € 500.000. Labour is normally 3-5 times the cost of the equipment, combining the costs of the new technologies discussed above will average to € 350.000. Five times this amount equals 1.75 million.

Adding these numbers together, € 350.000 for energy capture and usage equipment, € 1.750.000 for labour, € 500.000 for the redesign, equals € 2.6 million. The cost of adding additional standard equipment, such as navigation etc. and installation is estimated to € 400.000. Combined, this gives a rough estimate of € 3 million. This value is of the same order of magnitude as the retrofit cost of the energy observer, which is 4 million euros.

4.9 Annual expenses

After the construction of the ship, it has to be maintained and looked after, this includes annual costs. This is calculated using a tool from Luxyachts. Below, a breakdown of the costs can be seen. This is dependent on input sliders on the left. The base input is the length of the boat, which is 90ft. As it is intended to charter the vessel, the owner is not going to be using this boat for pleasure and private trips too often, therefore the owner's input can be reduced. Fuel and dockage are also reduced as the ship does not need additional fuel, it is excluded from the calculation.

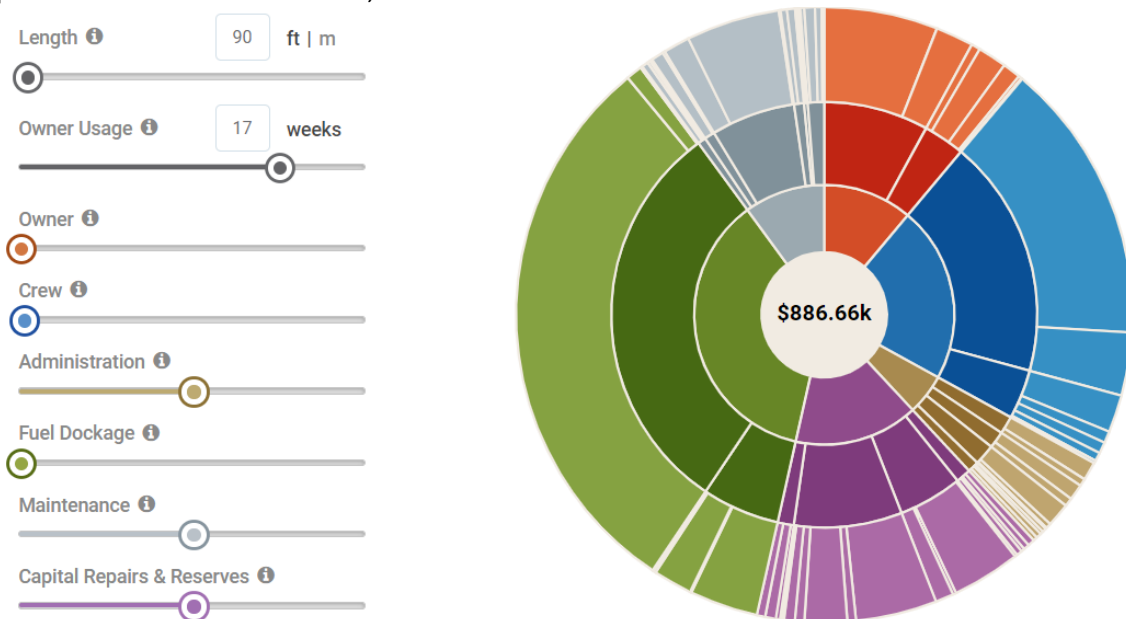


Figure 115: Luxyacht cost calculator [42]

Since the ship runs on solar and hydrogen power refuelling is not necessary and can therefore be deducted. This is a big factor in the annual cost, the difference is 30% in savings for fuel. However, the whole installation is more costly at purchase. The engineering cost can be reallocated for the cost in taking care of the electric and hydrogen power system. The total of the expenses is € 744.500 but without the fuel cost, the operating cost is € 514.500 annually. [42]

Owner	\$99,750	^	Maintenance	\$90,243	^
Provisions	\$71,400	∨	Bridge	\$5,520	∨
Services	\$28,350	∨	Deck	\$7,020	∨
Crew	\$196,568	^	Engineering	\$57,390	∨
Salaries	\$162,750	^	Interior	\$6,720	∨
Permanent crew	\$132,966	∨	Galley	\$2,520	∨
Dayworkers	\$29,784		Annual shipyard	\$11,073	∨
Supplemental costs	\$33,818	∨	Annual Operating Expenses	\$759,434	
Administration	\$45,756	^	Capital Repairs & Reserves	\$138,451	∨
Insurance	\$12,250	∨	Total Expenses*	\$886,662	
Regulatory	\$11,500	∨			
Financial management	\$14,316	∨			
Office	\$7,690	∨			
Dockage & Fuel	\$327,117	^			
Dockage & port fees	\$52,938	∨			
Fuel & transport	\$274,179	∨			

Figure 117: Luxyacht cost calculator 2 [42]

Figure 116: Luxyacht cost calculator 3 [42]

4.10 Income

In order to recuperate the annual expenses as well as the cost for retrofitting the ship, some options of generating income will be explored.

4.10.1 Charter as research vessel

The first possibility is to charter the catamaran for a period of time on a private basis. With a purpose such as research expeditions. The tasks of a research vessel can be: hydrographic survey, oceanographic research, fisheries research, coastal research, pipe inspection, etc.

For example, Foras na Mara Marine Institute has two vessels, the Celtic Explore and the Celtic voyager for charter as research vessels. Their functions are fisheries research and coastal research. They are both 100ft ships and therefore close to the size of the Alinghi 5. Their prices are € 19.000 and € 8.500 per day. [43]

The European Marine Board shared that on average their research vessels are in operation for 116 days (or 16.5 weeks). If the Alinghi 5 is deployed in a similar manner an income can be generated between € 986.000 and € 2.204.000 per year. [44]

4.10.2 Charter for pleasure

A second option is to charter the vessel for pleasure. Doing so for a given period of time. Let us assume 16.5 weeks to be equal to the previous example. For this to work, the yacht has to be furnished with luxury items and be designed in a different way, for maximal comfort.

Yachts this size are usually rented out for € 50.000 per week. This would yield € 825.000 annually.

Day charter is also possible, for yachts carrying 12 people, the price usually amounts to € 5.500 per day. Recalculated equals € 638.000 per year. [45] [46]

4.10.3 Charter for daytrips and island transport

Providing a ferry service to one of the nearby islands such as Ibiza is a third option. Current prices go from €44 to €330 per ticket. The voyage takes a little less than 5h so the route Valencia – Ibiza could be done twice a day with a normal ferry, however they travel up to 33 knots. Using the Alinghi 5 would traverse with only half the speed, implying only one trip per day. With 12 persons on board, this yields € 528 to € 3960 per day or € 61.250 to € 460.000 per year.

With the same optic, Valencia – Palma can be done. Prices average around 260 per trip, which makes € 3.120 per day or € 362.000 annually. [47]

4.11 Evaluation

First to evaluate is the solar powered propulsion method in comparison with an internal combustion engine system. In the table below the cost of the new system is shown. As well as the time for a return on investment (ROI), it is calculated by determining the time it takes to recover the investment cost by substituting the fuel cost. The ROI for the propulsion system is 9.13 years.

<i>Solar vs internal combustion engine</i>	
<i>cost for installation</i>	
equipment	€350.000
installation	€1.750.000
total	€2.100.000
<i>fuel cost</i>	
annual cost	€230.000
<i>ROI (y)</i>	9,13

Table 23: Solar vs internal combustion engine

A breakdown is presented of the equipment and their estimated cost, as mentioned before. The total of the retrofit is given along with the annual operating cost. These values are needed to determine the ROI for the suggested methods of making an income.

<i>Total cost: retrofit of the boat</i>	
energy capture equipment	€350.000
solar panels	€28.100
battery	€33.210
wind turbines	€6.180
electric motor system	€102.280
fuel cell	€74.000
electrolyser	€46.000
compressor	€46.000
hydrogen storage	€6.500
labour	€1.750.000
design	€500.000
additional equipment	€400.000
<i>total</i>	<i>€3.000.000</i>
<i>Annual cost of the boat</i>	
operating cost	€514.500

Table 24: Retrofit of the boat

In the last table the comparison between the three main options is made. An initial ROI is calculated to show the return time for the fabrication of the ship. Afterwards the ROI is calculated including the operation cost, evaluating the total scheme.

As it shows, island transport and day trips are not profitable. This is mainly because ferries go get their passengers to the desired location as soon as possible, allowing multiple trips per day. The Alinghi 5 is too slow for this purpose making this the least favourable option.

Weekly charter for pleasure comes second but still has a relatively long ROI time of 9.66 years and day charter has a ROI of 24.29 years. Worth mentioning that for this purpose the ship has to be built in a luxurious way. Generally, the lifecycle time of a ship is 30 years and every 5 years an expensive survey has to happen makes this option also not ideal.

The last and best option is to configure the ship as a research vessel. This yields the largest profit and a ROI of 2 to 6 years. The income can be expected to be between 1 and 2 million per year. Therefore, it makes the most sense transforming the Alinghi 5 into a research vessel.

<i>Income</i>	€	<i>Initial ROI (y)</i>	<i>ROI (y)</i>
<i>Charter as research vessel</i>			
lowest case	986.000	3,04	6,36
highest case	2.204.000	1,36	1,78
<i>Charter for pleasure</i>			
week charter	825.000	3,64	9,66
day charter	638.000	4,70	24,29
<i>Island transport and daytrips</i>			
lowest case Valencia Ibiza	61.250	48,98	not profitable
highest case Valencia Ibiza	460.000	6,52	not profitable
average Valencia Palma	362.000	8,29	not profitable

Table 25: ROI

5 CONCLUSIONS



5 Conclusions

This chapter evaluates the solutions and whether the research objectives are achieved.

- Objective: “Energy technology and - storage selection: researching which methods of hydrogen production and storage are available. Determining which method is most viable for the purpose. Characterising the chosen devices and implementation in combination with the solar panel. Incorporation in the model ship.”

Evaluation: Both solar and hydrogen energies were thoroughly explored, as well as the current and future vision on technologies in the autonomous maritime sector. The selection of converting and storing energy in hydrogen form is made. The technologies chosen for this purpose are electrolysis and fuel cell technology, combined with compressed gas storage. Devices such as the electrolyser and fuel cell were subjected to several tests. This was done in order to fully characterise their behaviour to assess their optimal operating condition and to find their limitations. Finally, the devices were combined with the solar panel in one circuit to operate in coherence.

- Objective: “Solar panel capture characterization: the optimal solar technology which is industrially available for the application is amorphous silicon. A commercial sized panel will be fitted into the proposed model. The setup will be characterized and analysed for evaluating the power generation and its possibilities. Analysis will be done to determine the significant parameters and make adjustments for optimization.”

Evaluation: A literature review was conducted in order to have a better understanding of the current technologies on the market, and which one is best suited for maritime use. Next, the solar panel was characterised to find the optimal power point, its efficiency, fill factor, IV - and PV curve. A data acquisition program was configured to log full days of testing and make the characteristics. The solar cell was further analysed in combination with the electrolyser and motor to determine the optimal cooperation setup.

- Objective: “Model catamaran: using the available catamaran design, a model will be engineered to fit on the power system. This will be done by using 3D additive manufacturing.”

Evaluation: Inspired by the Alinghi 5 a 3D model of the catamaran was designed. The catamaran accommodates the hydrogen parts. Buoyancy calculations were made in order to verify floatability of the hull. Additive manufacturing was the chosen method to manufacture the model catamaran. A study was done in order to find the optimal material and 3D printer settings. Finally, the parts were printed and assembled.

- Objective: “Power system integration: Finally, a test rig will be assembled with the required electric motor, propeller, and power unit. From there on, the design can be further improved, and the assembly can be characterized and evaluated.”

Evaluation: all the parts were assembled. The solar panel, the hydrogen parts and a remote-control steering system were added and fitted into the 3D printed catamaran. An electric system was designed to change power modes by the use of pilot switches. They allow you to switch to sailing electrically or on hydrogen power. Subsequently, an operational performance evaluation was carried out, this is the

characterisation of the model ship that includes the calculation of the sailing times in the different modes. This coupled the results of the individual experiments to the actual conditions of the model ship. To finalise with advice for the optimal transition of sailing modes.

In addition, an economical study was made to find a logical purpose for the Alinghi 5. In the future the ship can be retrofitted to a research vessel for coastal missions. Calculations are made and a rough estimate is determined for the cost of the construction and the new equipment. With these numbers, a supplementing return on investment is made as well.

The general conclusion is that the main goals and objectives have been met. A functional autonomous 3D printed solar catamaran has been made and can be remote controlled. The model serves as an interesting proposal for sustainable maritime transportability combining solar and hydrogen as renewable energies. The results of this project demonstrate the viability of the development for fully sustainable maritime mobility as a first step in eliminating fossil fuels in navigation.

6 REFERENCES AND OTHER SOURCES OF INFORMATION



6 References and other sources of information

- [1] Alinghi, "The 33rd america's cup," [Online]. Available: <https://www.alinghi.com/33rd-america%E2%80%99s-cup>. [Accessed 05 01 2021].
- [2] A. Brink, "Arthur's Column," 08 06 2010. [Online]. Available: <https://www.adriaan.com/tag/alinghi-5-catamaran/>. [Accessed 05 01 2021].
- [3] IMO, "Autonomous shipping," [Online]. Available: <https://www.imo.org/en/MediaCentre/HotTopics/Pages/Autonomous-shipping.aspx>. [Accessed 05 01 2021].
- [4] T. S. Rana, "The Future of the Maritime Industry: Autonomous Shipping," 23 07 2019. [Online]. Available: <https://www.icnnational.com/the-future-of-the-maritime-industry-autonomous-shipping/>. [Accessed 06 01 2021].
- [5] Rolls Royce, "Autonomous ships The next step," 2016. [Online]. Available: www.rolls-royce.com/marine. [Accessed 06 01 2021].
- [6] Det Norske Veritas, "Energy Transition Outlook 2019," DNV-GL, 2019. [Online]. Available: <https://eto.dnvgl.com>. [Accessed 20 01 2021].
- [7] Energy efficiency and renewable energy, "Hydrogen and Fuel Cell Technologies Office Multi-Year Research, Development, and Demonstration Plan," U.S. department of energy, [Online]. Available: <https://www.energy.gov/eere/fuelcells/downloads/hydrogen-and-fuel-cell-technologies-office-multi-year-research-development>. [Accessed 20 02 2021].
- [8] Alternative Energy Tutorials, "Alternative Energy Tutorials," 2021. [Online]. Available: <https://www.alternative-energy-tutorials.com>. [Accessed 20 01 2021].
- [9] E. Becquerel, "Mémoire sur les effets électriques produits sous l'influence des rayons solaires," *Comptes Rendus* 9, vol. 1935, pp. 561-567.
- [10] E. Seale, "Solar Cells, Shedding a little light on photovoltaics," 28 02 2002. [Online]. Available: http://solarbotics.net/starting/200202_solar_cells/200202_solar_cell_use.html. [Accessed 20 01 2021].
- [11] A. Dixon, "Photovoltaic energy conversion: theory, present and future solar cells," 1981. [Online]. Available: <https://www.sciencedirect.com/topics/engineering/amorphous-silicon-solar-cel>. [Accessed 20 01 2021].
- [12] A. Shah and J. Meier, "Towards very low-cost mass production of thin-film silicon photovoltaic (PV) solar modules on glass," in *Thin Solid Films*, Elsevier, 2005, pp. 292-299.
- [13] A. M. Green, "Recent Developments in Photovoltaics," *Solar Energy*, vol. 76, no. 1-3, pp. 3-8, 2004.

- [14] Fraunhofer ISE, "Photovoltaics Report (PDF)," 2014. [Online]. Available: https://en.wikipedia.org/wiki/Crystalline_silicon#cite_note-Green1-46.
- [15] J. A. Luceno-Sanchez, A. M. Diez-Pascual and R. P. Capilla, "Materials for Photovoltaics," *State of Art and Recent Developments, International Journal of Molecular Sciences*, 2019.
- [16] Askdifference, "Irradiation vs. Radiation," 06 03 2018. [Online]. Available: <https://www.askdifference.com/irradiation-vs-radiation/>. [Accessed 20 01 2021].
- [17] SunWise U.S., "How UV Index is Calculated," *Environmental Protection Agency*, 2015.
- [18] A. Karafil, "Temperature and Solar Radiation Effects on Photovoltaic Panel Power," 08 2016. [Online]. Available: <https://www.researchgate.net>. [Accessed 20 01 2021].
- [19] Hydrogen Europe, "Hydrogen basics," 2017. [Online]. Available: <https://www.hydrogeneurope.eu/hydrogen-basics-0>. [Accessed 29 01 2021].
- [20] S. Shen, M. Zhang and D. Urry, "Horizon Renewable Energy Science Education Manual," Horizon Educational Group, 300 North La Salle Street Suite 4925 Chicago IL 60654 USA.
- [21] Hydrogen Europe, "Hydrogen storage," 2017. [Online]. Available: <https://www.hydrogeneurope.eu/hydrogen-storage>. [Accessed 29 01 2021].
- [22] Hydrogen Europe, "Electrolysers," 2017. [Online]. Available: <https://www.hydrogeneurope.eu/electrolysers>. [Accessed 29 01 2021].
- [23] Hydrogen Europe, "Fuel Cells," 2017. [Online]. Available: <https://www.hydrogeneurope.eu/fuel-cells>. [Accessed 29 01 2021].
- [24] J. Bae, "Fuel Processor Lifetime and Reliability in Solid Oxide Fuel Cells," Elsevier, 2021. [Online]. Available: <https://www.sciencedirect.com/topics/engineering/fuel-reforming>. [Accessed 29 01 2021].
- [25] Axiom Test Equipment, "Keithley 2601," 2021. [Online]. Available: <https://www.axiomtest.com/Meters>. [Accessed 17 02 2021].
- [26] T. L. Nelson A.Kelly, "Increasing the solar photovoltaic energy capture on sunny and cloudy days," *Solar Energy*, vol. 85, no. 1, pp. 111-125, 2011.
- [27] C. Kap-Seung, J. Ahn and J. Lee, "An Experimental Study of Scale-up, Oxidant, and Response Characteristics in PEM Fuel Cells," *IEEE Transactions on Energy Conversion*, vol. 29, no. 3, pp. 727-734, 2014.
- [28] T. Tolga, "Energy and exergy analyze of PEM fuel cell: A case study of modeling and simulations," *Energy*, vol. 143, pp. 284-294, 15 01 2018.
- [29] Y. Semih, B. Kubilay and D. K. Kerim, "3D printed solar Catamaran model design and embedded sensing system application," *International journal of 3d printing technologies and digital industry*, vol. 2, no. 3, pp. 12-21, 2018.

- [30] GE Additive, "What is Additive Manufacturing?," [Online]. Available: <https://www.ge.com/additive/additive-manufacturing>. [Accessed 2021 02 21].
- [31] Simplify 3D, "Ultimate 3D Printing Materials Guide," [Online]. Available: <https://www.simplify3d.com/support/materials-guide/>. [Accessed 21 02 21].
- [32] K. Van Dokkum, Ship knowledge, BV Vlissingen: Dokmar maritime publishers, 2016.
- [33] "Energy Observer," 2017. [Online]. Available: https://en.wikipedia.org/wiki/Energy_Observer. [Accessed 05 03 2021].
- [34] Mindtech by Asime, "Energy Observer, the first ship propelled by renewable energies docks in Spain on its round-the-world voyage," MTechV, 09 05 2019. [Online]. Available: <https://mindtechvigo.com/en/energy-observer-the-first-ship-propelled-by-renewable-energies-docks-in-spain-on-its-round-the-world-voyage/>. [Accessed 05 03 2021].
- [35] SunWatts, "30kW solar kit CSUN 390 XL, SMA Sunny Boy," 2021. [Online]. Available: <https://sunwatts.com/30kw-solar-kit-csun-390-xl-sma-sunny-boy/>. [Accessed 05 03 2021].
- [36] Watt U Need, "Ecorote 1kW grid injection wind kit," 2014. [Online]. Available: <https://www.wattneed.com/en/wind-turbine/21137-wind-turbine-ecorote-1000w-0768563817113.html?preconfig=1:1|1:1|1:1>. [Accessed 05 03 2021].
- [37] OceanVolt, "Twin shaftfrive 20," [Online]. Available: <https://oceanvolt.com/twin-shaftdrive-20/>. [Accessed 05 03 2021].
- [38] FuelCellStore, "5kW Hydrogen Fuel Cell Power Generator G-HFCS-5kW72V," [Online]. Available: <https://www.fuelcellstore.com/fuel-cell-stacks/high-power-fuel-cell-stacks/g-hfcs-5kw72v-5000w-hydrogen-fuel-cell-power-generator>. [Accessed 05 03 2021].
- [39] Pure Energy Centre, "Hydrogen Electrolyser," [Online]. Available: <https://pureenergycentre.com/hydrogen-electrolyser/>. [Accessed 05 03 2021].
- [40] Pure Energy Centre, "Hydrogen compressor," [Online]. Available: <https://pureenergycentre.com/hydrogen-compressor/>. [Accessed 05 03 2021].
- [41] Boc , "Hydrogen N5.0 (CP Grade H2) Cylinder," The Linde Group, [Online]. Available: <https://www.boconline.co.uk/shop/en/uk/l-200bar-hydrogen-cp-grade-290628-l>. [Accessed 05 03 2021].
- [42] Luxyachts, "Yacht cost calculator," [Online]. Available: <https://www.luxyachts.com/yacht-cost-calculator>. [Accessed 01 03 2021].
- [43] Foras na Mara Marine Institute, "Vessel Rates," 2020. [Online]. Available: <https://www.marine.ie/Home/site-area/infrastructure-facilities/research-vessels/vessel-rates>. [Accessed 05 03 2021].

- [44] Marine board, "Next Generation European Research Vessels Current Status and Foreseeable Evolution," www.marineboard.eu, Zoeck, 2019.
- [45] Boats at sea, "Orion 90," [Online]. Available: <https://www.boatsatsea.com/charter-yacht-orion-90>. [Accessed 05 03 2021].
- [46] Yanpy, "Yacht rentals in Majorca," 2020. [Online]. Available: <https://www.yanpy.com/en/yacht-rentals-majorca>. [Accessed 05 03 2021].
- [47] Ferryhopper, "Ferry from Valencia to Ibiza," [Online]. Available: <https://www.ferryhopper.com/en/ferry-routes/direct/ferry-valencia-ibiza>. [Accessed 05 03 2021].
- [48] Kabanize, "Cycle Time as Normal (Gaussian) Distribution," [Online]. Available: http://www.muelaner.com/wp-content/uploads/2013/07/Standard_deviation_diagram.png. [Accessed 20 02 2021].
- [49] Big salty, "UV Index Forecast for Valencia," 17 10 2020. [Online]. Available: <https://bigsalty.com/en/uv/forecast/8010/>.
- [50] Alinghi, "Le innovazioni su Alinghi 5," [Online]. Available: <https://ammiraglio61.wordpress.com/2010/02/10/le-innovazioni-su-alinghi-5/>.

7 ANNEXES



7 Annexes

7.1 Additional pictures





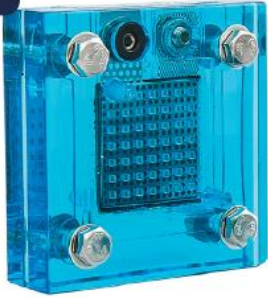
7.2 Datasheets

Horizon PEM electrolyser

Horizon
Educational

PEM Electrolyzers

FCSU-010



Product Description

Produce hydrogen and oxygen using only pure water and an external power source. Take your pick of power sources, all available from Horizon: small solar panels, wind turbines, mechanical hand cranks or batteries.

Features

- ✓ Converts water into hydrogen and oxygen
- ✓ Fully compatible with the Horizon education range

Content

- ✓ Set of 5 PEM Electrolyzers
- ✓ Tubing
- ✓ Pins
- ✓ Banana cables / connecting leads
- ✓ Syringe
- ✓ User Manual:

Specifications

Dimensions	54x54x17 mm
Total weight:	69.7 g
Input voltage	1.8 V ~ 3V (DC)
Input current	1A
Hydrogen production rate	7 ml/min (1A)
Oxygen production rate	3.5 ml/min (1A)

Packing Information

Case Pack Quantity (1 unit = set of 5):	1
Master Pack Quantity (units):	24
Packaging Type:	cardboard
20' Container (units):	6550
40' Container (units):	13355
Unit Box Length (cm/in):	21.2 / 8.35
Unit Box Width (cm/in):	15 / 5.91
Unit Box Height (cm/in):	9.7 / 3.82
Unit Volume (Litres/Cubic Meters):	3.1 / 0.003
Unit Box Weight (kg/lbs):	0.57 / 1.26
Case Pack Length (cm/in):	63 / 24.80
Case Pack Width (cm/in):	44 / 17.32
Case Pack Height (cm/in):	35 / 13.78
Case Pack Volume Litres/Cubic Meters):	97.0 / 0.097
Case Pack Weight (kg/lbs):	14.7 / 32.41

*The cartons' size may vary between ±1-2 cm.



Logistics Information

Item UPC-Code:	N/A
Item HS-Code:	-
Manufactured in:	Shanghai, China
Local Warehouse	Prague, Czech Republic
FOB Harbor:	Los Angeles, USA
First Ship Date:	available now
Minimum Order:	24

*All the information in this datasheet is subject to change without notice. In case of doubt please contact the Horizon sales team.

www.HorizonEducational.com

Cebekit reversible fuel cell

cebekit



PEM REVERSIBLE FUEL CELL C-7121

TECHNICAL SPECIFICATIONS OF THE CELL PEM

Function electrolyzer

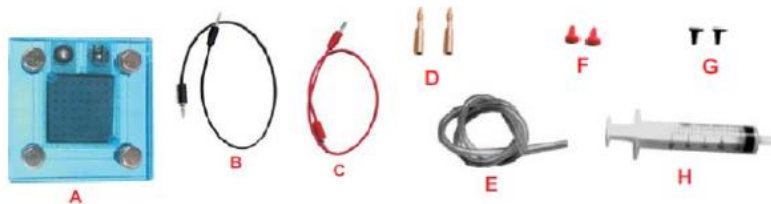
Input voltage.....1,7V – 3V (DC)
Consumption.....0,7 A @ 2 V
Half of hydrogen production.....5ml/min.
average production of oxygen.....2,5 ml/min.

Fuel cell Function

Output voltage.....0,6 V (DC)
Output current.....300 mA.
Output power.....180 mW

CONTENT

- A PEM reversible cell
- B Black wire plugs
- C Red cable with plug
- D Two brass pins
- E Flexible tube
- F Two red caps
- G Two black color caps
- H Syringe for hydration



Size..... 54 x 64 x 17 mm

Weight.....14 gr.

INTRODUCTION

Cell PEM (Polymer Electrolyte Membrane) that combines the functions of electrolyzer and fuel cell into a single component. Operation reversible: when connected to a generator of electricity (photovoltaic solar cell, turbine generator with crank, batteries, etc ...) and oxygen to produce hydrogen from deionized water (acts as an electrolyzer). By applying an electric charge generated electricity from hydrogen (fuel cell acts like).

Perfect for science labs, technology classrooms and demonstrations on hydrogen technology. Also for power portable computers and robots.

GENERAL SAFETY INSTRUCTIONS

- 1 - This cell is intended only for adults who have enough knowledge of fuel cells to develop their own projects by themselves or over 14 supervised by an adult who has read and understood the instructions in this manual.
- 2 - Before using this equipment should read and understand these instructions.
- 3 - Tools are required to mount this unit. We must pay due attention when being handled tools to avoid injury.
- 4 - Some small pieces are fragile, need to be handled carefully to avoid breaking them.
- 5 - Do not use any portion, element or component of the cell supplied for any purpose other than those specified in this manual. The cell may not be disassembled.
- 6 - At the end of each use to drain all the components containing water, hydrogen and oxygen.
- 7 - Wash your hands after working or experimenting with fuel cells

WARNING FOR THE CORRECT USE OF THE CELL

- 1 - Use only distilled water. Using distilled water will not damage the electrodes of the fuel cell. The fuel cell uses a carbon-catalyst Platinum nano, these particles are very sensitive to impurities that are always present in the water not distilled. When you see that the fuel cell starts to rust, it means that their experiments did not use distilled water.
- 2 - Before making sure you've electrolysis cell well hydrated by injecting water into the syringe. Leave the water on the inside with 5-10 minutes for complete hydration.

www.cebekit.com - info@cebekit.com

User manual Horizon fuel cell



PEM Fuel Cell

Product Ref No. : (FCSU-012)

Specifications:

High performance PEM fuel cell specifications:

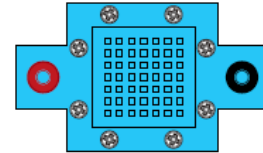
- Dimensions (w x h x d): 32mm x 32mm x 10mm
- Total Weight: 27.3grams
- Output Power: 270mW
- Output Voltage: 0.6V (DC)
- Output Current: 0.45A
- Color: Blue

What is included:

- PEM Fuel cell

What you need:

- PEM Electrolyzer Fuel Cell
- Pins, Tubing
- 2 x banana cables/ Connecting leads
- Syringe
- Clincher
- Battery pack or solar panel
- Distilled water
- Gas containers



Note:

You can purchase the components used in the operation online at: <http://www.horizonfuelcell.com/store.htm>

Fuel Cell Experimentation:

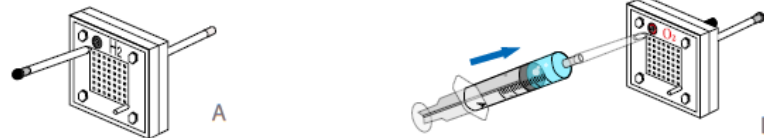
Before applying a load to the fuel cell, you must first create the hydrogen and oxygen gasses needed by the fuel cell for the conversion of chemical energy into electrical energy. This can be performed by using Horizon PEM electrolyzers and outer/inner gas containers to create and capture the hydrogen and oxygen gasses. These inner/outer containers are made primarily for educational demonstration, and you may also use small balloons as in the H-racer or small syringes to capture the gasses.

PEM Electrolyzer- User Directions

Preparation of the Electrolyzer and Solar/Battery Powered Hydrogen Production

1. Place the Electrolyzer onto a flat surface. Cut 2 x 4cm length pieces of rubber tube and insert a black pin into the end of one tube. Place the tube with the black pin into the top pin on the hydrogen side (with black terminal). Place the other tube firmly onto the top input nozzle on the oxygen side (see A).

2. Fill the syringe with DISTILLED water. On the red (oxygen) side of the electrolyzer, connect the syringe to the uncapped tube. Fill the electrolyzer until water begins to flow out of the tube. Place a red plug into the short tube located on the Oxygen side of electrolyzer. Let settle for 3 min (see B).



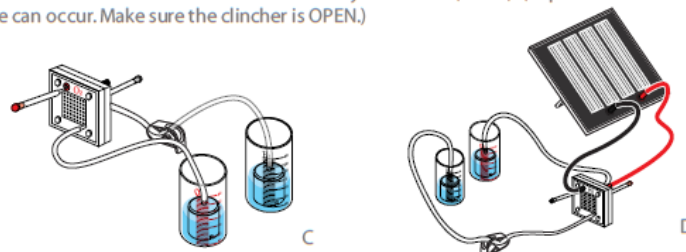
3. Place the outer water/gas containers onto a flat surface. Fill with distilled water up to the "0" line.

4. Place inner containers into outer cylinders minding that the gaps are not blocked by inner plastic rims. Make sure the water is still level to the "0" line. If not, remove some water with the syringe so that water level is at "0" line. Cut out two 20cm lengths of tubing.

5. Place one tube through the holes on the white clincher, with the clincher 4 cm from the end of the tube. Connect the tubes to the top nozzles on the inner containers. If the tubing is connected to the inner cylinders lastly there will be no air trapped inside the inner containers.

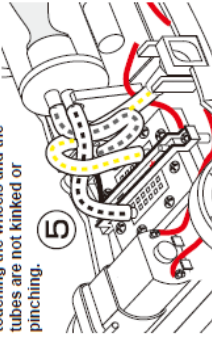
6. Connect the other end of one of the tubes to the bottom end of the black hydrogen side of the electrolyzer. Connect the end of the other tube to the bottom end of the red oxygen side of the electrolyzer (see C).

7. Connect the electrolyzer to the solar panel using the corresponding cables and expose to direct sunlight. You can also use a Horizon battery pack and two AA batteries to connect to the electrolyzer as well (see D). (Important: make sure connections are correct or permanent damage can occur. Make sure the clincher is OPEN.)



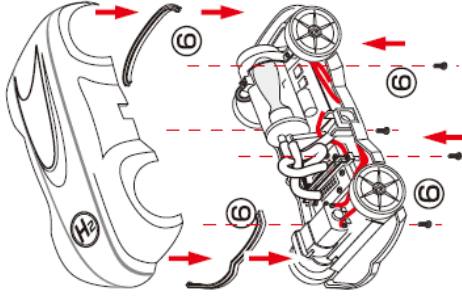
H-racer 2.0 assembly guide

Warning: Make sure these connections are correct. Any other connection will not allow proper operation of the car and its fuel cell power system. Also ensure the wires are not touching the wheels and the tubes are not kinked or pinching.



6. Place the front and rear bumpers onto the bumper frames on the chassis.
 *Be careful not to place the bumpers upside down. Make sure the rear bumpers fit correctly onto the frame.

Position the body of the car onto the chassis. Align the holes on the chassis with the holes on the car body top. Use a screwdriver (not included) to attach the body to the chassis using the set of 4 large screws and make sure the screws are entered straight into the chassis. Do not tighten the screws until all screws are partially entered into the chassis. Drive the screws into the chassis until no gaps are left between the body and the chassis.



Remove the H2 sticker from its backing and position it on the car accordingly.

4. Position the fuel cell onto the square slot located in the middle of the car chassis. The positive mark on the fuel cell should be positioned on the side with the red cable, and the negative mark on the side with the black cable. Push the fuel cell into the chassis.

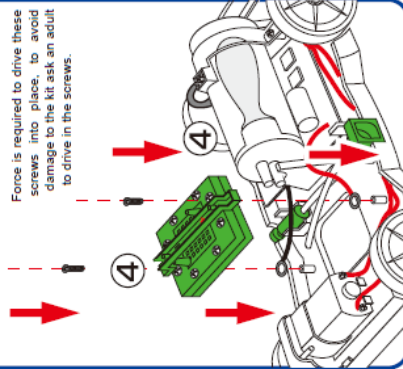
Position the black cable terminal between the fuel cell holder and the fuel cell end plates, and position the red cable terminal in the same manner on the opposite side. Make sure the holes are aligned.

Align the fuel cell holder with the two holes on the car chassis. Place the screws into the screw holes and make sure the screws are entered through the cable terminal holes and straight into the chassis.

*Please note there are two types of screws. The smaller screws are used for the fuel cell and the larger screws are used for the car body.

Use a screwdriver to attach the fuel cell end plate and the red & black cable terminals to the screw holes on the chassis. Make sure the metal terminals from the cables are closely touching the fuel cell end plates. Do not tighten the screws until the two screws are partially entered into the chassis. Drive the screws into the chassis making sure all the parts are connected tightly without moving.

Force is required to drive these screws into place, to avoid damage to the kit ask an adult to drive in the screws.



5. Connect one end of the flexible tubes to the lower nozzle on the storage cylinder and the other end of the flexible tube to the nozzle on fuel cell located nearest to the motor. Connect the other end of the flexible tube on the refueling input valve to the other nozzle located on the fuel cell. Connect the purging valve tube to the upper nozzle located on the storage cylinder. Make sure all tubes are properly positioned as in diagram.

H-racer 2.0 ASSEMBLY GUIDE



Model No.: FC-JJ-23



Warning
 To avoid the risk of property damage, serious injury or death:

This kit should only be used by persons 12 years old and up, and only under the supervision of adults who have familiarized themselves with the safety measures described in the kit. Keep small children and animals away as it contains small parts that could be swallowed. The fuel cell generates gases that are very easily ignited. Read the instructions before use and have them ready for reference.

Battery operation instructions:

1. The removing and inserting of batteries is to be conducted by the adults only. When inserting the batteries make sure that you are doing so with the correct polarity (the positive end of the battery must match up with the "+" and the negative end of the battery must match up with the "-" indicated on the battery pack) and then close the battery compartment.
2. Non-rechargeable batteries are not to be recharged, and standard batteries or new and used batteries are not to be mixed and should be used separately.
3. Different types of batteries such as rechargeable, alkaline and standard batteries or new and used batteries are not to be mixed and should be used separately.
4. The two spare red/black cables are not to be inserted into an AC socket.
5. Exhausted batteries are to be removed from the battery compartment.

H-racer 2.0

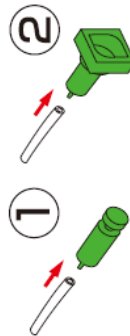
ASSEMBLY GUIDE

What do you need?

- H-Racer 2.0
- AA batteries=2 Units
- Water=25ml
- LR44 batteries=3 Units

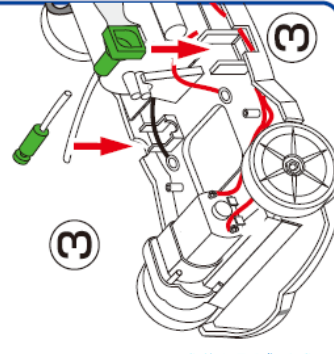
1. Connect one of the flexible tubes to the small purging valve. Make sure the tube is inserted all the way into the base of the purging valve nozzle.

2. Connect another flexible tube to the nozzle of the refueling input valve. Make sure the tube is inserted all the way into the base of the nozzle of the refueling input valve.



TIP: To fit the flexible tubes onto the nozzle of the valve, connect the nozzle of the tube into the nozzle of the valve until the tube is snugly fixed to the base of the nozzle.

3. Place the refueling input valve above the opening on the left side of the chassis. Make sure the red cable is positioned above the refueling input valve tubing. Slide the refueling input valve onto its mount located at the opening on the side of the chassis. With a downward motion, click the valve into place ensuring it is smoothly aligned with the outer surface of the chassis.



Xunzel solar panel



xunzel™

applied Solar and Wind Energy

FICHA TÉCNICA

SOLARTHIN™ Series

Paneles solares fotovoltaicos para la carga y el mantenimiento de baterías de 12V

SOLARTHIN™ Especificaciones



GARDEN



LAND



CARAVAN



MARINE





SOLARTHIN 2.5W-12V

SOLARTHIN 7W-12V

SOLARTHIN 20W-12V

Modelo	Pmax	V	Vmp	Imp	Voc	Rango Temperatura	Conector	Peso	Dimensiones (mm)	Longitud del cable (mm)
SOLARTHIN 2.5W-12V	2.5W	12V	15V	167mA	21.5V	-40 °/+80 °C	XU1	450gr	325 x 125 x 22	1800
SOLARTHIN 7W-12V	7W	12V	15V	467mA	21.5V	-40 °/+80 °C	XU1	1.36kg	325 x 340 x 22	1800
SOLARTHIN 20W-12V	20W	12V	15V	1330mA	21.5V	-40 °/+80 °C	XU1	8.0kg	325 x 940 x 22	2500

Accesorios incluidos:

Toma CLA Macho

Toma CLA Hembra

Pinzas Batería

Comprobador LED

Soportes para inclinar y fijar







MANTENIMIENTO Y CARGA DE BATERÍAS









L-1 106214-MA



Industry Leading Technology for Off-Grid, Off-Shore and Backup Power Applications












SENSOVANT

Smart Sensing

(+34) 968 162 005

www.sensovant.com

comercial@sensovant.com



© 2014-2015 Copyright Xunzel. Information contained in this document is subject to change without notice.

El diseño y todos los datos de esta ficha están protegidos por Ley y no pueden ser distribuidos, ni reproducidos, ni total ni parcialmente, ni publicados ni usados para ningún propósito sin el expreso consentimiento por escrito de XUNZEL. ©2014-2015 XUNZEL. Xunzel no se hace responsable de posibles errores tipográficos.

DAQ 9174 Ni 9129 Card Equipment pinout

Table 1. Signals by Mode

Mode	Pin					
	1	2	3	4	5	6
Voltage	T+	T-	—	HI	LO	—
Current	T+	T-	HI	—	LO	—
4-Wire Resistance	T+	T-	EX+	HI	EX-	LO
2-Wire Resistance	T+	T-	HI	—	LO	—
Thermocouple	T+	T-	—	HI	LO	—
4-Wire RTD	T+	T-	EX+	HI	EX-	LO
3-Wire RTD	T+	T-	EX+	—	EX-	LO
Quarter-Bridge	T+	T-	HI	—	LO	—
Half-Bridge	T+	T-	EX+	HI	EX-	—
Full-Bridge	T+	T-	EX+	HI	EX-	LO